University of Amsterdam

Simulating energy transfer of triplet excitons

Roan van Leeuwen

Submitted in part fulfilment of the requirements for the degree of
Master of Science in Computational Science on the
University of Amsterdam, July 18, 2018

Simulating energy transfer of triplet excitons

Master of Science Thesis

Author:
Roan van Leeuwen BSc
6353371, 10092102, 2528512 (VU)
Computational Science
University of Amsterdam

Supervisor:
dr. Ivan Infante
Theoretical Chemistry
Vrije Universiteit Amsterdam

Supervisor:
dr. Bruno Ehrler
Hybrid Solar Cells
AMOLF

Examiner:
dr. Jaap Kaandorp
Computational Science Lab
University of Amsterdam

Abstract

In the thrive for higher efficiency of solar panels, the use of singlet fission materials could be one of the solutions. Research on such materials has confirmed the existence of the singlet fission process in combination with energy transfer afterwards, for certain acceptor materials.
In this master thesis, the first aim was to computationally reproduce this experimentally observed energy transfer from tetracene, the singlet fission material, to a lead sulphide quantum dot, the acceptor material, using density functional theory, molecular dynamics and surface hopping algorithms. The second aim is to answer the question if and how the orientation of the tetracene with respect to the quantum dot influences the energy transfer.
The accuracy of the functionals used in this work was determined to be rough, especially for charge transfer states. After adjusting the (charge transfer) state energies, the energy transfer of triplet excitons from tetracene to quantum dots was successfully reproduced using the GFSH algorithm, with transfer times that are not contradicting the experimentally determined time frame. Analysis of the behaviour of the coupling during the simulated trajectory suggests that the distance between tetracene and the closest atom of the quantum dot ligands has a significant influence on the coupling. Finally, no clear dependencies are found between coupling and one of the other variables.

Contents

Abstract **i**

1 Introduction **1**

1.1 Introduction 1

1.2 Context 2

1.3 Problem 3

1.4 Outline 4

2 Background Theory **5**

2.1 Quantum Physics and Quantum Chemistry 5

2.1.1 Wave functions 5

2.1.2 The Schrödinger equation and the Hamiltonian 6

2.1.3 Quantum numbers 6

2.1.4 Photovoltaic Effect 7

2.1.5 Singlet and Triplet States 7

2.1.6 Singlet Fission 8

2.1.7 Tetracene 10

2.1.8 Pentacene 10

2.2 Computational Theory 11

2.2.1 Introduction 11

2.2.2 Density Functional Theory in general 11

2.2.3 Different Functionals 12

2.3 List of Symbols 13

3 Research Part I: Exploratory simulations using DFT 15

3.1 Introduction 15

3.1.1 Background 15

3.1.2 Materials 15

3.1.3 Geometry of the Materials 16

3.1.4 Outline 16

3.2 Theory 17

3.2.1 Introduction 17

3.2.2 TheoDORE 17

3.3 Method 18

3.3.1 Method 1: DFT with Different Functionals using ADF 18

3.3.2 Method 2: DFT with Different Functionals using Orca and TheoDORE . 20

3.4 Results and Analysis 21

3.4.1 Tetracene Results 21

3.4.2 Tetracene Analysis 21

3.4.3 Pentacene Results 23

3.4.4 Pentacene Analysis 24

3.5 Discussion 26

3.6 Conclusion 26

4 Research Part II: Energy Transfer from Tetracene to Quantum Dot with Non-Adiabatic Molecular Dynamics 27

4.1 Introduction 27

4.1.1 Description 27

4.1.2 Quantum Dot 27

4.1.3 Literature 28

4.1.4 Objective 28

4.1.5 Outline 29

4.2 Experimental Research 29

4.3 Theory 31

4.3.1 Introduction 31

4.3.2 Molecular Dynamics 31

4.3.3 Fewest-switches surface hopping 32

4.3.4 Classical path approximation 33

4.3.5 GFSH 34

4.4 Method 35

4.4.1 Introduction 35

4.4.2 Starting geometry determination with CP2K 35
4.4.3 Trajectory Calculation using MD by CP2K 36
4.4.4 Recalculation of Hamiltonians and coupling with QMWorks 36
4.4.5 Simulation of the Energy Transfer with PYXAID 37
4.5 Setups 38
4.5.1 Preparation: approximating the charge-transfer state energies 38
4.5.2 Different ligands 39
4.6 Results and analysis 43
4.6.1 Hamiltonian Results 43
4.6.2 Hamiltonian analysis 48
4.6.3 Energy transfer results 55
4.7 Discussion 61
4.7.1 Error Margins 61
4.7.2 Further uncertainty 61
4.7.3 Surface hopping 62
4.7.4 Coupling 63
4.8 Conclusions 64

5 Conclusion **65**

5.1 Summary of Thesis Achievements 65
5.2 Applications 66
5.3 Future Work 66

A Coordinates **68**

A.1 Tetracene Monomer 68

A.2 Tetracene Dimer 69

A.3 Pentacene Monomer 72

A.4 Pentacene Dimer 73

A.5 PbS+7C and Tetracene 76

A.6 PbS+9C and Tetracene 82

B Excitation energy results **89**

B.1 Tetracene 89

B.2 Pentacene 90

C Coupling of Setup 9C versus variables **91**

Bibliography **93**

Chapter 1

Introduction

1.1 Introduction

Solar panels are increasingly used for generating electricity all over the world. Despite this rising usage of solar panels, their efficiency is still rather limited, with energy efficiency values around 20% for panels on the market, and of 28.8%[52, 25] as a maximum obtained under lab conditions. There are promising processes within a range of materials that can potentially improve the efficiency of solar energy systems, such as carrier multiplication. In organic materials, carrier multiplication's equivalent is called singlet exciton fission, which has experimentally been observed in certain materials. To use the benefits of singlet fission, one needs to eliminate or significantly reduce the losses that necessary processes, such as energy transfer, cause. By computationally reproducing experimentally observed energy transfer of excitons generated by singlet fission, the aim of this thesis is to find out how energy transfer can be made more efficient. To do so, question how the ideal placement of the donor with respect to the acceptor is, needs to be answered.

1.2 Context

Global warming is almost generally accepted as a big problem, for which solutions have to be found with an increasing urgency. Hence, one of the currently interesting fields of research is finding full-fledged alternatives to fossil energy. Solar panels are one of the alternatives that are already on the market. Although the usage of solar panels is increasing rapidly, their efficiency is still relatively low, since roughly 20% of the energy of light reaching the panel is converted into energy. In lab situations, higher efficiencies are obtained, up to 28.8%[52, 25].

A big part of the loss of efficiency is caused by the fixed band gap, or HOMO-LUMO gap for the case of organic molecules. The loss is caused by the spectrum of the sun, which is well spread over a big range of wavelengths. Photons with an energy equal to the band gap can provide excitations without loss of energy. Photons with lower energy will not be absorbed. Hence, all energy of these photons can be considered as losses. The photons with higher energy than the band gap can be absorbed, but will reduce in energy to the lowest excited state. Hence, the difference between the energy of the photon and the energy of the lowest excited state is also lost energy. Combining this calculation of losses with the solar spectrum results in the Shockley-Queisser limit, describing the maximum efficiency for monocrystalline materials. Under these conditions, the optimal band gap is at 1.34 eV, with a theoretical maximum energy efficiency of 33.7%[52].

One of the solutions that might help overcoming the Shockley-Queisser limit and hence might help improving the efficiency of future solar panels, is the use of materials with carrier multiplication capabilities. In organic materials, this process is called singlet fission. Herein, an electron is excited to form an excited state called the singlet exciton, which converts into two triplet excitons. Hence, one of the requirements for a material to allow singlet fission to take place, is that the singlet excitation is roughly two times higher in energy than the triplet excitation, compared to the ground state energy.

A singlet fission material on its own will not be able to exceed the Shockley-Queisser limit, but in combination with other materials it might. For useful solar applications it is therefore important that the energy transfer from singlet fission materials to the second, acceptor, material

is as efficient as possible. An important aspect herein is the energy transfer time. If the energy is transferred faster, there is less time and hence less probability for processes causing losses, such as recombination, to take place.

This research focusses on the energy transfer from singlet fission materials into quantum dots. This has experimentally been observed for setups from tetracene to lead sulphide quantum dots[64], as well as from pentacene to lead selenide quantum dots[59]. In the experiment with tetracene, the quantum dot ligand length is varied to show an exponential decrease in transfer efficiency. This indicates that the transfer mechanism is Dexter energy transfer[**?**]. Knowing that the energy transfer does occur, the next challenge is to optimise the transfer. Using computational techniques, we aim to give insights in the ideal positioning of a singlet fission material, represented by a single tetracene molecule, with respect to the acceptor, a lead sulphide quantum dot. To do so, the focus is solely on the energy transfer process. Hence, the singlet fission process is ignored, which leads to an initial situation where the triplet exciton is located at the tetracene molecule. Using density functional theory, molecular dynamics and surface hopping algorithms, the electron transfer from tetracene to the quantum dot is simulated and analysed.

1.3 Problem

In the experiments performed in labs, the energy transfer from tetracene and pentacene to quantum dots has been confirmed to take place. However, it is hard to determine the exact microscopic distance and orientation between donor and acceptor. With simulations of the situation, it can easily be seen how the donor is orientated with respect to the acceptor. Using computational techniques, we want to find out how the setup influences the energy transfer.

The first target of the research is to computationally reproduce the energy transfer from tetracene to lead sulphide quantum dots. As a next step, we want to know how the different angles influence the energy transfer: how should the tetracene molecule be rotated around its longest and its smallest axis, to observe optimal energy transfer? Furthermore, we also want to obtain information on the role of the intermolecular distance. Should the distance be as small as possible? And does the positioning and length of the ligand influence the energy

transfer?

1.4 Outline

In the remainder of this thesis, the aim is to find answers to the posed research questions. This research covers various parts of different fields of science. Therefore, Chapter 2 describes the theory and background behind the relevant parts of chemistry, physics and informatics. This includes a short explanation of quantum physics and the photovoltaic effect, as well as a brief description of singlet and triplet states and the singlet fission process. Furthermore, density functional theory, the computational technique that is the basis of the majority of the computations performed for this thesis, is explained in this chapter.

Hereafter, the research is described, divided into two different parts. In the first part, Chapter 3, exploratory density functional theory computations are performed on tetracene monomers and dimers. Pentacene monomers and dimers were also analysed in the same way, as a reliability check. For both materials, different types of functionals are used to give insights in the accuracy and speed of calculating the excited states of the setups.

In Chapter 4, the second research part, molecular dynamics algorithms are used to simulate the dynamics of a setup in which a tetracene molecule is placed close to a lead sulphide quantum dot. The setups are analysed for two different ligands with both thousands of unique time steps.

The final chapter, Chapter 5, summarises the conclusions that can be drawn from the results. Furthermore, this chapter describes if, how, and to which extent, the results and conclusions are able to provide answers to the research questions.

Chapter 2

Background Theory

Background Theory Statement

In this section, we take a deeper look into the theory behind the occurring phenomena. The two main parts of this section are 'Quantum Physics and Quantum Chemistry' (2.1) and 'Computational Theory' (2.2). The symbols that are used are as much as possible in line with the corresponding references, and are only altered in case of duplicate symbols or meanings.

2.1 Quantum Physics and Quantum Chemistry

2.1.1 Wave functions

In classical mechanics, $x(t)$ would describe the position of an object, e.g. a particle, over time t. In quantum mechanics, the same particle is described by its wave function, Ψ[27]. The wave function is related to the probability to find the particle between a and b $p_{a<x<b}$, as

$$p_{a<x<b} = \int_a^b \|\Psi(x,t)\|^2 dx. \tag{2.1}$$

In this case, Ψ is dependent of time (t) and a one-dimensional space coordinate (x).

2.1.2 The Schrödinger equation and the Hamiltonian

The wave function obeys the Schrödinger equation[54], which can be denoted as[27]

$$\hat{H}\Psi = E\Psi \quad \text{or} \quad \hat{H}\Psi = i\hbar\frac{\delta}{\delta t}\Psi \tag{2.2}$$

depending on Ψ being time-independent or time-dependent, respectively. Herein, $\hat{H}$ is the Hamiltonian operator, and E are the allowed energies. Furthermore, the values E can be seen as the eigenvalues and expectation values of $\hat{H}$, with the Ψ-functions being the corresponding eigenfunctions.

The Hamiltonian operator for a single particle can be described as

$$\hat{H} = -\frac{\hbar^2}{2m}\nabla^2 + V, \tag{2.3}$$

in which m is the mass of the particle, $\hbar$ is Planck's constant divided by 2π, ∇ is the nabla operator and V describes the potential.

2.1.3 Quantum numbers

The state of a particle, say an electron, is defined by quantum numbers. There are two numbers that determine the energy of the electron. These are the principal quantum number n and the azimuthal quantum number l. The number n is restricted to be a positive integer, whereas l can have all values from 0 to $n-1$, thus $l = 0, 1, 2, \ldots n-1$.

The other two quantum numbers defining the state of a particle, are the magnetic quantum number m_l and the secondary spin quantum number m_s. These quantum numbers are restricted to the values $m_l = -l, -l+1, -l+2, \ldots, l-1, l$ and $m_s = -s, -s+1, \ldots, s-1, s$, where s is the (primary) spin quantum number, which is $s = \frac{1}{2}$ for a single electron.

2.1.4 Photovoltaic Effect

The n and l numbers indicate the orbital that the electrons are in. The Pauli exclusion principle states that two identical fermions (electrons, for example) cannot occupy the same state. Hence, the orbital with the lowest energy ($n = 1 \rightarrow l = 0$) can only hold two electrons, since m_l has to be zero and the spin can be either $\uparrow$ ($m_s = \frac{1}{2}$) or $\downarrow$ ($m_s = -\frac{1}{2}$). The bands with low energy, which have a higher probability to be filled, are called valance bands, the higher energy band is called the conduction band. The band gap energy E_g is the difference in energy between the valence and the conduction band.
A photon may be absorbed and excite an electron from the valance to the conduction band. This process is called photoconductivity and the energy of the photon evidently has to satisfy[68]

$$E_{photon} \geq E_g. \tag{2.4}$$

Using p–n junction, the positive side (p, with a lack of electrons) is connected to the negative side (n, with an excess of electrons), creating a potential difference, which, upon photo excitation can generate a current. This process is called the photovoltaic effect.

2.1.5 Singlet and Triplet States

In a system consisting of two electrons such as an exciton, multiple spin configurations are possible. For the singlet state, the quantum number s is zero, resulting in the configuration:

$$\frac{1}{\sqrt{2}}(\uparrow\downarrow - \downarrow\uparrow), \text{ with } m_s = 0. \tag{2.5}$$

The triplet states are the three possible configurations for the spin quantum number $s = 1$[27]:

$$\begin{gathered} \uparrow\uparrow \text{ , with } m_s = 1; \\ \frac{1}{\sqrt{2}}(\uparrow\downarrow + \downarrow\uparrow), \text{ with } m_s = 0; \\ \downarrow\downarrow \text{ , with } m_s = -1. \end{gathered} \tag{2.6}$$

The ground and first excited singlet state are denoted as S_0 and S_1, whereas the energetically lowest triplet state is denoted as T_1. There are multiple ways to generate triplet states and the generation method that is studied in this thesis is fission of singlet excitons.

2.1.6 Singlet Fission

An organic chromophore that is excited to a higher singlet state is able to share its excitation energy with a neighbouring organic chromophore in the ground state. This results in two neighbouring chromophores in excited triplet states. The process is called singlet fission and a schematic representation is included in figure 2.1[56]. For singlet fission to take place rapidly,

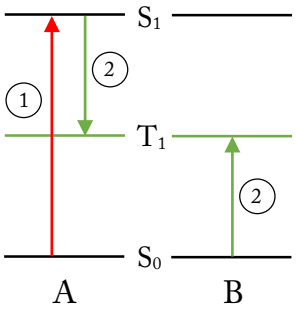

Figure 2.1: a schematic representation of singlet fission; at step 1, chromophore A is excited to state S_1, denoted as $A(S_1)$; at step 2 the singlet fission takes place, converting $A(S_1) + B(S_0)$ to $A(T_1) + B(T_1)$.

there several of conditions that need to be satisfied; not all of them are well known.[56] The biggest requirement is the presence of two organic molecules for which the energy of the excited singlet state is approximately twice the energy of the triplet state ($E(S_1) \gtrsim 2\,E(T_1)$).
The most direct description of the singlet fission process is based on the reverse triplet-triplet annihilation from Merrifield's theory[13, 32]:

$$S_1 \Leftrightarrow {}^1(\mathrm{TT}) \Leftrightarrow T_1 + T_1. \tag{2.7}$$

Herein, ${}^1(\mathrm{TT})$ is an intermediate state of two correlated triplets, which from now on is called multiple exciton state (ME). Although some researchers supported this direct mechanism[76], the estimated direct coupling matrix element was about two orders of magnitude too small to explain the singlet fission timescale in pentacene[8, 14]. To explain the rapid fission, the

existence of quantum superposition between S_1 and ME was suggested[14]:

$$S_0 \rightarrow [S_1 \Leftrightarrow \mathrm{ME}] \rightarrow \mathrm{ME}' \rightarrow T_1 + T_1, \tag{2.8}$$

in which $[S_1 \Leftrightarrow \mathrm{ME}]$ is the superposition, and ME′ is the multiple exciton state that is no longer coupled to S_1. However, this equation does not include charge transfer states (CT), which are believed to play a role in the fission mechanism in tetracene crystallites, pentacene dimers and pentacene crystallites[13, 8, 9]. Charge transfer states are the result of an electron that is

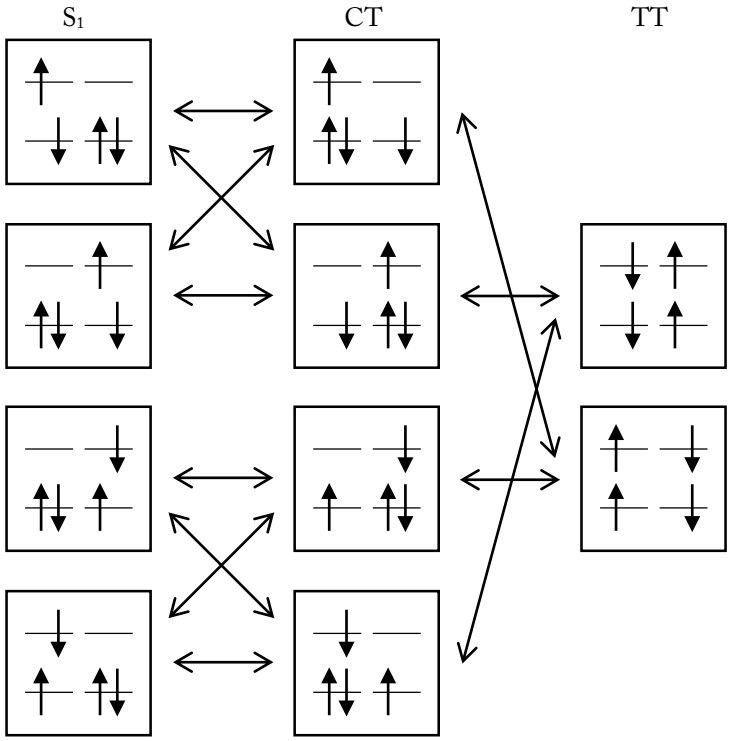

Figure 2.2: a simplified schematic representation of the allowed spin configurations and transitions of the states S_1 (one molecule in S_1 and the other in S_0), CT (the charge transfer state) and TT (the triplet-triplet state)[26]. In every square, the top lines are the LUMO and the bottom lines the HOMO; the horizontal separation distinguishes the two molecules.

excited to a neighbouring molecule, as schematically shown in figure 2.2. With the inclusion of charge transfer states, the fission mechanism could be written as[39]:

$$S_0 \rightarrow [S_1 \Leftrightarrow \mathrm{CT} \Leftrightarrow \mathrm{ME}] \rightarrow \mathrm{ME}' \rightarrow T_1 + T_1, \tag{2.9}$$

where $[S_1 \Leftrightarrow \mathrm{CT} \Leftrightarrow \mathrm{ME}]$ is a quantum superposition state between the Frenkel exciton (S_1), the charge transfer state and the multiple exciton state. This is a rather general notation, whereas some studies indicate that the process might be material and/or structure dependent. In pentacene dimer, charge transfer states behave as high-lying virtual states in a super-exchange

mechanism engendering ultra-fast fission[39, 8]. In pentacene crystallites on the other hand, ultra-fast fission requires the involvement of charge transfer states, which are in this case lower-lying due to the polarizability of the surrounding molecules, mixing with the adiabatic singlet exciton S_1[9]. Efficient singlet fission has only been found in a select number of molecules, including, as already mentioned, pentacene and tetracene[39, 77, 3].

2.1.7 Tetracene

Tetracene consists of four alkene rings, see figure 2.3 (a). Singlet fission in tetracene is an uphill process, since excitation energy of the S_1 state is lower that the sum of the excitation energy of two triplet states, $E(S_1) < E(2\,T_1)$. The excitation energy of S_1 and T_1 are 2.32 eV and 1.25 eV for a tetracene crystal at room temperature[66].

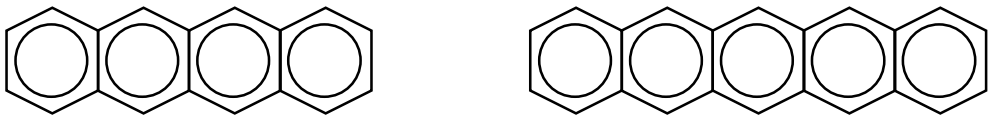

Figure 2.3: tetracene (a) and pentacene (b) molecular structure

2.1.8 Pentacene

The pentacene molecule is shown in figure 2.3 (b). The excitation energies in pentacene are favorable for singlet fission. For a monomer, the excitation energies are 2.3 eV for S_1 and 0.86 eV for T_1[77, 29, 11]. In crystal structure, the excited-state energy of S_1 is 1.83 eV[65].

2.2 Computational Theory

2.2.1 Introduction

As already mentioned in the introduction, this is a theoretical research zoomed in to very small scales. Hence, the computations are performed with software and algorithms developed in the theoretical chemistry research field. Albeit multiple techniques are to be used, the majority of the computations is based on one method, called Density Functional Theory (DFT). This section describes the background of DFT, as well as the differences between a couple of the relevant functionals.

Since this is the only general method, no other computational methods are described at this point. The remaining methods and algorithms that are used are described specifically in theory sections in the chapters they are used in.

This section is based on, and uses the notations of, an article written by Cramer and Truhlar[15].

2.2.2 Density Functional Theory in general

Density functional theory provides a method for the computation of energies, charge distributions and wave functions. The electronic energy of the computed system can be approximated as:

$$E = T_n + \varepsilon_{ne} + \varepsilon_{ee} + \varepsilon_{xc}. \tag{2.10}$$

Herein, T_n is the kinetic energy of non-interacting electrons, ε_{ne} the interaction between the electron distribution and the nuclei, ε_{ee} contains the interaction energy of the spin densities with each others and with themselves, described by the classical Coulomb energy.

The remaining energies and energetic corrections are described by the exchange-correlation energy, ε_{xc}. This ε_{xc} corrects for the lack of interactions in T_n, and the unphysical interactions of the electrons with themselves, which are included in ε_{ee}. Also, ε_{xc} includes exchange energy, taking into account the exchange of electron variables due to indistinguishability, and correlation energy, taking into account that multiple single-electron spin densities put together are not equal

to one many-electron spin density. ε_{xc} is written as a functional of the spin-density and it is called the spin-density functional[15] or exchange-correlation functional[73].

These densities of a system can be calculated using the occupied Kohn-Sham spin-orbitals, $\psi_{j\sigma}$, as

$$\rho_\sigma = \sum_{j}^{\text{occ}} |\psi_{j\sigma}|^2. \tag{2.11}$$

The Kohn-Sham spin-orbitals can be computed with self-consistent field calculations, and the σ and j represent the spin number and other quantum numbers, respectively. With the usage of Kohn-Sham theory comes one of the limitations of DFT. Kohn-Sham theory is not able to treat all open-shell systems or excited states well. Still, Kohn-Sham theory remains the most accurate available approach for most cases. Furthermore, there are functionals that can overcome these disadvantages.

The existence of the density functional is confirmed by the Hohenberg-Kohn theorem[30]. However, there is no closed-form expression for the functional, and improving the approximations of the functional can not be done by a systematic route. This does not mean that no useful approximations exist. In the next subsection, 2.2.3, the different type of functionals are described.

2.2.3 Different Functionals

The first approximation to a density functional is the Dirac-Slater approximation, which is an approximation to exchange[16, 55]. Taking correlation into account by calculations on uniform electron gas, results in the local spin density approximation (LSDA), depending only on spin densities and not on derivatives of the density, nor on orbitals[12, 70, 47].

As a next step, a dependence on the gradients of the spin densities can be added. These type of functionals are called generalised gradient approximations (GGAs). One of the numerous GGAs was developed by and named after Perdew, Burke, and Ernzerhof, hence called PBE[45].

Both of the two thusfar mentioned types of functionals, LSDA and GGAs, include self-exchange and self-correlation. As a result of these unphysical and hence unwanted additions, calculations with such functions turn out to calculate too small HOMO-LUMO gaps.

Self-exchange and self-correlation can be eliminated by including respectively Hartree-Fock exchange and kinetic energy density[46, 6, 75]. The addition of Hartree-Fock exchange results in functionals called hybrid GGAs or hybrid functionals. If kinetic energy density is added, the functionals are called meta functionals. The combination of the two results in hybrid meta functionals. The hybrid functional that is by far the most popular, is called B3LYP[57]. Hybrid functionals, such as B3LYP, have the advantage that they overcome the problems with open-shell systems and excited states as caused by Kohn-Sham theory.

Out of all the available functionals, new functionals are created that combine multiple functionals to a curtain extent. The last group of functionals worth mentioning is called the range-separated functionals. These functionals combine different methods for calculating short-range and long-range exchange. CAM-B3LYP is such a range-separated functional, combining the B3LYP functional with a long-range correction called Coulomb-attenuating method (CAM)[73, 60].

2.3 List of Symbols

CT	charge transfer state
E	total energy
ε_{ee}	interaction energy between electrons
ε_{ne}	interaction energy of electrons with nuclear framework
ε_{xc}	exchange-correlation energy/functional
$\hat{H}$	hamiltonian operator
h	original Planck's constant
$\hbar$	Planck's constant h divided by 2π, i.e. $\hbar = 1.054572 \times 10^{-34} Js$ [27]
HOMO	highest occupied molecular orbital
i	complex component
j	collection of all quantum numbers, except spin
l	azimutal quantum number
LUMO	lowest unoccupied molecular orbital

m_l	magnetic quantum number
m_s	secondary spin quantum number
ME	multiple exciton state of two combined triplets
n	principal quantum number
Ψ	wave function, mostly unrestrained
ψ	wave function, mostly restrained to specific variables, dimensions and/or conditions
ρ	spin density
σ	spin quantum number
s	(primary) spin quantum number
S_n	n'th excited singlet state, with S_0 the ground state
T_n	kinetic energy
T_1	the lowest excited triplet state
^{1}(TT)	combined state of two triplets, mostly depicted as ME
V	total potential energy
v	local potential function
W	interaction compontent of E
w	interaction function
∇^2	Laplacian, which depends on the used coordinate system; for cartesian coordinates, it is defined as: $(\frac{\partial^2}{\partial x^2} + \frac{\partial^2}{\partial y^2} + \frac{\partial^2}{\partial z^2})$
$\uparrow$	spin up, i.e. $m_s = \frac{1}{2}$
$\downarrow$	spin down, i.e. $m_s = -\frac{1}{2}$

Chapter 3

Research Part I: Exploratory simulations using DFT

3.1 Introduction

3.1.1 Background

In this chapter, DFT calculations are performed on the singlet fission materials. Since there are many different functionals that all have certain qualities and downsides, it is needed to get an impression of the results that the different functionals deliver, as well as the computational time it takes to use them.
In the research performed for this chapter, the focus is mostly on the ground states and excited states, the excitation energies and for the acceptor materials on the band gap.

3.1.2 Materials

The exploratory DFT calculations are performed on two different singlet fission materials: tetracene and pentacene. Both are studied as a monomer and as a dimer. The monomer is interesting, since it provides a good insight in all the locally excited states. The dimer is

complementary to the monomer, because it allows the existence of charge transfer states, as well as delocalised states.

For tetracene, the first excited singlet state is 2.35 eV higher than the ground state, measured in crystal structure with emission spectra for prompt fluorescence. The first excited triplet state is 1.25 eV, determined with emission spectra for delayed fluorescence.[66]

In the crystal structure, the first excited singlet state of pentacene is determined to be 1.83 eV higher than the ground state, where the first excited triplet state is 0.73 eV higher than the groundstate[38].

3.1.3 Geometry of the Materials

For the monomers, a geometry optimisation is performed with the PBE functional in the ADF software package[62, 19, 5]. For the dimers, the structures are build by ADF-BAND[61, 72, 21, 20, 48] using lattice parameters taken from literature[40, 41]. Geometry optimisations are run with the PBE functional.

3.1.4 Outline

The remainder of this chapter starts with a section that describes how software package TheoDORE is able to determine electron-hole localisation variables quantitatively. Thereafter, the method section describes the two methods used for calculating the relevant data. The results and analysis section is split into multiple subsections for tetracene and pentacene. The last two sections of this chapter are the Discussion and Conclusion parts.

3.2 Theory

3.2.1 Introduction

In this section, the software and its underlying theory that are specifically needed for this chapter, are described. In this chapter, a package called TheoDORE is the only used software that is not covered by Chapter 2. Descriptions of TheoDORE and the theory behind TheoDORE are provided in the next subsection[50].

3.2.2 TheoDORE

TheoDORE can be used to calculate quantitative information on the localisation of, and distance between, the electron and the hole. To do so, TheoDORE starts with the transition density matrix (1TDM), denoted as

$$D_{\mu\nu}^{OI} = \langle \Phi^O | \hat{a}_\mu^\dagger \hat{a}_\nu | \Phi^I \rangle, \tag{3.1}$$

where $a^\dagger$ and a are the creation and annihilation operators, respectively. Then, the charge transfer number of fragments A and B is written as[51]

$$\Omega_{AB} = \frac{1}{2} \sum_{\mu \in A} \sum_{\nu \in B} [(\mathbf{D}^{0I}\mathbf{S})_{\mu\nu}(\mathbf{S}\mathbf{D}^{0I})_{\mu\nu} + D_{\mu\nu}^{0I}(\mathbf{S}\mathbf{D}^{0I}\mathbf{S})], \tag{3.2}$$

in which the summation runs over all atomic basis functions μ and ν of A and B, respectively. Now, the total amount of charge separation [50] can be calculated by

$$\omega_{CT} = \frac{1}{\Omega} \sum_{B \neq A} \Omega_{AB}, \tag{3.3}$$

resulting in a value between 0 and 1, due to scaling by Ω. A value of $\omega_{CT} = 0$ indicates a local excitation, and a complete charge transfer state results in $\omega_{CT} = 1$. Ω can be physically interpret as a measure of the single-excitation character of an excitation, and it can be calculated

as

$$\Omega = \mathrm{tr}(\mathbf{D}^{I0}\mathbf{S}\mathbf{D}^{0I}\mathbf{S}). \tag{3.4}$$

Herein, $\mathbf{D}^{I0}$ is the transpose of $\mathbf{D}^{0I}$.

TheoDORE can furthermore be used for giving an expectation value of exciton size, which is defined as the distance between the electron and hole,

$$d_{exc} = \sqrt{\langle|\vec{x}_h - \vec{x}_e|^2\rangle_{exc}}. \tag{3.5}$$

This distance can be calculated from the output of computations using

$$d^2_{exc} = \frac{1}{\Omega}\sum_{\xi\in\{x,y,z\}}\Big(\mathrm{tr}(\mathbf{D}^{I0}\mathbf{M}^{(2)}_{\xi}\mathbf{D}^{0I}\mathbf{S}) - 2\ \mathrm{tr}(\mathbf{D}^{I0}\mathbf{M}^{(1)}_{\xi}\mathbf{D}^{0I}\mathbf{M}^{(1)}_{\xi}) + \mathrm{tr}(\mathbf{D}^{I0}\mathbf{S}\mathbf{D}^{0I}\mathbf{M}^{(2)}_{\xi})\Big). \tag{3.6}$$

Where $M^{(k)}_{x,\mu\nu}$ can be calculated using the atomic orbitals χ_μ and χ_ν, as

$$M^{(k)}_{x,\mu\nu} = \int \chi_\mu(r)x^k\chi_\nu(r)dr. \tag{3.7}$$

3.3 Method

3.3.1 Method 1: DFT with Different Functionals using ADF

This subsection describes the time-dependent density functional theory simulations that are performed with the ADF software [62, 19, 5]. Within ADF, one needs to define a number of computational properties. These properties include the basis set, the integration accuracy, a frozen core option and a relativity option. Furthermore, the Tamm-Dancoff Approximation (TDA) can be turned on or off. Any other options are kept at default.

In general, increasing the accuracy, the basis set functions and turning on the other options results in better results, but also in a significantly longer computation time. For most simulations, not too high quality properties are chosen, to keep the computational time convenient. As a benchmark, a couple of simulations with higher quality are performed on tetracene, to see

if the lower quality simulations are appropriate or not.

Tetracene

All the functionals, with the corresponding properties, that were used for tetracene, are listed in table 3.1.

	PBE	PBE (high qual.)	B3LYP	B3LYP (high qual.)	CAM-B3LYP	CAMY-B3LYP	MO6-2X
mon/dim	both	both	both	both	both	both	both
sing/trip	both	both	both	both	both	sing	both
Basis Set	DZP	TZ2P	DZP	TZ2P	DZP	DZP	DZP
Integ. Acc.	normal	verygood	normal	verygood	normal	normal	good
Frozen C.	small	none	none	none	none	none	none
Relativity	none	none	none	none	none	none	none
TDA	off	off	off	off	both	off	on
ADF	2014.08	2014.08	2014.08	2014.08	2016.01	2014.08	2014.08

Table 3.1: the functionals with their corresponding properties as used during the calculation of the excitation energies of tetracene. The row labels stand for monomer/dimer; singlet/triplet excitations; basis set; integration accuracy; frozen core; relativity; Tamm-Dancoff Approximation turned on or off; and the ADF version used.

Pentacene

All the functionals, with the corresponding properties, that were used for pentacene, are listed in table 3.2.

From the results of these computations, the excitation energies are obtained. Furthermore, information about the exciton can be determined with additional software, as described in the next subsection.

	PBE	B3LYP	CAM-B3LYP	CAMY-B3LYP	MO6-2X
mon/dim	both	both	both	both	both
sing/trip	both	both	both	sing	both
Basis Set	DZP	DZP	DZP	DZP	DZP
Integ. Acc.	normal	normal	normal	normal	good
Frozen C.	small	none	none	none	none
Relativity	none	none	none	none	none
TDA	off	off	both	off	on
ADF	2014.08	2014.08	2016.01	2014.08	2014.08

Table 3.2: the functionals with their corresponding properties as used during the calculation of the excitation energies of pentacene. The row labels stand for monomer/dimer; singlet/triplet excitations; basis set; integration accuracy; frozen core; relativity; Tamm-Dancoff Approximation turned on or off; and the ADF version used.

3.3.2 Method 2: DFT with Different Functionals using Orca and TheoDORE

In the excited states of the tetracene dimer, it is interesting to know where the electron and the hole are located. The software package TheoDORE (Theoretical Density, Orbital Relaxation and Exciton analysis) provides a method to give a quantitative description of the electron-hole distribution over the molecules/segments, as well as a expectation value for the distance between the electron and the hole. Since the output from ADF cannot be parsed to be used with TheoDORE, a different DFT program is used to obtain the analysis.

ORCA is used to do comparable calculations to the previous ADF calculations, but has the additional benefit that its output can be analysed by TheoDORE. To do so, the Orca output is parsed into compatible data by cclib[42].

3.4 Results and Analysis

3.4.1 Tetracene Results

From the literature, we know what the energies of the first excited triplet and singlet state (T_1 and S_1) are. The triplet state is 1.25 eV, the singlet state is 2.32 eV in crystal structure and 2.88 eV for the monomer[66]. All three values are relative to the ground state energy.

The T_1 and S_1 states for the different functionals are displayed in table 3.3.

	PBE	PBE (hq)	B3LYP	B3LYP (hq)	CAMY-B3LYP	CAM-B3LYP	CAM-B3LYP (TDA)	M06-2X
T_1 (mon)	1.39	1.39	1.23	1.22	N.A.	-0.14	1.42	1.21
S_1 (mon)	2.17	2.15	2.45	2.42	2.69	2.75	3.03	2.92
T_1 (dim)	1.27	1.25	1.18	1.18	N.A.	-0.38	1.37	1.17
S_1 (dim)	1.30	1.28	1.90	1.85	2.56	2.68	2.87	2.75

Table 3.3: the excitation energies of the corresponding states as calculated for the corresponding functionals with the settings as described in the method section of tetracene, section 3.3.1. All values for the excitation energies are in eV and are relative to the ground state energy. The excitation energies of the remaining four triplet and four singlet states are enclosed in Appendix B.1.

The data from TheoDORE for tetracene is enclosed in figure 3.1.

3.4.2 Tetracene Analysis

Monomer

For the monomer, the calculated energetic values for T_1 are stable and accurate. The values never differ by more than 0.2 eV from the reference value. The range-separated functionals are also delivering stable and accurate values for S_1, again not differing by more than 0.2 eV from the literature value. The non range-separated functionals are having a more trouble determining S_1, underestimating the values by 0.4-0.7 eV.

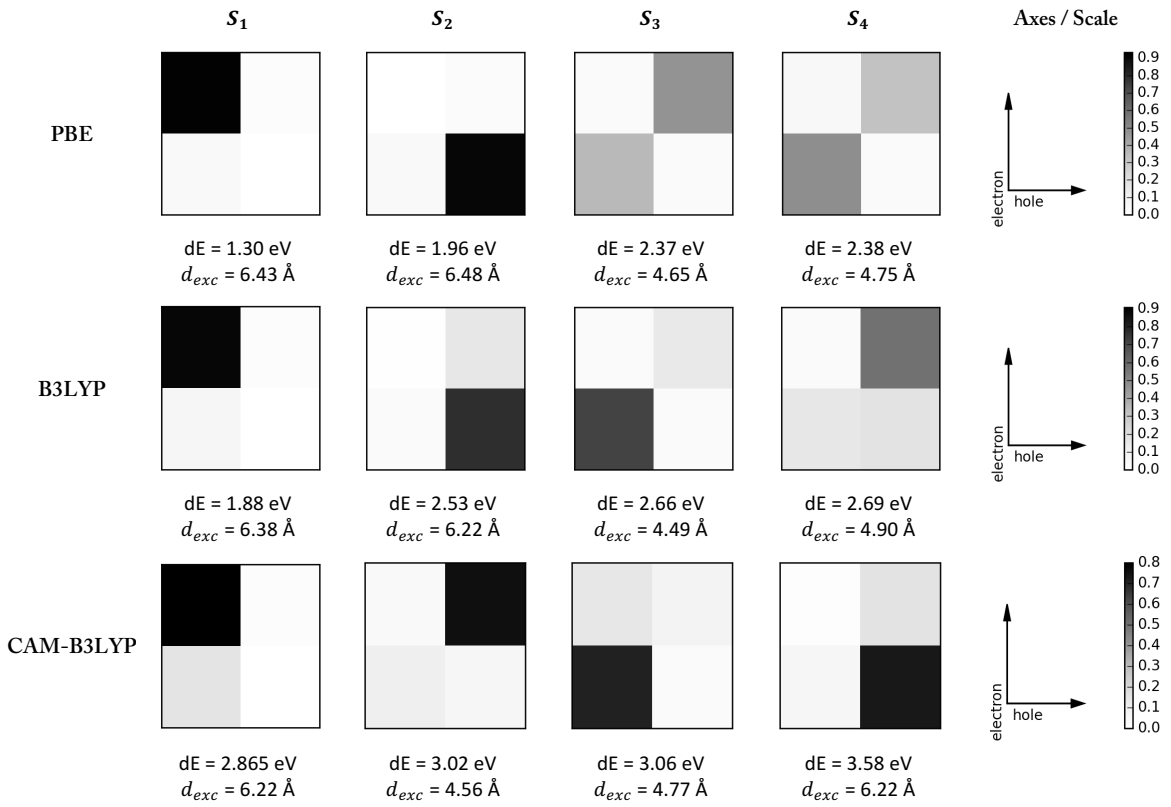

Figure 3.1: Electron and hole localisation for tetracene, obtained by TheoDORE. The 2×2 squares display where the electron and the hole are. The bottom/top squares indicate that the electron is located at molecule A/B, whereas the left/right squares indicate that the hole is located at molecule A/B. Hence, PBE(S_1) is a charge-transfer state, where the electron is at molecule B and the hole is at molecule A. Likewise, CAM-B3LYP(S_2) is mostly a local excitation at molecule B and PBE(S_3) is delocalised over the two atoms (molecule B is slightly more populated).

Dimer

The values for T_1 are comparable to the values obtained for the monomer. Again, the difference with the reference value is never bigger than 0.2 eV. We can now determine further, how the electron and hole are distributed.

For the singlet states, one can decide how the electrons and holes are distributed over the two molecules using the TheoDORE software. Due to limitations in (combining multiple types of) software, TheoDORE can only be used on the PBE, B3LYP and CAM-B3LYP functionals.

For PBE, the first two singlet excitations are charge transfer (CT) states. They are too low,

compared to the literature value. However, the first non-CT state, where the exciton is delocalised over the two molecules, is calculated to be at 2.37 eV. For B3LYP and CAM-B3LYP, the first non-CT states are at 2.66 eV and 3.02 eV, respectively. Further differences in the results are the localisation of the exciton. In PBE's results, it is almost evenly delocalised over the two molecules. For the results of CAM-B3LYP, the exciton is localised at one of the molecules for roughly 80%.

The analysis as performed by TheoDORE makes clear that the energetically lowest singlet states for the dimer are solely CT-states. However, one expects the CT-states to be higher in energy than the excited states without charge-transfer properties. For tetracene, this idea is backed by theoretical computations[76].
TheoDORE limits the possibilities of analysis to the singlet states. For these singlet states, the energy of the lowest non CT-states are underestimated by the PBE functional and also, albeit to a lesser extent, by the B3LYP functional. The CAM-B3LYP functional, on the other hand, slightly overestimates the energy of this non-CT singlet state. With values of respectively 1.30 eV and 1.88 eV, the PBE and B3LYP functionals are not even close to finding the right energies for the CT-states. The CAM-B3LYP functional however, gets a lot closer to a realistic value, with a CT-state energy of 2.87 eV. The exact energetic value to compare with is hard to determine, although it is likely that it is slightly higher than the S_1 excitation. For instance, for pentacene the CT-state energy on a dimer is estimated to be 0.23 eV higher compared to the energy of the normal S_1 state[38].

3.4.3 Pentacene Results

For pentacene, the excitation energies for a monomer are 0.86 eV for T_1 and 2.3 eV for S_1 [77, 29, 11]. In crystal structure, the excitation energy for S_1 is 1.83 eV[65]. The results for the first singlet and triplet excited states for the monomer and the dimer are listed in table 3.4.

The TheoDORE analysis on the electron and hole makes clear that all of these three S_1 states are CT-states. The first non CT-states are at 1.84 eV, 2.11 eV and 2.49 eV, for PBE, B3LYP

	PBE	B3LYP	CAMY-B3LYP	CAM-B3LYP	CAM-B3LYP (TDA)	M06-2X
T_1 (mon)	0.93	0.71	N.A.	-0.90	0.95	N.A.
S_1 (mon)	1.62	1.89	2.14	2.20	2.50	N.A.
T_1 (dim)	0.72	0.62	N.A.	-0.96	0.89	0.70
S_1 (dim)	0.78	1.28	1.89	2.06	2.17	2.04

Table 3.4: the excitation energies of the corresponding states as calculated for the corresponding functionals with the settings as described in the method section of pentacene, section 3.3.1. All values for the excitation energies are in eV and are relative to the ground state energy. The excitation energies of the remaining four triplet and four singlet states are enclosed in Appendix B.2.

and CAM-B3LYP, respectively.

All the useful data that are provided by Orca and TheoDORE, are enclosed in figure 3.2.

3.4.4 Pentacene Analysis

Monomer

The calculated values for the energy of the first excited triplet states are relatively stable, except for CAM-B3LYP when the TDA is not used. For the remaining functionals, T_1 for B3LYP is the most inaccurate, but only 0.24 eV away from the literature value.
The energies of the monomer's S_1 states tend to be underestimated by the software, with the PBE functional deviating the most, by 0.7 eV.

Dimer

For the dimer, things get more complicated. From literature, we know that the energies for the CT-state and first non-CT S_1 excitation for a pentacene dimer are estimated to be 2.03 eV and 1.80 eV, respectively[38]. It is hard to tell how accurate these values are, but it does confirm the idea that the CT-state should not be the lowest in energy. Due to technical limitations by the TheoDORE package, only the singlet states can be analysed properly. For the singlet excitations, it becomes clear that the lowest calculated states are CT-states, just like we have seen with tetracene. The CT-states that are the lowest excitations according to PBE and

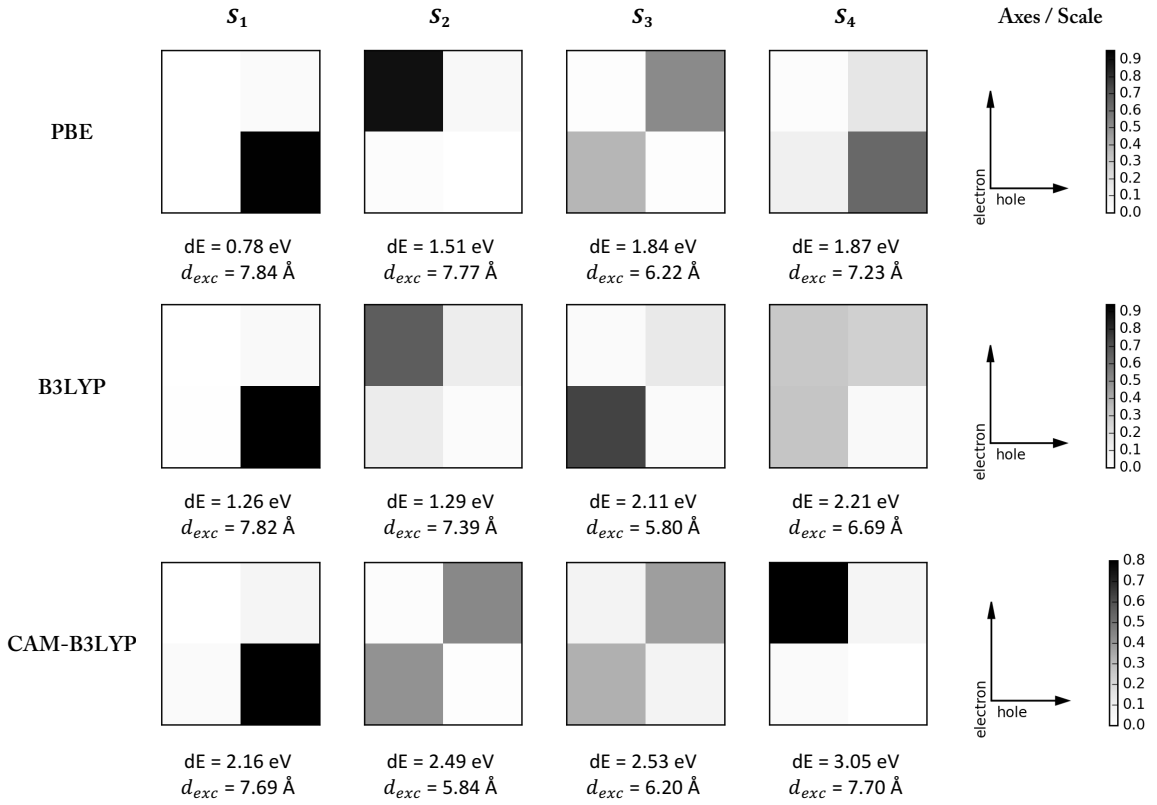

Figure 3.2: Electron and hole distribution for pentacene, obtained by TheoDORE. The 2×2 squares display where the electron and the hole are. The bottom/top squares indicate that the electron is located at molecule A/B, whereas the left/right squares indicate that the hole is located at molecule A/B. Hence, PBE(S_1) is a charge-transfer state, where the electron is at molecule A and the hole is at molecule B. Likewise, B3LYP(S_3) is mostly a local excitation at molecule A and CAM-B3LYP(S_2) is delocalised over the two atoms (molecule B is slightly more populated).

B3LYP, are far too low. The question remains however, whether all the states are too low in energy, or if it is only the CT-states energies that are underestimated.

If we only take a look at the non CT-states, the S_1 energy from the PBE functional, i.e. 1.84 eV, is closest to our reference values of 1.83 eV and 1.80 eV, obtained on crystal and dimers, respectively [65, 38]. The B3LYP and CAM-B3LYP functionals tend to overestimate the excitation energies for the S_1 state in a pentacene dimer, while all three functionals are underestimating the energy of the CT-state.

3.5 Discussion

The results make clear that there are high error margins. However, due to the way the functionals are built, i.e. with trial and error, it is hard to specify the exact error that should be taken into account. The determined values for the energy in combination with the information that TheoDORE provides, suggests that especially the computed CT-states are quite unreliable. Nonetheless, one should also be careful with the interpretation of the non-CT states. The energies of these states differ less than the CT-state energies, but the localisation of the hole and the electron are not consistent over the results from the three different functionals.

3.6 Conclusion

For all the four situations, the calculations of the energetic value of T_1 is relatively stable, with the error being 0.24 eV at most. For S_1, the calculations are less accurate. The range-separated functionals are doing well on the monomers, with dE $<$ 0.2 eV. For the dimers, the range-separated functionals are also doing relatively well, since the error is never bigger than 0.41 eV. The non range-separated functionals however, have big errors for both the monomers (up to 0.73 eV) and the dimers (up to 1.6 eV).
Analysis makes clear that the errors of the energy of the dimers are mostly caused by underestimations of the energy of the charge transfer states. Since the systems in the next chapter are bigger, the range-separated functionals are, in most occasions, computationally too expensive. Hence, one has to take the potential errors into account, especially in the charge-transfer state situations.

Chapter 4

Research Part II: Energy Transfer from Tetracene to Quantum Dot with Non-Adiabatic Molecular Dynamics

4.1 Introduction

4.1.1 Description

In this chapter we study the process of energy transfer of a triplet exciton located at tetracene, to a lead-sulphide quantum dot (PbS QD). In this introduction, we start by explaining what a quantum dot is. Thereafter, a summary is given of experimental research that has been done on this matter. Lastly, I describe what the objectives and outline of this chapter are.

4.1.2 Quantum Dot

Quantum dots (QD) are colloidal particles that are very interesting for fields with optoelectric purposes or applications. The first reason why QDs are interesting is that the optical and electronic properties, such as the band gap, are dependent of the particle size and can hence

accurately be tuned[23, 33].

The surfaces of the QDs are terminated by ligands that guarantee the solution processability of the QDs. Research has shown that these ligands also influence the optoelectric properties of the QDs. Experiments make clear that the energy levels of the quantum dots can be shifted significantly by changing the ligands[10]. Furthermore, the light absorption can be increased significantly by shortening the ligands[23]. QDs can be used as light-harvesting materials, but they have also succesfully been used as emissive acceptor materials, for energy transfer from singlet fission materials[64, 59].

4.1.3 Literature

The energy transfer process from triplet excitations to quantum dots has been observed in multiple experimental articles[64, 59]. In this research, the aim is to computationally reproduce the triplet transfer from tetracene to PbS QDs, as observed in MIT's experiments[64]. A summary of the relevant parts of the article is provided, just after this introduction.

4.1.4 Objective

From the experimental results, we know that the energy transfer occurs within 10ns. In the research described in this chapter, the first aim is to reproduce the energy transfer observed in the described experiments. After this, the next step is to provide useful insights in the properties of, and the influences on the transfer process. Different methods of analysis are used to obtain information about the possible occurrence of quantum tunnelling, the adiabaticity of the process, the role of the charge-transfer states, the influence of the position of the tetracene with respect to the QD and the influence of the ligand.

4.1.5 Outline

In the next section, 4.2, the already mentioned experimentally observed energy transfer from tetracene to PbS QDs is summarised.
Hereafter, section 4.3 describes the theory behind the steps and algorithms that are specifically used in this chapter for the determination of the trajectories (molecular dynamics) and the surface hopping (FSSH, CPA and GFSH).
After this theory section, the method section, 4.4, gives an in-depth description of al the steps performed for obtaining the geometries, the trajectories and the surface hopping results.
In the next section, 4.5, the two used setups are described, as well as their behaviour over time.
Thereafter, the results and analysis are enclosed (4.6). This includes an analysis of the coupling between tetracene and the quantum dot, and the influences of their mutual orientation hereon, as well as the simulations of the surface hopping process.
Naturally, this section is followed by a discussion (4.7) and a conclusion (4.8).

4.2 Experimental Research

The described process of singlet fission has been observed in multiple molecules. For the purpose of converting light into useable energy, the excited electrons need to be extracted from the singlet fission material. This chapter describes an overview of an experimental research performed at MIT by Thompson et al[64]. Herein, it is experimentally shown that energy transfer of triplet excitons from tetracene (the singlet fission material) to lead sulphide (PbS) quantum dots (the acceptor material) is possible, and dependent of ligand and/or intermolecular distance. All mentioned data, formulas and figures of this chapter refer to the cited MIT article.
In the first part of the research, the excitation spectrum of a thin film of PbS nanocrystals coated with a 20-nm-thick film of tetracene is measured. Near-infrared emission is detected after exciting the tetracene layer. The presence of energy transfer from tetracene to PbS can be confirmed, since the peaks in the PbS excitation spectra appear at the same energies as in the absorption spectra of tetracene.

For the next step, the wavelength-dependent quantum yield of photons from the nanocrystal is used,

$$\mathrm{QY}(\lambda) = \mathrm{QY}_{\mathrm{NC}} \left(\frac{\mathrm{ABS}_{\mathrm{NC}}(\lambda) + \eta_{\mathrm{fis}}\eta_{\mathrm{ET}}\mathrm{ABS}_{\mathrm{Tc}}(\lambda)}{\mathrm{ABS}_{\mathrm{NC}}(\lambda) + \mathrm{ABS}_{\mathrm{Tc}}(\lambda)} \right). \tag{4.1}$$

Herein, $\mathrm{ABS}_{\mathrm{NC}}$ is the absorption of the nanocrystal, $\mathrm{QY}_{\mathrm{NC}}$ is the intrinsic quantum yield of the nanocrystal, $\mathrm{ABS}_{\mathrm{Tc}}$ is the absorption of the tetracene, η_{fis} is the yield of excitons in tetracene after singlet exciton fission and η_{ET} is the exciton transfer efficiency from tetracene to the nanocrystal. Fitting this function to the measured curve provides a value for $\eta_{\mathrm{fis}}\eta_{\mathrm{ET}} = 1.80 \pm 0.26$. The fact that $\eta_{\mathrm{fis}}\eta_{\mathrm{ET}}$ is greater than one proofs that the energy transfer is dominated by triplet excitons, since efficient triplet generation by singlet fission is the only explanation if more excitons are transferred than there are photons absorbed.

During the process, multiple ligands are used to passivate the surface of the nanocrystal. The

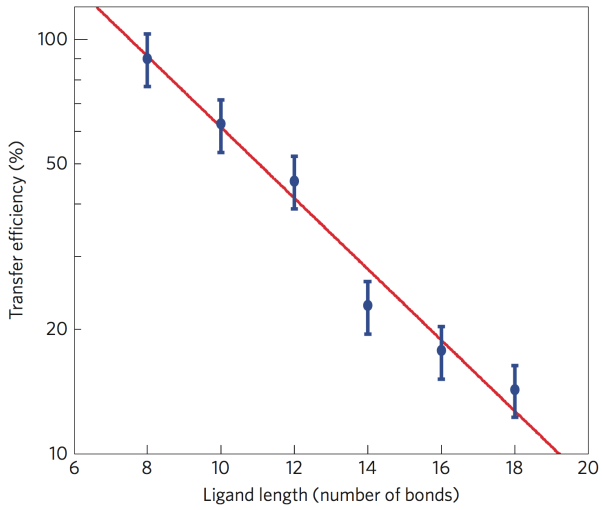

Figure 4.1: MIT's figure, showing a distinct correlation between the energy transfer efficiency and number of carbon-carbon single bonds in the nanocrystal ligand. The diagonal line is an exponential fit on the data, and the vertical bars represent the estimated uncertainty.

ligands vary in length, from oleic acid (OA, the longest), to caprylic (octanoic) acid (CA, the shortest). Figure 4.1 shows the energy transfer efficiency as a function of the ligand length, measured in terms of the number of single carbon-carbon bonds. This figure makes clear that there is a direct correlation between the length of the ligand on the quantum dot, and the efficiency of the energy transfer. The question remains however, whether it is the ligand itself, the increased intermolecular distance, or a combination of the two, which causes the decrease

of efficiency.

4.3 Theory

4.3.1 Introduction

In this section, all the theoretical approaches and background that have not yet been mentioned but are relevant for this chapter, are written out in detail. This section is divided into subsections describing (the background of) the different methods that were used.
The subsections are in the same order as in the research. Hence, first the process of molecular dynamics is explained. The next step is the simulation of energy transfer over time, of which the theory is described in three subsections.
The first of these last three subsections describes the general theory behind the fewest-switches surface hopping method (FSSH). The next subsection explains what the classical path approximation is, which can be used in combination with FSSH. The last subsection describes a method called global flux surface hopping, which is a modification of FSSH that allows transitions trough higher-lying states.

4.3.2 Molecular Dynamics

If one wants to simulate the movement of atoms over time, molecular dynamics (MD) is a relatively simple but reliable method to do so.
The most basic system of MD is purely mechanical and contains N atoms, in a fixed volume V, with an energy $E = T + E_p$. Herein, the kinetic energy T is the sum of the classical kinetic energy of all individual atoms ($\frac{1}{2}\sum_i m_i v_i^2$) and E_p is the interatomic potential energy. Such a system with fixed volume is called a microcanonical ensemble, or NVE.
The equation of motion can be determined by the Verlet algorithm, as[22, 17]:

$$\mathbf{R}_i(t+\delta t) = 2\mathbf{R}_i(t) - \mathbf{R}_i(t-\delta t) + \frac{\delta t^2}{M_i}\mathbf{f}_i(t) + \mathcal{O}(\delta t^4) \tag{4.2}$$

$$\mathbf{V}_i(t) = \frac{1}{2\delta t}\left[\mathbf{R}_i(t+\delta t) - \mathbf{R}_i(t-\delta t)+\right] + \mathcal{O}(\delta t^3). \tag{4.3}$$

Alongside of the Verlet algorithm, there is an other algorithm that is equivalent to it, which is called Velocity Verlet[22, 17]:

$$\mathbf{V}_i(t+\delta t) = \mathbf{V}_i(t) + \frac{\delta t^2}{2M_i}\left[\mathbf{f}_i(t) + \mathbf{f}_i(t+\delta t)\right] \tag{4.4}$$

$$\mathbf{R}_i(t+\delta t) = \mathbf{R}_i(t) + \delta t \mathbf{V}_i(t) + \frac{\delta t^2}{2M_i}\mathbf{f}_i(t). \tag{4.5}$$

In the four above-mentioned equations, $\mathbf{R}_i$ denotes the place of atom i, $\mathbf{V}_i = \dot{\mathbf{R}}_i$ the velocity of atom i, $\mathbf{f}_i$ the forces on atom i and M_i the mass of atom i. These algorithms are, despite its simplicity, efficient, numerically stable and furthermore conserve energy quite well.

For systems that keep the energy constant, instead of the volume, there are some slight adaptions needed in the algorithms. Such a system, called Canonical ensemble or NVT, obeys a relation between temperature and the expectation value of the kinetic energy[22, 17]:

$$\langle \sum_{i=1}^{N} \frac{\mathbf{P}_i^2}{2M_i} \rangle_{NVT} = \frac{3}{2} N k_B T, \tag{4.6}$$

with k_B the Boltzmann constant. To obey this formula, and hence keep the system at a constant temperature, one can add velocity rescaling to the algorithm. Herein, the velocities are rescaled every time the temperature deviates from the correct value by more than the threshold value. There are alternatives to velocity rescaling, such as adding a thermostat at the edges simulating a thermal bath, but they are not discussed in this thesis since they are not used.

4.3.3 Fewest-switches surface hopping

This section gives an overview of the fewest-switches surface hopping method (FSSH), and is, unless stated otherwise, citing to the Supporting Information of the main PYXAID article, [1]. In FSSH, the influences of deterministic (TD-SE) and stochastic factors are combined to simulate a time-evolving electron-nuclear system over multiple trajectories.

At every time step, the probability for the electron to hop from a certain state i to another

state j is calculated. This probability can be written out as

$$P_{i\to j}(t,dt) = \int_t^{t+dt} \frac{2}{c_i^*(t)c_i(t)} Re\left[\left(\frac{iH_{ij}}{\hbar}\right) c_i^*(t)c_j(t)\right] dt = \frac{2}{\hbar}\int_t^{t+dt} \frac{Re\left[d_{ij}c_i^*(t)c_j(t)\right]}{c_i^*(t)c_i(t)} dt. \quad (4.7)$$

Herein, c_i and c_j and their conjugates are part of the density matrix, as

$$\rho_{ij}(t) = c_i^*(t)c_j(t). \quad (4.8)$$

In the case that the computed probability $P_{i\to j}$ is negative, it is changed to zero. The probability of staying in the same state i can hence be denoted as

$$g_{i\to i}(t) = 1 - \sum_{j\neq i} g_{i\to j}(t), \text{ where } g_{i\to j}(t) = \max\left(0, P_{i\to j}(t)\right). \quad (4.9)$$

The first part of the name FSSH, "fewest switches", thanks its name to the fact that the number of hops is minimised. This is due to the FSSH probabilities being related to the flux of the populations of states, and not to the actual state populations, resulting in a minimisation of switches.[67]

So far, all factors were deterministic. In the last step, the stochastic factor is introduced by a random number $\xi \in [0,1]$. This ξ is compared to the probabilities to determine the next state j, which meets the requirement

$$\sum_{k=0}^{j-1} g_{i\to k}(t) < \xi \leq \sum_{k=0}^{j} g_{i\to k}(t). \quad (4.10)$$

4.3.4 Classical path approximation

The FSSH method can be updated to work within the Classical Path Approximation (CPA). CPA is valid under the assumption that the electronic dynamics are driven by the nuclear dynamics, and the nuclear dynamics are unaffected by the dynamics of the electronic degrees of freedom. Hence, this requires an absence of reorganisation, fragmentation, isomerisation and other significant structural changes under electronic excitations.[1]

In original FSSH, conservation of the total energy of the system is obtained by rescaling the velocity vectors of all atoms. Within FSSH-CPA, a different rescaling technique is used. Instead of the velocity, the transition probabilities are scaled, but only for energetically unfavourable transitions:

$$g_{i\to j}(t) \to g_{i\to j}(t) b_{i\to j}(t) \tag{4.11}$$

$$b_{i\to j}(t) = \begin{cases} exp\left(-\frac{E_j - E_i}{k_B T}\right) & E_j > E_i \\ 1 & E_j \leq E_i \end{cases}. \tag{4.12}$$

For these energetically unfavourable transitions, the scaling correction is the Boltzmann factor, in which k_B is the Boltzmann constant and T is the temperature.[1]

4.3.5 GFSH

In the previously described sections, the mechanism of FSSH is explained. An alternative for the simulation of surface hopping is an algorithm called global flux surface hopping (GFSH)[71]. This method is based on the same principles as FSSH, but it handles the hopping probability for classically forbidden transitions differently. These classically forbidden transitions cannot and should not be fully avoided, since the avoidance would create an unrealistic unbalance in the surface hopping simulations[43, 44]. The difference between FSSH and GFSH can be found in dynamical processes such as superexchange, where two states are indirectly coupled trough an intermediate state with higher energy. An example hereof is the singlet fission process as described in section 2.1.6, where the higher-lying charge transfer states play a key role, but are hardly populated[56, 8, 2, 7]. Hence, these hops would be forbidden in FSSH, but GFSH allows these transitions by altering the hopping probability[71]. Although singlet fission is not the process that is simulated in this research, GFSH will turn out to be useful. After all, the process to be simulated is a dexter energy transfer, between two states that are not directly coupled.

The major difference between FSSH and GFSH lies in the surface hopping probabilities. The entire set of quantum states is divided into two subgroups of states. This results in groups A

and B, i.e. one with reduced population and the other with increased population, respectively. Then, the hopping probability can be written as[71]:

$$g_{i\to j} = \frac{\Delta\rho_{jj}}{\rho_{ii}} \frac{\Delta\rho_{ii}}{\sum_{k\in A}\rho_{kk}} \text{ (if } i \in A \text{ and } j \in B), \tag{4.13}$$

herein, the population change of a quantum state is defined as

$$\Delta\rho_{ii} = \rho_{ii}(t + \Delta t) - \rho_{ii}(t). \tag{4.14}$$

After a surface hop, the energy is conserved in the same way as in FSSH.

4.4 Method

4.4.1 Introduction

For this part of the research, two different setups are analysed. For both setups, the same method is used. The order of the steps as performed in the research are

1. Starting geometry determination with CP2K (4.4.2)
2. Trajectory Calculation using MD by CP2K (4.4.3)
3. Recalculation of Hamiltonians and coupling with QMWorks (4.4.4)
4. Simulation of the Energy Transfer with PYXAID. (4.4.5)

The next subsections each describe a part of the method.

4.4.2 Starting geometry determination with CP2K

As a first step in the process, the starting geometry of the setup is determined. The facets of the PbS QD are terminated for fifty percent with hydrogen atoms and for the other fifty

percent with ligands. The ligands are distributed over the facets in a realistic and natural, and thus irregular, way, determined by in-house calculations for different research topics[23]. For efficiency reasons, the actual ligands are only placed on the facet close to the tetracene, the other ligands are kept as short as possible, i.e. a COOH termination. For different setups, the same ligand placement is used, to make sure that the ligand length is the only variable changing.

After the placement of the ligands, the tetracene is placed close to the facet with the actual ligands. The distance of the tetracene is chosen arbitrarily, in such a way that the distance is big enough to prevent bondings between the ligand and the tetracene, and at the same time small enough to encourage the transfer of the electrons.

After each described step, a geometry optimisation is run within CP2K, with the PBE functional. The last geometry optimisation furthermore checks, and possibly corrects, whether the intermolecular distance was chosen properly.

4.4.3 Trajectory Calculation using MD by CP2K

The geometry of the first point in time is determined in the previous subsection. For calculation of the remainder of the trajectory, the MD method as described in 4.3.2 is used. The computations are performed by the CP2K package, where the temperature is fixed at 300K, and multiple picoseconds are simulated, in steps of 1 fs.

In the trajectory, the starting point comes from a geometry optimised situation, and hence represents 0K. Therefore, the energy of the system starts low, and increases to a height where it stabilises. This 'warming up'-part, where the energy is not constant, is removed and thus not used in any of the remaining steps.

4.4.4 Recalculation of Hamiltonians and coupling with QMWorks

After the determination of the trajectory, the Hamiltonians need to be recalculated, due to technical incompatibilities. For this purpose, a python package called QMWorks-NAMD is

developed within the research group. Herein, the implementation of the computations of the non-adiabatic coupling is based on a method as used by Plasser et al[49].

4.4.5 Simulation of the Energy Transfer with PYXAID

The PYXAID package, which theory is described in sections 4.3.3-4.3.5, is used for the energy transfer simulation, using FSSH or GFSH. In this part, the relevant states are included, forming the active space. The energy levels of the states can be adjusted, to be closer to reality. The shifting of the energy happens in groups. The local excitation (LE) at tetracene is one group. The LE's on the PbS QD together form another group, and the last group contains al the CT-states. The energies of these groups are shifted relatively to each other.
The number of HOMO's and LUMO's that are included in the active space is determined by the alignment of the energy of the orbitals over time, which gives an indication for the relevant orbitals for the energy transfer process.
The simulations starts with a local excitation at the tetracene molecule. From there on, a thousand runs are performed over the longest available reliable part of the trajectory. The population of the states is averaged over these one thousand runs.
There are multiple settings that can manually be adjusted. One of them is the energy of the states. For both setups, eight different simulations are run, with the following settings:

1. FSSH with unchanged energy levels
2. FSSH with Tc LE lowered to 1.25 eV, and PbS band gap lowered to 1.0 eV, not changing the energy of the CT-states
3. FSSH with Tc LE lowered to 1.25 eV, and PbS band gap lowered to 1.0 eV, increasing the energy of the CT-states with 0.2 eV
4. FSSH with Tc LE lowered to 1.25 eV, and PbS band gap lowered to 1.0 eV, increasing the energy of the CT-states with 0.4 eV
5. GFSH with unchanged energy levels

6. GFSH with Tc LE lowered to 1.25 eV, and PbS band gap lowered to 1.0 eV, not changing the energy of the CT-states

7. GFSH with Tc LE lowered to 1.25 eV, and PbS band gap lowered to 1.0 eV, increasing the energy of the CT-states with 0.2 eV

8. GFSH with Tc LE lowered to 1.25 eV, and PbS band gap lowered to 1.0 eV, increasing the energy of the CT-states with 0.4 eV

4.5 Setups

4.5.1 Preparation: approximating the charge-transfer state energies

As a preparation to the main research, the tetracene and the QD have already been investigated in previous chapters. This led to useful results, providing insight in the orbitals and the energy of certain states. Furthermore, multiple experimental studies provide benchmarks for energies of excitations localised at tetracene, as well as the band gap of the PbS QD.
However, there is one type of state of which we do not know the energy beforehand. These are the charge-transfer states, in which only one electron has transferred, resulting in charged setups, i.e. $Tc^{+}PbS^{-}$ or $Tc^{-}PbS^{+}$.
A simple but rough approximation for the CT-state energy, can be calculated by[69]

$$E_{CT} = E_{cat} + E_{an} - \frac{ke^2}{\epsilon r}. \tag{4.15}$$

The last term describes a coulombic correction for the attraction between the charges. Herein, k is the coulomb constant, e is the charge that is separated and r is the separation distance. E_{CT}, E_{cat} and E_{an} are the energies of the CT, cationic and anionic system, with respect to the ground state energy, respectively. For the PbS-Tc system, this separation distance should have a value ranging from the shortest surface-to-surface QD-Tc distance (as a minimum) and the centre-to-centre QD-Tc distance (as a maximum distance).

For the initial geometry of the tetracene and PbS QD terminated by the shortest ligand, the CT-state energy is approximated to be 3.31-3.71 eV above the ground state energy, depending on chosen separation distance. The calculations of E_{an} and E_{cat} are performed with CP2K DFT/PBE/DZVP.

One should be aware of the roughness of such an approximation. In comparable calculations on smaller systems with reference CT-state energies, the approximated CT-state was on the low side. For the QD-Tc system however, the CT-state energy appears to be quite high, compared to the local excitations. Consequently, the energy of the CT-state is confirmed to be reasonably higher than the local excitation energies, but the precise CT-state energy remains rather indefinite.

4.5.2 Different ligands

One of the aims was to get insights in the possible influences of the ligand used on the PbS QD. Hence, the ligand length is varied in the same way as the experimental article. The consequence is that for every ligand, a unique path has to be determined with an MD simulation. Since an MD simulation for such a setup is very time-consuming, time limited the number of setups to two. In the first setup, the QD is terminated for 50% with heptane (7 carbon atoms). The second setup is terminated with nonane (9 carbon atoms) at the same positions. The other 50% are terminated with formic acid. The positions of the ligands were determined by a simulation run within the Theoretical Chemistry group of the VU.

Setup I

The first setup is for 50% terminated by ligands containing 7 carbon atoms. This setup is from now on referred to as 'Setup 7C'. An image of the initial setup is shown in figure 4.2. During the dynamics, the tetracene molecule slowly drifts away from the QD. For the entire simulated period, the distance, angles and curvature of the tetracene are determined. There are two distances determined, the center-to-center QD-Tc distance and the center-to-closest-facet

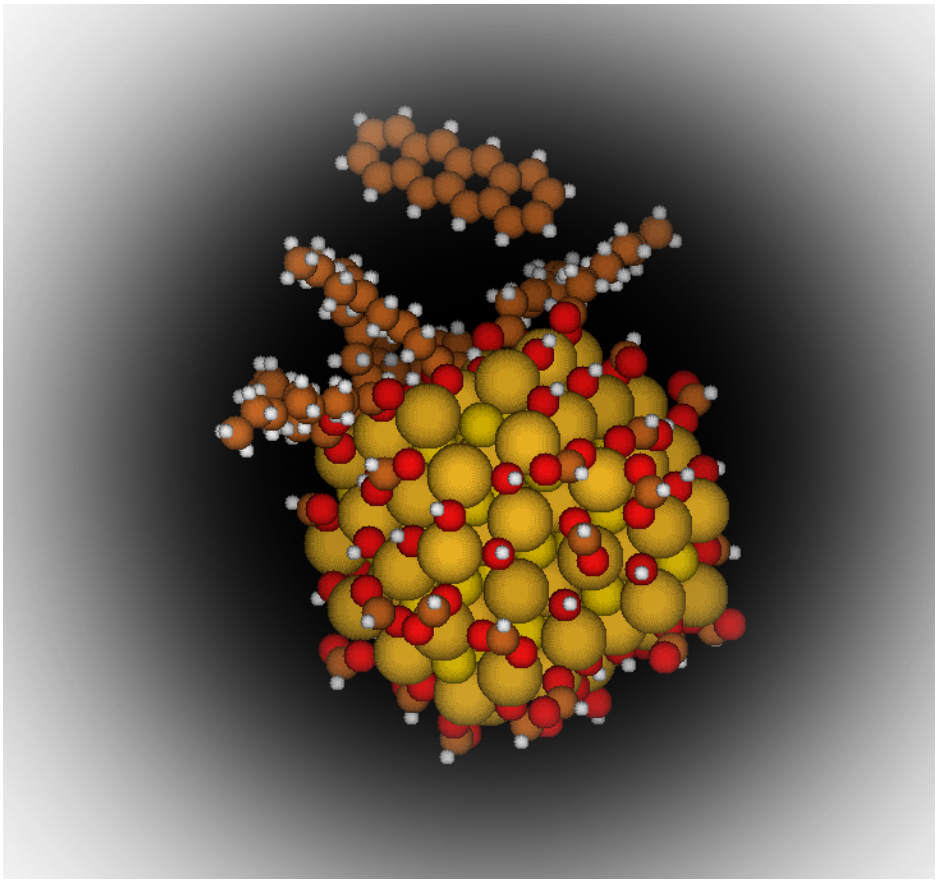

Figure 4.2: the geometry of the PbS QD with the heptane ligands at the relevant facet and the tetracene chromophore close to this facet. Picture taken at the first useful point in time.

QD-Tc distance. Out of the possible three angles, two are determined to be relevant. The first one represents the angle between the normal of the QD top facet and the longest axis of the Tc molecule (between the center of the two outer rings, through the two inner rings). This angle will from now on be referred to in figures as 'angle'. Since this angle is between the normal of the facet and the tetracene axis, when the tetracene is perpendicular to the QD facet, the angle is 0° and it is 90° when the two are parallel.

The second angle, which from now on we will call 'rotation', describes the rotation of the tetracene around its longest axis, oriented with respect to the QD. Hence this rotation is the angle between the normal of the QD top facet and the line through the C-C bond that unites the second and third carbon ring of tetracene. Again, the normal of the plane is taken, which means that a parallel tetracene molecule and QD top facet results in 90°, whereas 0° stands for a perpendicular situation.

The remaining third angle describes the rotation of Tc around the normal vector of the QD top facet. For symmetry reasons, this angle is not analysed.

The curvature of the Tc molecule is described by the parabolicity of the curve fitted trough tetracene surface, over the longest axis. Thus, this is the a in $y = ax^2 + bx + c$, which is zero for a straight line.

The distances, angles and curvature for the trajectory of the setup with the shorter ligand are displayed in figure 4.3.

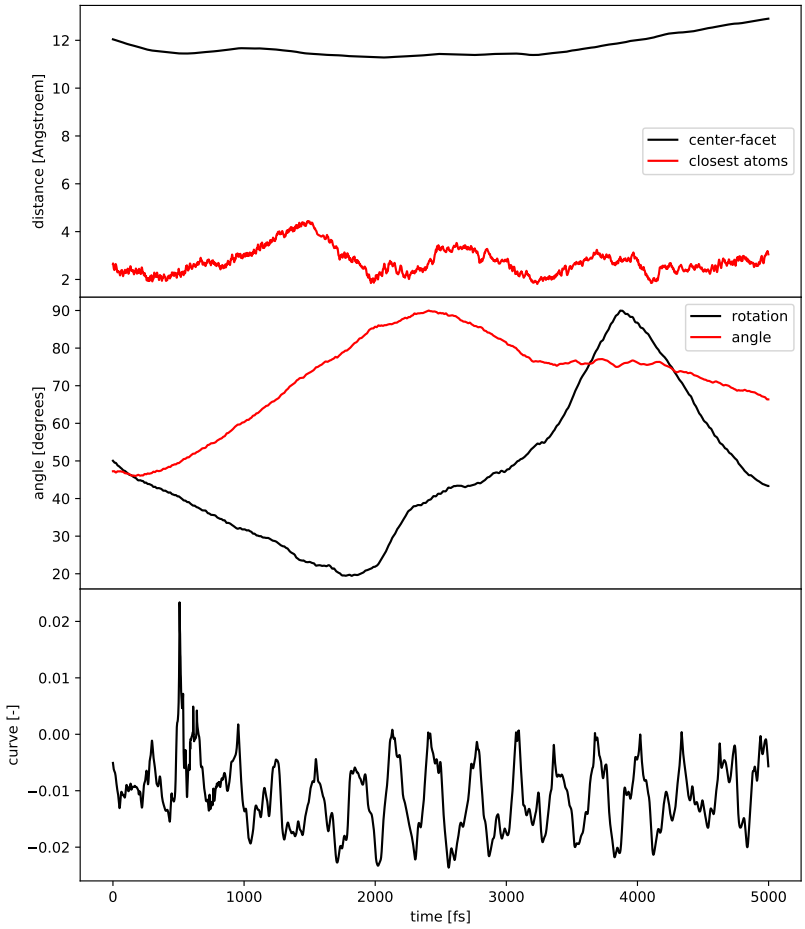

Figure 4.3: the behaviour of the orientation of the tetracene molecule with respect to the quantum dot (terminated with the 7C-ligand), for the entire trajectory.

Setup II

The second setup has the same initial coordinates as Setup I, with the addition of extra H and C atoms at the ligand ends, to extend the ligands from 7C to 9C. The results of the MD simulation are displayed in figure 4.4, using the same variables as for the first setup (figure 4.3).

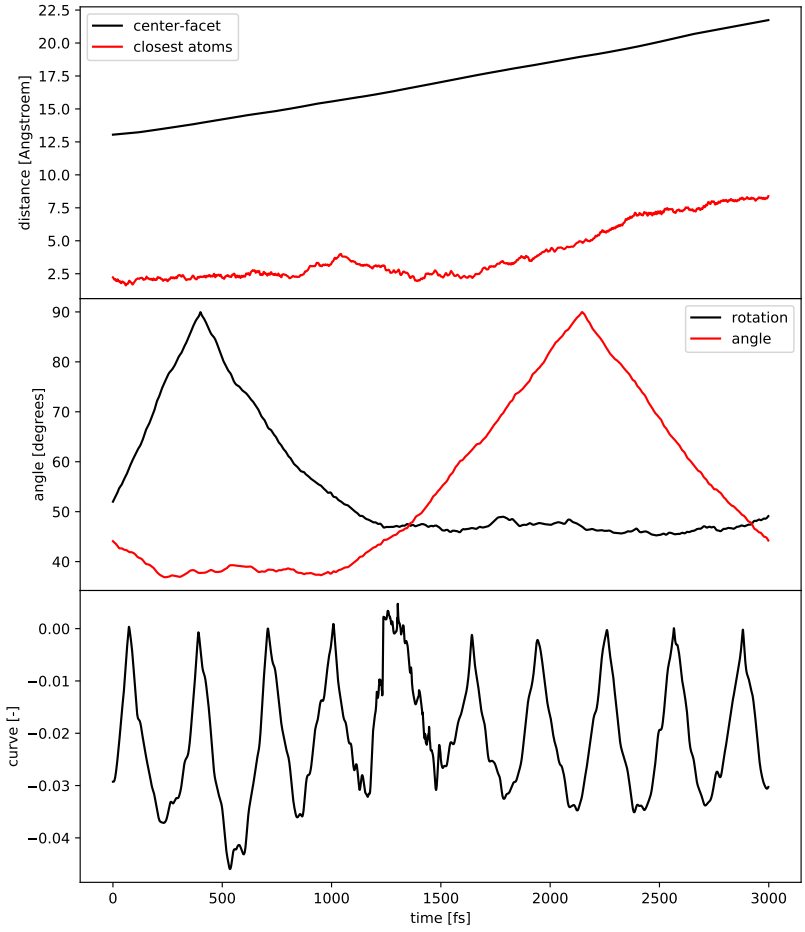

Figure 4.4: the behaviour of the orientation of the tetracene molecule with respect to the quantum dot (terminated with the 9C-ligand), for the entire trajectory.

Setup I vs Setup II

The most obvious difference between the trajectories of the two setups, is the separation between the QD and Tc. In the second setup, the Tc molecule moves away faster from the PbS QD. The most reasonable explanation is that the longer ligand results in a bigger expected value for the intermolecular distance. This behaviour is in line with the assumption of a relation between ligand length and intermolecular distance, made in the article describing the experimental research on the same matter[64].
In the two setups, the tetracene chromophores do not rotate in the same way, but this should not be of any influence for the results or analysis.
Furthermore, there is a slight difference in the way the tetracene bows over time. The curvature of the chromophore reaches higher values for the setup with the longer ligand. We have not found a clear explanation or cause for this difference.

4.6 Results and analysis

4.6.1 Hamiltonian Results

Real part: energy eigenvalues

After the calculation of the trajectories, the Hamiltonian files are known. The data of these files provides some insights in the behaviour of the orbitals over time. The real part of the Hamiltonian represents the energetic eigenvalues of the molecular orbitals. Herein, the alignment of the orbitals belonging to tetracene with respect to the PbS-orbitals can be seen. Figure 4.5 displays the real part of the Hamiltonians of 30 HOMOs and 30 LUMOs for Setup 7C, over time.

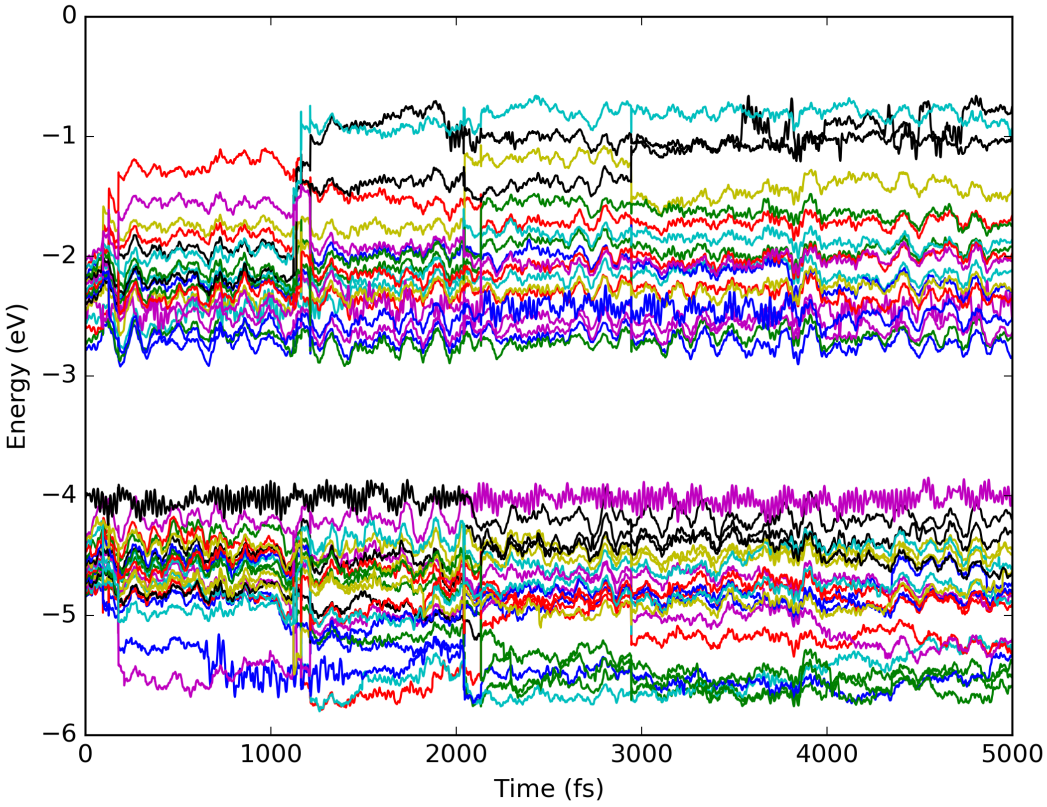

Figure 4.5: the molecular orbitals (30 HOMOs and 30 LUMOs) over time for Setup 7C. Due to computational difficulties, the program sometimes has problems following the same state, causing incorrect jumps between orbitals.

In this graph, the top HOMO, that starts black and ends purple, represents tetracene's HOMO. However, it should clearly not change color. The reason that this happens is that the software is not (always) able to keep track of which orbital is which, when they cross. At this moment, there is no solution to avoid this jumping.

The LUMO that belongs to tetracene switches even more often. It starts as the fifth LUMO in purple, then switches to cyan at 527, to purple at 1397, to blue at 2147 and back to purple at 3875.

These jumps cause trouble for the simulations of the energy transfer. Therefore, we have to stick to the parts of the trajectory where there are no jumps between the orbitals of interest. For the surface hopping simulations, the chosen trajectory is between 2980fs and 3860fs.

In the same way, the energy of the orbitals for Setup 9C are determined. Figure 4.6 shows the

behaviour of the energy of the orbitals over time.

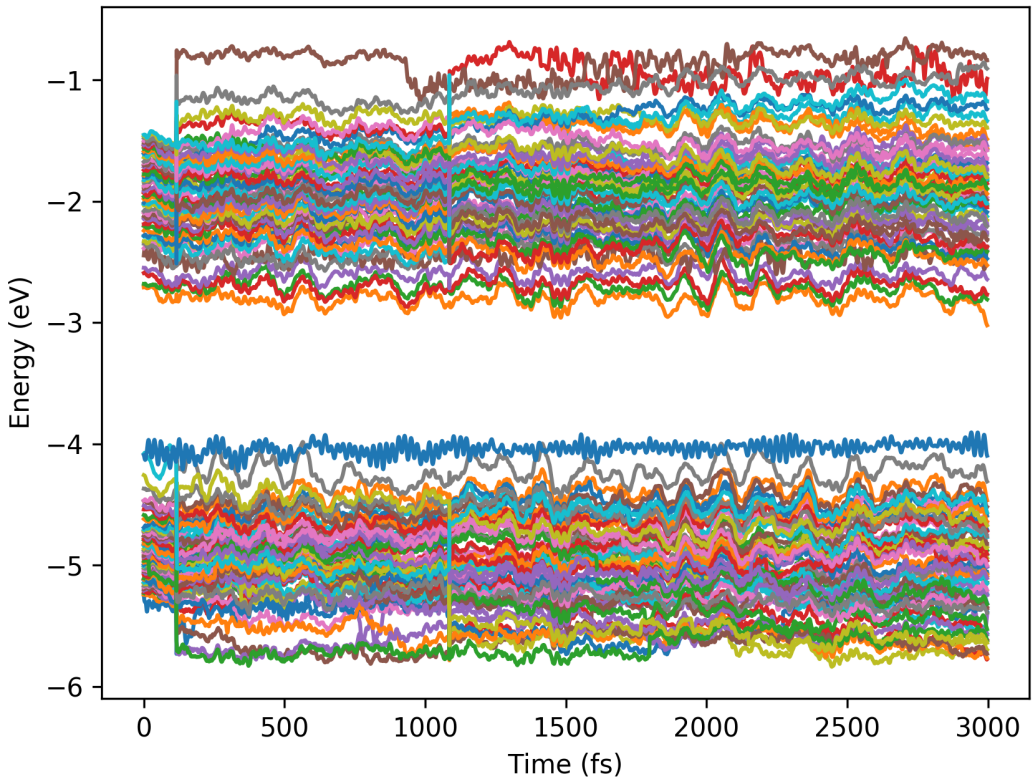

Figure 4.6: the molecular orbitals (50 HOMOs and 50 LUMOs) over time for Setup 9C. Due to computational difficulties, the program sometimes has problems following the same state, causing incorrect jumps between orbitals.

This figure makes clear that the Tc HOMO is most of the time not close to the PbS HOMOs, whereas the Tc LUMO is well within the conduction band of the QD. For an unknown reason, there is a number of inexplicable transitions between the orbitals that should not be there. Luckily, the number of time points with inexplicable transitions is lower than for Setup 7C. For the surface hopping calculations of Setup 9C, the timeframe from 1150fs to 3000fs is used.

Imaginary part: coupling

The complex parts of the Hamiltonian represent the coupling. This coupling defines how well two molecular orbitals are coupled with respect to each other. The complex Hamiltonian array

consists of the coupling of all the orbitals with all the other orbitals. For energy transfer, the electron on the Tc LUMO has to hop to one of the PbS LUMOs, and the hole on the Tc HOMO has to hop to one of the PbS HOMO's, which is equivalent to an electron hopping from one of the PbS HOMO's to the Tc HOMO. These Dexter energy transfer obeying combinations of coupling are the coupling values that are relevant. Hence, in figure 4.7, two (sums of) couplings are visualised. The first one is the sum of the coupling of the Tc LUMO with all of the PbS LUMOs. The second line represents the sum of the coupling of the Tc HOMO with all of the PbS HOMOs. At the time points where two orbitals were mixing, it is sometimes hard to determine exactly which is the orbital corresponding to tetracene. One does not want to accidentally include the coupling between two PbS-orbitals, since it is relatively high. To make sure that there is no PbS-PbS coupling in the sum, the sum at the switching points is simplified to solely include the coupling between the two states that are switching. Hence, even at the switching time point, one of those two orbitals belongs to the tetracene molecule. In figure

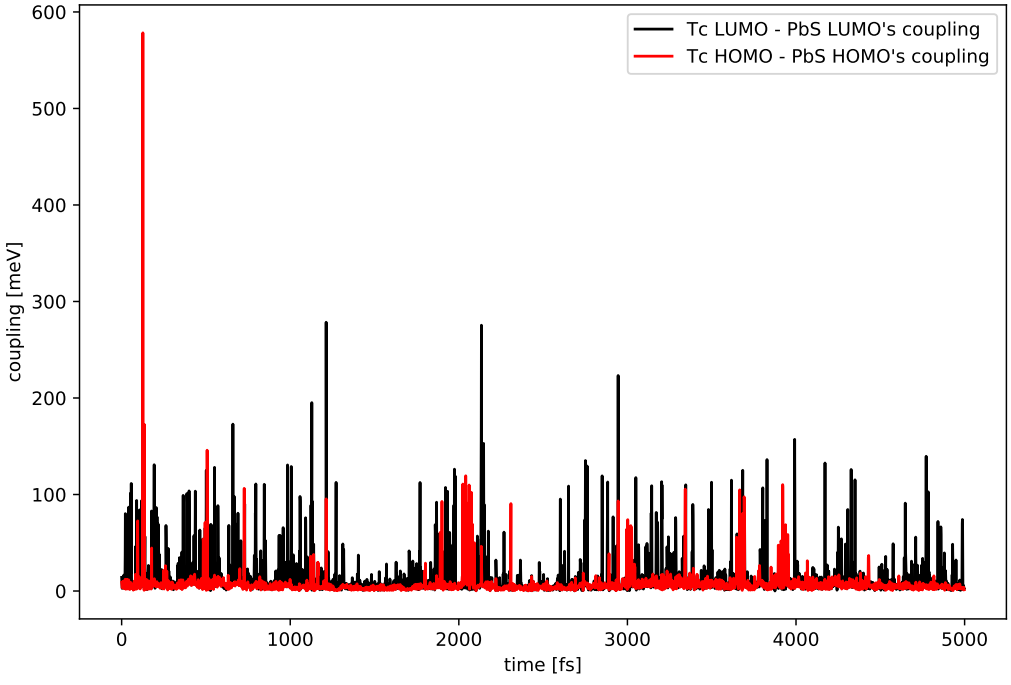

Figure 4.7: the coupling of the Tc LUMO with all the PbS LUMOs (in black) and the coupling of the Tc HOMO with all the PbS HOMOs in red for Setup 7C.

4.8, the coupling is visualised over time in the same way as for Setup 7C. Hence, one line

corresponds to the sum of the coupling between the Tc HOMO and all the PbS HOMOs and the other line corresponds to the sum of the coupling between the Tc LUMO and all the PbS LUMOs.

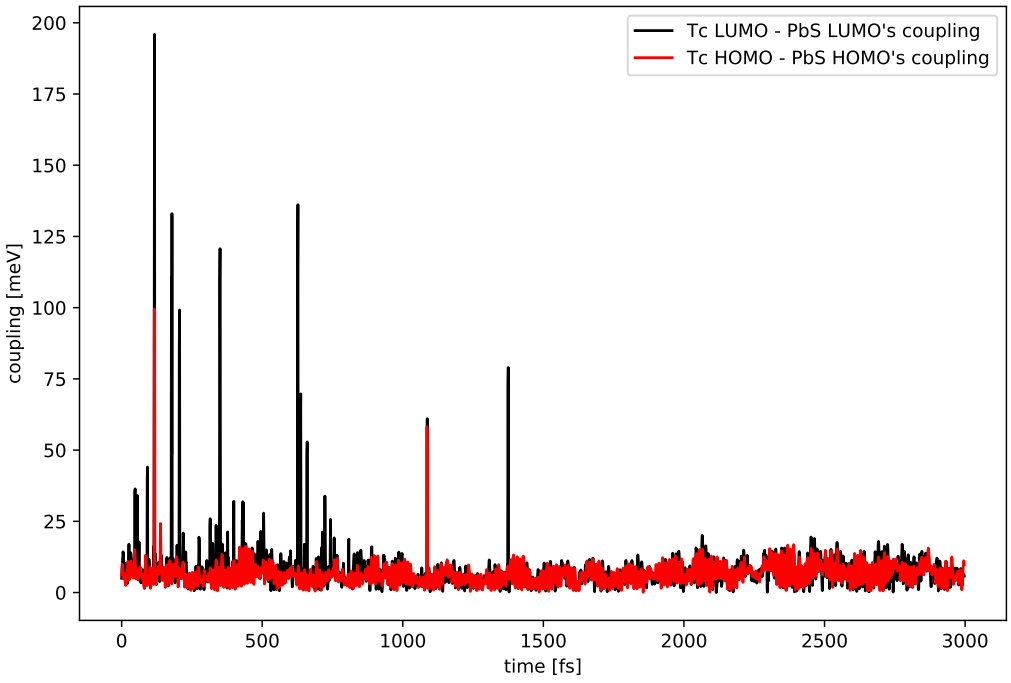

Figure 4.8: the coupling of the Tc LUMO with all the PbS LUMOs (in black) and the coupling of the Tc HOMO with all the PbS HOMOs in red for Setup 9C.

Apart from the summing, these coupling values are unmodified. Both coupling figures are bumpy. There are narrow peaks at the points where the coupling is high, but there is hardly any average coupling values; it is either maximum coupling or (almost) no coupling. This makes it hard to easily find a correlation between the coupling and one or more of the trajectory variables. In the next subsection, 4.6.2, a closer look is taken at the coupling in combination with these variables.

In figure 4.7 of Setup 7C, the coupling is relatively steady over time. The density of the peaks changes somewhat, but the height of the peaks stays the same. There is one outlier in the HOMO-HOMO coupling at the start of the trajectory, reaching a value of 578meV. We could not find a clear explanation for this coupling being so high.

Furthermore, there are more coupling peaks for the LUMO-LUMO coupling than for the HOMO-HOMO coupling. The most likely explanation for this difference is that the Tc LUMO is in the band of the PbS, whereas the Tc HOMO is slightly above the PbS HOMOs.
Figure 4.8 of Setup 9C, makes clear that the coupling is a lot weaker. In the beginning the LUMO-LUMO coupling has clear peaks, but they vanish over time. The reason behind this disappearance of coupling could be the rapidly increasing distance over time (figure 4.4), which will be analysed in the next subsection (4.6.2).
The coupling of the Tc HOMO with the PbS HOMOs stays rather low for the entire trajectory. This is likely caused by the energetic gap between the Tc HOMO and the PbS HOMOs.

4.6.2 Hamiltonian analysis

General

The Hamiltonians contain a lot of valuable information. It is interesting to find out whether a certain angle or distance between the Tc and PbS QD provides a higher coupling. Since the complexity of the coupling data, caused by the peaks as well as by the number of (potential) variables having influence, the structure of the data is modified. Each variable is divided into 10 or 20 bins over the range of the corresponding variable. This is done linearly, so that all bins have the same size. After this, the coupling values are appointed to the bin where they belong, based on this single variable. For every bin, the containing coupling values are averaged. This forms a dataset for each orientational variable: distance, rotation, curvature.
This analysis of the orientational variables combined with the coupling is followed by a spectral density analysis of the orbitals. This is calculated as the Fourier transform of the normalised autocorrelation function of a pair of molecular orbitals over a reliable range of time in the MD trajectory.

Distance

The first variable to be analysed is the distance between the two molecules. For Setup 7C, figure 4.9 suggests that the closest intermolecular distance influences the coupling. Even though the range of the distance, i.e. the range of the x-axis, is rather small, there is a negative trend visible. To keep the figure clear, a line is used instead of a histogram type of figure.

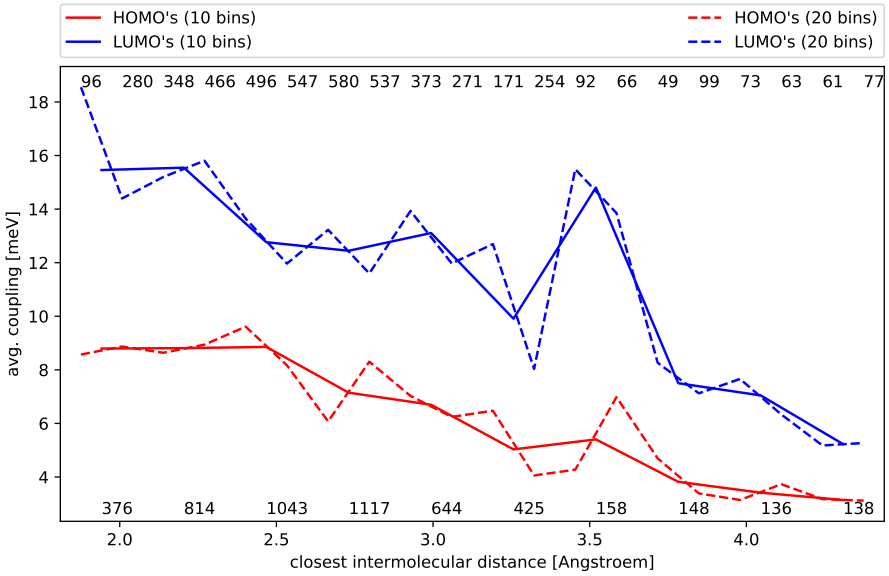

Figure 4.9: the coupling of setup 7C averaged per closest intermolecular distance bin, one set of 10 bins (solid lines) and one set of 20 bins (dashed lines); the number of coupling values belonging to a bin is displayed at the top (for 20 bins) and bottom (for 10 bins) of the figure.

The above figure is based on the smallest distance between atoms of PbS and Tc. In figure 4.10, the averaged coupling is plotted against the distance between the center of Tc and the center of the PbS facet that is terminated with ligands.

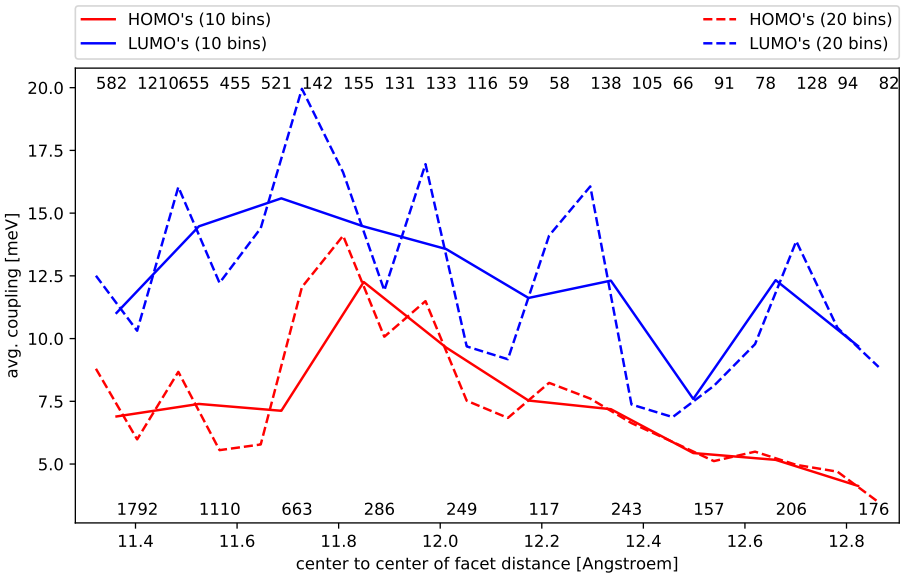

Figure 4.10: the coupling of setup 7C averaged per distance bin, one set of 10 bins (solid lines) and one set of 20 bins (dashed lines); the number of coupling values belonging to a bin is displayed at the top (for 20 bins) and bottom (for 10 bins) of the figure.

In this figure, it is hard to find a trend between the distance and the coupling. The combination of the two above graphs suggests that it is not the distance from the tetracene to the quantum dot self that is important, but the distance between the tetracene and the closest ligand on the quantum dot. For Setup 9C, the same type of analysis can be done. However, due to the absence of a variety of coupling peaks, the bin-sorted data for Setup 9C does not make any sense. For completeness, these figures for Setup 9C are included in Appendix C, but one should be aware that the analysed signal might be closer to noise than to reliable data.

Rotation

The next interesting variable is the orientation, in terms of rotation of the tetracene molecule with respect to the QD. In figure 4.11, the bins for the variable 'rotation' are plotted. The rotation describes the rotation of the tetracene around its longest axis, where a rotational value of 0° describes a perpendicular situation, and hence 90° means the facet and tetracene are parallel.

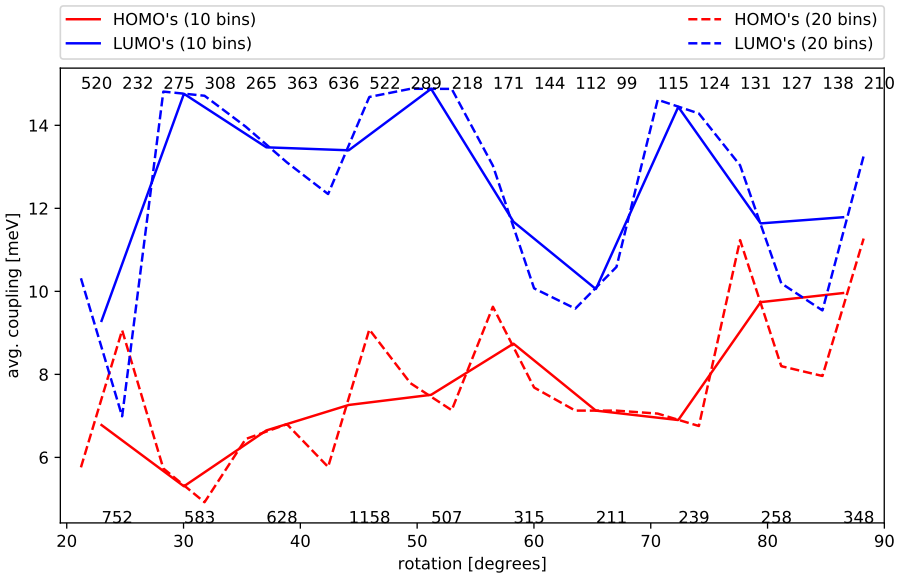

Figure 4.11: the coupling of setup 7C averaged per rotational bin, one set of 10 bins (solid lines) and one set of 20 bins (dashed lines); the number of coupling values belonging to a bin is displayed at the top (for 20 bins) and bottom (for 10 bins) of the figure.

Based on the shape of the curves in figure 4.11, it is hard to find a relation between the coupling and the rotation. There is no clear trend visible, and the curve is unexplainable bumpy.

Next to the rotation around the longest tetracene axis, there is another rotational variable which I denote as angle. It is the angle between the longest axis of the tetracene and the normal of the closest QD facet. A first look at figure 4.12 makes clear that the left half of the figure has a higher averaged coupling than the right side of the figure. Hence, one could conclude that the coupling is better in a diagonal situation ($45-65°$) than in a parallel position ($80-90°$). However, one has to be cautious. The trajectory results in an enormous sample over spacial variables. However, these variables, such as distance and angle might be entangled, in such a way that for instance the parallel/perpendicular angle only occurs at small/big distance. Taking a look at the average intermolecular distance per angular bin, the distance is roughly equal for the bins in the range of 55° to 90°, with values between 4.8Åand 5.8Å. However, the average intermolecular distance when the angle is between 45° and 52°, is 2.6Å. This could be a reason for the most left bins having higher average coupling, but it does not explain the average coupling peaks around $60° - 65°$.

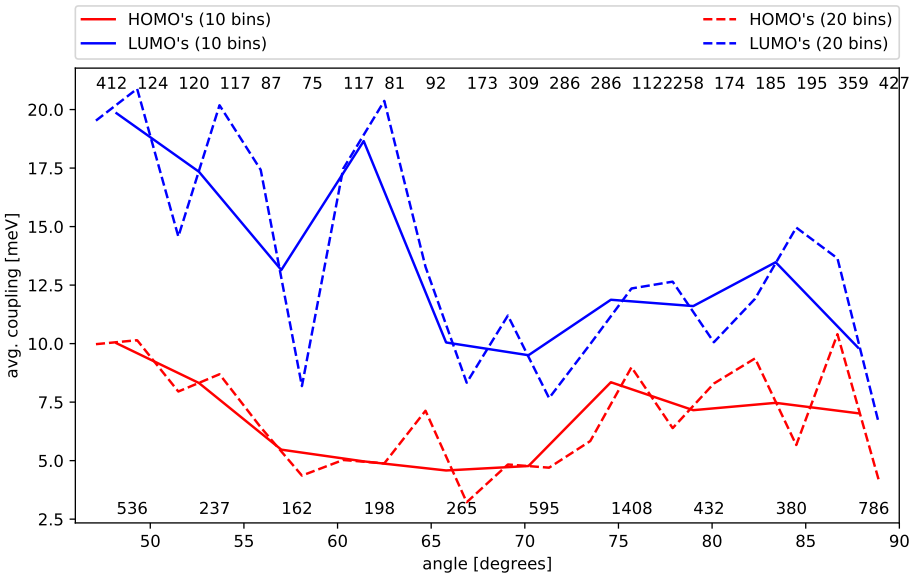

Figure 4.12: the coupling of setup 7C averaged per angular bin, one set of 10 bins (solid lines) and one set of 20 bins (dashed lines); the number of coupling values belonging to a bin is displayed at the top (for 20 bins) and bottom (for 10 bins) of the figure.

Again, for the data of Setup 9C, the graphs are enclosed in Appendix C, but they are considered irrelevant due to the lack of coupling during the trajectory.

Curvature of tetracene

As a last variable that might play a role in the coupling, is the curvature of the tetracene. Tetracene's parabolicity is determined as the measure for the curvature of the molecule. Hence, a value of 0 means an entirely flat molecule, whereas values of higher absolute values correspond to a highly bowed molecule. The bins for different values of parabolicity are displayed in figure 4.13. In figure 4.13, the absolute values of the parabolicity are used, since there is no difference between positive and negative values due to symmetry. The figure has two or three peaks for the coupling between the LUMOs. The first peak is close to zero, which corresponds to a straight, unbowed, tetracene molecule. The second peak is roughly at a parabolicity of 0.010, which is 2 to 3 meV higher than the lowest average couplings between the LUMOs. The average intermolecular distance does not differ significantly between the bins, i.e. between 2.65 and 3.45Å. Furthermore, the bins with the highest average intermolecular distance do not have the

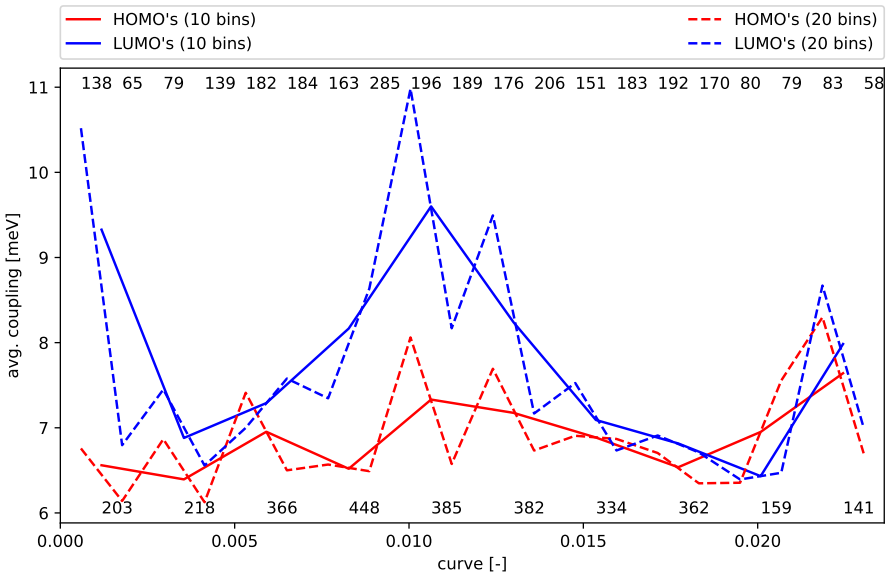

Figure 4.13: the coupling of setup 7C averaged per parabolicity-bin, one set of 10 bins (solid lines) and one set of 20 bins (dashed lines); the number of coupling values belonging to a bin is displayed at the top (for 20 bins) and bottom (for 10 bins) of the figure.

lowest average coupling. Hence, the peaks are not caused by a difference in distance. However, this does not mean that the conclusion is that at certain curvatures of the molecule, the coupling is significantly higher. The differences in average coupling are relatively small. The difference in range is less than 5meV and combining this knowledge with the number of datapoints, we can not rule out that the differences are caused by coincidence.

Spectral Density

Besides the coupling, the energy of the molecular orbitals also contains valuable information. The spectral density can be determined from these energy values. The spectral density for the LUMO of tetracene and the PbS LUMO is displayed in figure 4.14. The peeks in the region 200-400 cm^{-1} make clear that slow vibrations with low frequency play an important role of the correlation between the orbitals of the tetracene and the quantum dot. Since these vibrations are really slow, they likely take place in the quantum dot. Over the relevant combinations of orbitals, the height, energy and number of these low energy peeks varies slightly, but they never leave the energetic region between 200 and 400 cm^{-1}.

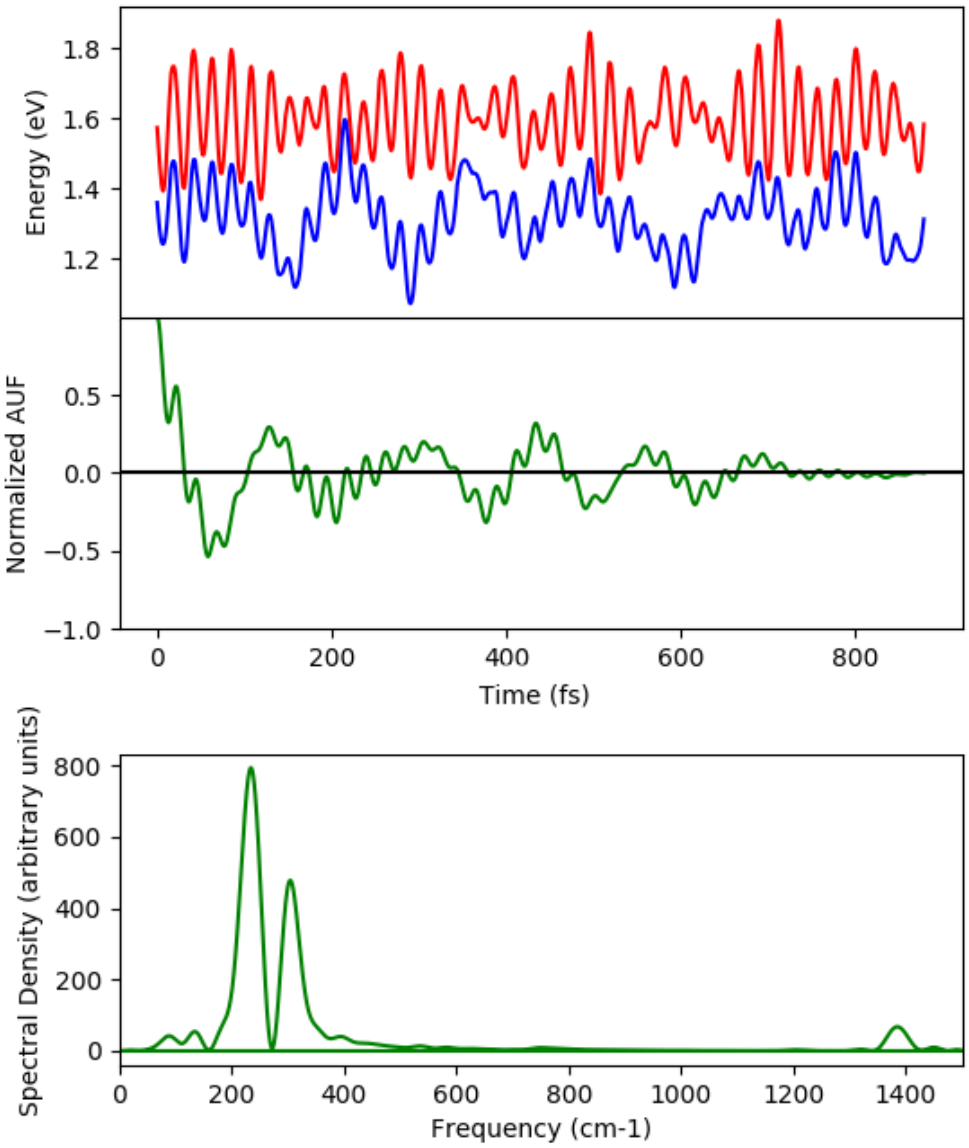

Figure 4.14: The energy levels of the Tc LUMO and PbS LUMO (top, red and blue respectively), the normalised autocorrelation function between these two (middle), and the spectral density (bottom). The last is calculated as the Fourier transform of the Normalised AUF.

The other peek, at 1385 cm^{-1}, is the same for all relevant combinations of orbitals. This peek is more interesting, since it describes which phonon plays an important role in the correlation between the donor and acceptor states. With frequency calculations in ADF[62, 19, 5] on the tetracene molecule and the ligand, it can be determined which vibration belongs to the frequency of 1385 cm^{-1}. The momentum of the vibration is drawn in figure 4.15.

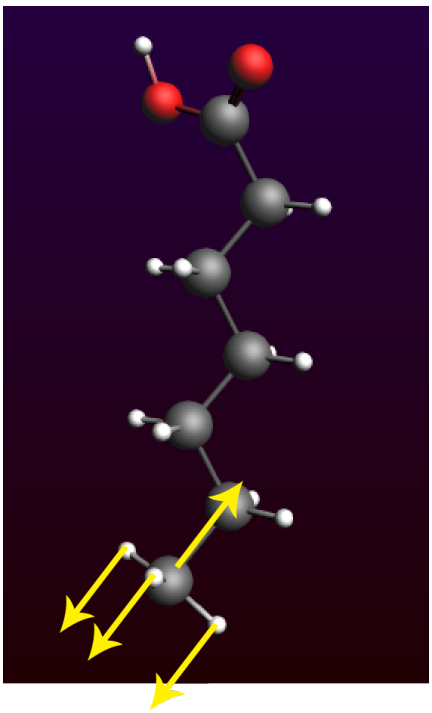

Figure 4.15: the direction of movement of the vibration that plays a role in the correlation between the tetracene and quantum dot states. The movement goes back and forth over the yellow arrows, starting in the directions drawn.

4.6.3 Energy transfer results

Setup 7C: FSSH

For Setup 7C, the chosen timeframe is from 2980fs and 3860fs. The simulation of the surface hopping with the FSSH algorithm and no changes to the energy level, is enclosed in figure 4.16.

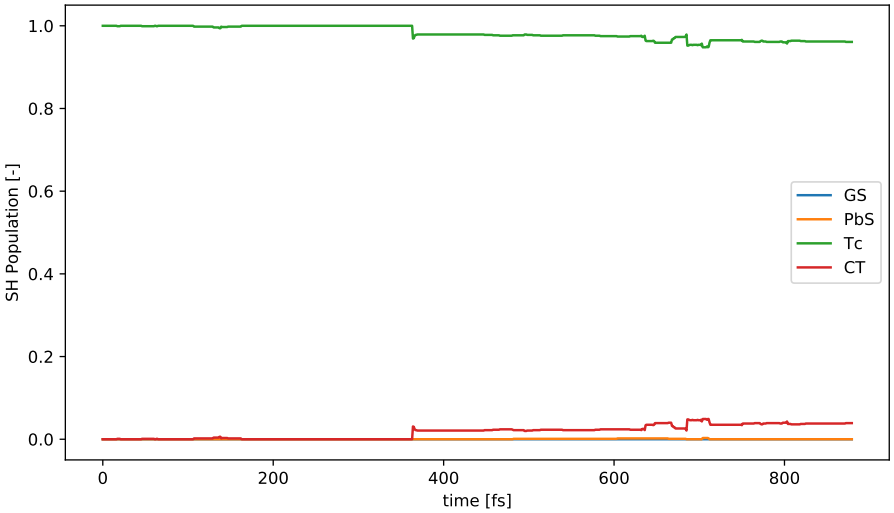

Figure 4.16: the surface hopping simulated over time for Setup 7C. The FSSH-algorithm is used, with unaltered energy levels, i.e. $E_{LE(Tc)} = 1.595$ eV and the bandgap of PbS is 1.459 eV. The energy of the lowest charge transfer state is 1.318 eV. All energetic values are averaged over the time of the relevant trajectory.

Figure 4.16 makes clear that the CT-states are populated over time, but none of the states localised at PbS are populated. The most obvious reason is that the CT-states are the lowest in energy, which therewith makes it the most likely state to be populated.

As a logical next step, the energy levels are altered to more realistic values. The average PbS bandgap is lowered to 1.0 eV and the average energy of the excited state at tetracene is lowered to 1.25 eV. As described in section 4.5.1, it is hard to determine the energy of the CT-states, but it is save to conclude that they are reasonably higher than the locally excited states. Therefore, multiple simulations are performed, with different energies for the CT-states. The energy of the CT-states is increased with 0 eV, 0.2 eV, 0.4 eV.

Of those three energy configurations, only the first (PbS 1.0 eV; Tc 1.25 eV; CT 1.3 eV) shows some energy transfer, albeit very little. In 1000 simulations, only one run shows energy transfer. Hence, assuming continuation at the same pace, this would mean that 90% of the energy transfer is completed after 1.2 ns. One has to note that the CT-state energy is still likely to be smaller than in reality.

The other two of the three energy configurations (PbS 1.0 eV; Tc 1.25 eV; CT 1.5 or 1.7 eV),

are probably closer to reality. However, no CT is observed at all in the 2000 runs that these two simulations jointly performed. Hence, it is a logical next step to change the SH-algorithm to GFSH, since it relies less on CT-states.

Setup 7C: GFSH

For the GFSH method, simulations are performed for the same energetic configurations, which can be listed as:

1. Tc: 1.595 eV; PbS: 1.459; CT: 1.318 eV;
2. Tc: 1.250 eV; PbS: 1.000; CT: 1.318 eV;
3. Tc: 1.250 eV; PbS: 1.000; CT: 1.518 eV;
4. Tc: 1.250 eV; PbS: 1.000; CT: 1.718 eV.

Just like the first configuration with FSSH, the same energetic configuration only causes population of the CT-states when GFSH is used.
For configuration 2, in 12 of the one thousand runs the exciton is transferred. This would mean that 90% of the initial energy is transferred after 0.17 ns, if the transfer continues at a similar rate. However, the transfer might be too fast since the energy of the CT-state is at some points still lower than the energy of the exciton at tetracene.
Hence, it is interesting to look at configurations 3 and 4, where the CT-state energy is higher. Figure 4.17 shows the transfer for configuration 3.

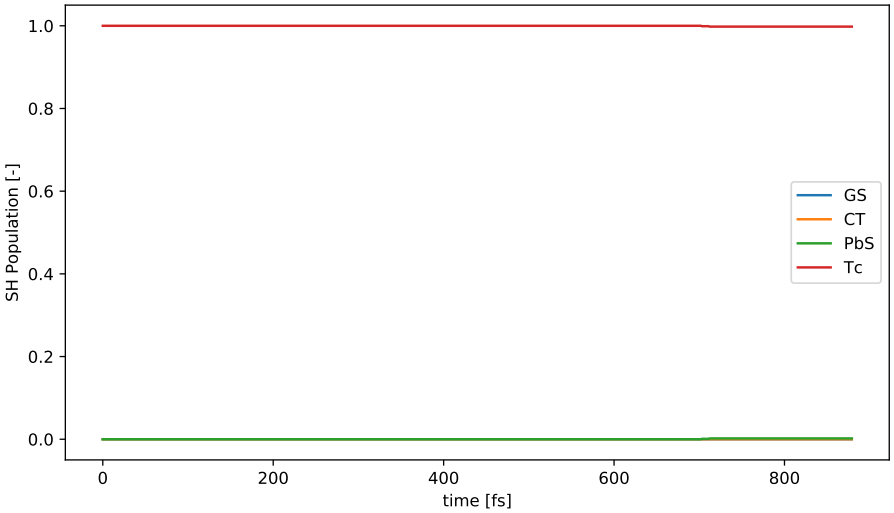

Figure 4.17: the surface hopping simulated over time for Setup 7C. The GFSH-algorithm is used, with more realistic energy levels, i.e. $E_{LE(Tc)} = 1.25$ eV and the bandgap of PbS is 1.0 eV. The energy of the lowest charge transfer state is 1.518 eV. All energetic values are averaged over the time of the relevant trajectory.

It is hard to see by eye, but after 1000 runs, 2 excitons are transferred to the PbS QD. This means that 90% of the initial excitons will be transferred after 1.0 ns, under the assumption that the transfer rate is the same.

Figure 4.18 shows that the transfer for configuration 4 happens more quickly than for configuration 3. At the end of the simulation, 6 out of the 1000 runs showed energy transfer. Hence, this would result in a transfer time of 0.3 ns for 90% of the initial excitons, assuming the transfer rate does not change.

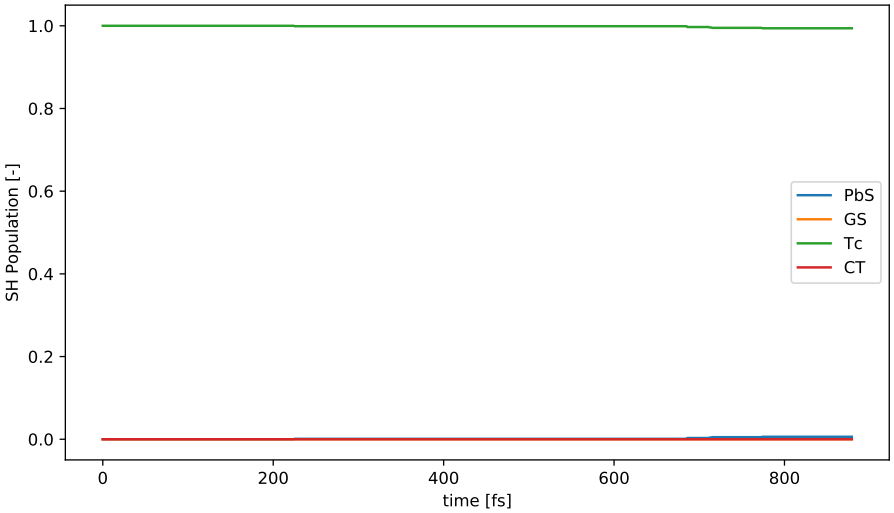

Figure 4.18: the surface hopping simulated over time for Setup 7C. The GFSH-algorithm is used, with more realistic energy levels, i.e. $E_{LE(Tc)} = 1.25$ eV and the bandgap of PbS is 1.0 eV. The energy of the lowest charge transfer state is 1.718 eV. All energetic values are averaged over the time of the relevant trajectory.

Setup 9C: FSSH

As we have seen for Setup 7C in combination with FSSH, FSSH does not show energy transfer when the CT-states are energetically unfavourable to populate. For Setup 9C, the same modifications are made to the energy levels, resulting in these 4 configurations:

1. Tc: 1.592 eV; PbS: 1.415; CT: 1.228 eV;
2. Tc: 1.250 eV; PbS: 1.000; CT: 1.228 eV;
3. Tc: 1.250 eV; PbS: 1.000; CT: 1.428 eV;
4. Tc: 1.250 eV; PbS: 1.000; CT: 1.628 eV.

Even though the unaltered CT-state energy is lower than for Setup 7C, no energy transfer nor charge transfer is observed at all for any of the four configurations. The energy levels are the same or even more CT-favourable compared to the energy levels of Setup 7C. Hence, the reason for the absence of CT is likely to be something else than the energy differences. The most likely

reason for the lack of CT is that the coupling between the relevant orbitals is very low. Herein, the bigger distance between tetracene and PbS is likely to play a role.

Setup 9C: GFSH

For the same four configurations, the GFSH algorithms is also used. Figure 4.19 contains the surface hopping simulation of the first, energetically unaltered, configuration.

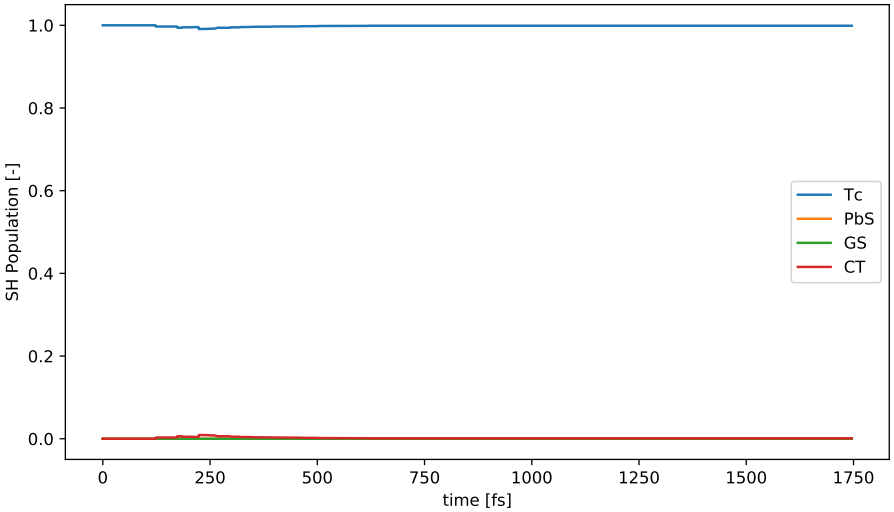

Figure 4.19: the surface hopping simulated over time for Setup 9C. The GFSH-algorithm is used, with unaltered energy levels, i.e. $E_{LE(Tc)} = 1.529$ eV and the bandgap of PbS is 1.415 eV. The energy of the lowest charge transfer state is 1.228 eV. All energetic values are averaged over the time of the relevant trajectory.

This figure shows that some of the CT-states are temporarily populated, before the electron hops back to the excitonic state at Tc. There is no energy transfer from Tc to PbS. For the remainder of the configurations, there is no CT, and thus no energy transfer, at all.
The explanation is likely to be, as mentioned for the FSSH part of Setup 9C, that the coupling for this setup is remarkably low.

4.7 Discussion

4.7.1 Error Margins

During computational analysis and/or simulations, it is very important to clarify the error margins for the results obtained. Due to the nature of the majority of the used algorithms, it is hard to determine clear error margins. But we can be sure that the error margins are more than significant.
During the process:

- the geometry is optimised (with DFT);
- which is used as a starting point for the remainder of the trajectory calculated with MD (with DFT);
- the resulting trajectory is used for recalculation of the Hamiltonians (with DFT);
- which are used for the simulation of surface hopping.

Due to the nature of the development of the DFT functionals, which can well be described as a method of trial and error, it is almost impossible to determine a good guideline for the possible size of errors, especially if there is very little reference data. From chapter 3, we already know that the error for the energy levels could reasonably be more than ten percent. The error for non-quantitative data, such as wave functions is even harder to determine. Nonetheless, knowing that the final data is the result of computations performed on DFT-computed data based on DFT-data based on DFT-data, it is fair to say that one has to be extremely careful drawing conclusions from the data.

4.7.2 Further uncertainty

Next to the errors caused by the computational imperfections, there are also differences between the experimental setup and the computational setup. In the computational setup, there is only

one tetracene molecule. However, in the experimental reality there is an entire nanocrystal of tetracene. This not only has an influence on the energy, but also on the wave function, which is believed to be delocalised over multiple molecules[9]. Within PYXAID, the energy can be corrected for, but possible differences in wave functions and coupling values can not be corrected for. Furthermore, there are multiple QDs in the experiment, whereas the simulation only allowed the presence of one QD. For PbS QDs, the number also plays a role, but it is likely to be a smaller role than for tetracene.

4.7.3 Surface hopping

Within the surface hopping computations, there is two fields in which changes can be made after the determination of the trajectory to achieve as realistic as possible energy transfer. The first is by changing the SH-algorithm, and the second is by shifting the energy levels.

Taking a closer look at the energy levels, in combination with the previously analysed CT-state energies(4.5.1), it is most likely that the configurations with the highest and second-highest CT-state energies are the most reliable configurations. Four the other configurations, the CT-state energies are not increased, resulting in CT-states that are at some times energetically favourable to populate. As far as we can decide, this is an unphysical phenomenon.

Continuing with the configurations with increased CT-state energies, there is a clear difference between FSSH and GFSH. In GFSH there is still energy transfer visible for these configurations, whereas there is no CT when FSSH is used. Since the energy levels are close to reality and since the energy transfer has experimentally been observed, it is clear that GFSH results in a surface hopping simulation that it closer to reality.

Due to described inaccuracies in the behaviour of the orbitals over time, only small parts of the trajectory were used. This limits the observed energy transfer, and the only method to determine the transfer time for the entire energy is to “extrapolate” the energy transfer in an exponential way.

This extrapolation resulted in transfer times of 0.3 and 1.0 ns for 90% of the initial excitons. Literature reports that the energy transfer happens within < 10 ns[64]. Hence, the results of

the calculated transfer times are not contradicting the experiments.
However, since there is only one starting point of the trajectory for each setup, and since the total time of the trajectory was limited, it is impossible to obtain any new insights from the surface hopping data, other that the transfer time is in line with the experiment. Hence, this is one of the reasons why it was interesting look at the coupling.

4.7.4 Coupling

In an ideal alignment between the QD and the tetracene, the Tc HOMO would be slightly in the QD valence band, and likewise the LUMO would be slightly in the conduction band. In the obtained orbitals, the HOMO is higher in energy than the HOMO of the QD, whereas the LUMO is probably further in the conduction band than an ideal practical setup would demand. Therefore, the Tc LUMO - QD LUMOs coupling is on average likely to be overestimated, while the Tc HOMO - QD HOMOs coupling is on average likely to be underestimated.
Furthermore, the coupling signal itself is hard to analyse due to its nature of being either maximal or minimal. Therefore, it was more interesting to analyse modified data, that might be best described as 'coupling density', in which the coupling is averaged over a certain range of a variable.
The creation of the coupling density bins make the data rather rough, since multiple thousands of data points are converted into averaged values for a limited number of bins, which represent the new data. Hence, it is not possible to draw rock-solid conclusions from this data. However, the data clearly indicates that the coupling depends on the distance between tetracene and the acceptor's (including ligand) closest atom, rather than the distance between tetracene and the closest acceptor facet (excluding ligand). Further research will be needed to confirm or reject this suggested dependence.

4.8 Conclusions

After the analysis of the data and a closer look at the reliability of the obtained results, it is necessary to determine which conclusions can be drawn.

For the surface hopping simulations, it has become clear that it is very important to choose suitable values for the parameters, in particular the value of the energies. When the correct energy levels are chosen, energy transfer, albeit little, is observed for Setup 7C in the simulations when GFSH is used. The timeframe is far too short to simulate complete energy transfer. Using exponential extrapolation, an indication of the transfer time can be determined at values of 0.3 ns and 1.0 ns. These transfer times are in line with the time frame as described in the literature (i.e. < 10 ns). For Setup 9C, there is no energy transfer observed. This is possibly caused by an unrealistically large distance for the majority of the trajectory, resulting in low coupling between the orbitals of the donor and acceptor.

For the analysis of the coupling, no clear conclusions can be drawn due to the roughness of the modified data as well as the presence of unknown but significant errors. Taking this into consideration, the data for Setup 7C still suggests that the distance between tetracene and the closest atom of the ligand is the biggest influence on the coupling, whereas the distance between the tetracene and the closest acceptor facet seems to be less important. However, for confirmation of this hypothesis, it needs to be backed by further research. For the relation between the angle/rotation and coupling, no clear correlation can be observed.

For Setup 9C, there was no analysis possible since the density of the coupling peaks was too low.

Chapter 5

Conclusion

5.1 Summary of Thesis Achievements

During the process of the research and the analysis of its results, a number of interesting results, relations and conclusions have become clear. The first part of the research determines the performances of different functionals. The conclusion that is most relevant for the remainder of the calculations is that the PBE functional is not accurate for local states and the same functional struggles determining the charge transfer states and their energies.

The second part of the research, the surface hopping simulation, makes clear that the transfer of energy from tetracene to PbS quantum dots can be reproduced using the GFSH algorithm in combination with the correct energy levels, resulting in energy transfer times that are within the experimentally determined timeframe (i.e. $< 10ns$). Besides this confirmation, no new information can be deducted from the surface hopping results.

Analysis of the Hamiltonians on which the surface hopping calculations are based, indicates that the coupling at least depends on the distance between tetracene and the closest ligand atom. In the same simulated period of time, the distance between tetracene and the closest PbS facet does not change the coupling significantly. Hence, this indicates that the coupling is more dependent of the distance of tetracene with the closest ligand, than that it is dependent of the distance between tetracene and the closest PbS facet. Due to the roughness of the modified data

and the error margins in the prior calculations, this relation can not be definitively concluded until it is backed by further research.
For the rotation and angle of the tetracene molecule with respect to the quantum dot, it was not possible to determine if and how it affects the coupling.

5.2 Applications

This research was performed entirely computationally. However, the actual application that we are interested in, i.e. solar panels, also has to work in reality, and preferably with an optimal efficiency. Hence, for the practical experiments regarding the same matter, it is useful to get a better insight into the energy transfer process. One of the questions for which it is hard to derive the answer from the experimental results, is what the optimal placement of the tetracene molecule with respect to the quantum dot and its ligands is. This research can be considered as a first step towards unveiling the ideal placement.

5.3 Future Work

There are a couple of questions that could not be answered by the research performed for this thesis. These questions could be answered in future work on the same two materials. A first suggestion for future work could be to improve the size of the quantum dot, hopefully resulting in a better alignment of the tetracene HOMO with the HOMOs of the quantum dot. This should overcome the low HOMO-HOMO coupling. Also, one could create more and/or longer trajectories. If the number of different points in time is increased greatly, that would solve a number of problems: the averaged data (the bins) would be less rough and also less prone to irregularities caused by entanglement of multiple variables. Also, this would increase the range of angles and rotations observed, which for this research were not fully utilised.
With these improvements applied, resulting in more than enough datapoints and a better HOMO-HOMO coupling, one can solidly determine for each variable what its influence on the

coupling is.

Appendix A

Coordinates

A.1 Tetracene Monomer

Atom	X	Y	Z
1 C	−2.215 320 214	−0.642 978 562	0.079 949 647
2 C	−2.006 654 312	0.709 639 415	0.095 730 478
3 C	−0.684 101 596	1.238 613 393	0.031 010 992
4 C	0.395 798 352	0.401 375 856	−0.047 826 168
5 C	0.226 827 512	−1.016 901 219	−0.067 219 313
6 C	−1.119 143 868	−1.555 241 828	−0.001 353 828
7 H	3.770 225 791	−8.507 336 923	−0.423 042 593
8 C	−1.302 380 481	−2.935 308 136	−0.019 149 476
9 C	−0.216 487 39	−3.826 542 902	−0.099 434 849
10 C	1.131 176 099	−3.287 525 51	−0.165 383 138
11 C	1.307 122 416	−1.891 599 928	−0.146 846 228
12 C	2.217 069 191	−4.178 760 277	−0.245 668 511
13 C	2.033 832 578	−5.558 826 585	−0.263 464 159
14 C	0.687 861 198	−6.097 167 193	−0.197 598 674
15 C	−0.392 433 706	−5.222 468 485	−0.117 971 759

16 C	0.518 890 358	−7.515 444 269	−0.216 991 819
17 C	1.598 790 305	−8.352 681 805	−0.295 828 979
18 C	2.921 343 022	−7.823 707 828	−0.360 548 465
19 C	3.130 008 924	−6.471 089 85	−0.344 767 634
20 H	−3.228 866 348	−1.048 532 858	0.129 544 288
21 H	−2.855 537 081	1.393 268 51	0.158 224 606
22 H	−0.537 577 468	2.320 369 79	0.044 794 606
23 H	1.409 462 52	0.806 633 472	−0.097 433 628
24 H	4.143 555 058	−6.065 535 554	−0.394 362 275
25 H	−2.316 744 761	−3.340 271 467	0.030 504 005
26 H	2.320 974 421	−1.485 348 99	−0.196 444 076
27 H	3.231 433 471	−3.773 796 945	−0.295 321 992
28 H	−1.406 285 712	−5.628 719 423	−0.068 373 911
29 H	−0.494 773 811	−7.920 701 885	−0.167 384 359
30 H	1.452 266 177	−9.434 438 203	−0.309 612 593

Table A.1: the optimised coordinates of a tetracene monomer, as used in the calculations.

A.2 Tetracene Dimer

Atom	X	Y	Z
1 C	−1.090 614 808	−1.224 294 788	2.243 515 193
2 C	−1.854 750 323	−1.913 408 852	3.236 440 827
3 C	−2.000 827 406	−1.383 022 88	4.495 973 741
4 C	0.434 906 516	0.217 658	0.320 812 707
5 C	1.188 042 053	0.902 606	−0.656 558 403
6 C	1.345 470 465	0.386 055 516	−1.947 224 687
7 C	2.106 783 128	1.075 298 422	−2.942 460 256

8 C	2.244 687 57	0.547 824 24	−4.204 365 44
9 C	0.897 086 064	−1.392 588 082	−3.621 051 457
10 C	0.731 008 469	−0.883 316 641	−2.291 181 048
11 C	−0.930 264 053	−1.741 289 939	0.953 775 215
12 C	1.641 313 091	−0.698 233 974	−4.545 315 998
13 C	−1.401 713 259	−0.135 017 178	4.836 694 761
14 C	−0.651 681 57	0.557 103 562	3.915 483 449
15 C	−0.477 691 566	0.045 944 456	2.587 863 73
16 C	0.272 180 431	0.731 102 812	1.627 500 592
17 C	−0.016 040 214	−1.568 874 81	−1.329 365 361
18 C	−0.176 914 793	−1.055 822 95	−0.022 310 529
19 H	−2.333 687 239	−2.853 543 378	2.970 564 78
20 H	−2.589 869 429	−1.919 241 195	5.235 231 324
21 H	1.673 660 812	1.840 770 52	−0.392 819 338
22 H	2.588 413 568	2.014 410 89	−2.677 863 431
23 H	2.829 781 024	1.085 180 72	−4.946 132 084
24 H	0.405 893 249	−2.328 760 122	−3.878 245 496
25 H	−1.415 314 534	−2.679 428 393	0.688 948 701
26 H	−0.505 802 494	−2.504 464 17	−1.595 241 291
27 H	1.771 538 116	−1.098 651 761	−5.549 397 925
28 H	0.761 045 953	1.666 959 604	1.894 550 168
29 H	−1.539 291 751	0.269 177 096	5.838 007 601
30 H	−0.164 130 018	1.495 215 122	4.172 808 572
31 C	5.769 742 256	3.448 231 145	−4.571 164 907
32 C	5.089 394 039	4.062 246 585	−3.547 031 359
33 C	4.899 588 568	3.391 040 749	−2.295 877 136
34 C	4.194 210 522	3.984 544 482	−1.243 882 341
35 C	4.544 593 765	1.975 341 435	0.150 772 406
36 C	5.259 450 994	1.385 042 834	−0.915 661 864

37 C	5.443 438 979	2.055 805 919	−2.129 616 444
38 C	6.152 210 386	1.458 688 394	−3.222 513 658
39 C	6.293 900 699	2.130 904 933	−4.414 283 842
40 C	2.274 521 651	3.167 281 33	4.557 801 576
41 C	2.408 159 087	3.836 817 311	3.363 550 952
42 C	3.110 168 991	3.236 237 253	2.267 540 692
43 C	3.289 340 494	3.904 133 477	1.051 332 351
44 C	4.002 989 215	3.313 168 392	−0.015 459 459
45 C	4.354 644 554	1.305 126 536	1.379 972 694
46 C	3.654 225 017	1.901 107 919	2.433 634 064
47 C	3.471 868 689	1.233 229 153	3.687 772 134
48 C	2.799 138 36	1.850 373 521	4.714 975 251
49 H	5.914 911 194	3.970 736 851	−5.514 623 469
50 H	4.664 034 616	5.055 250 156	−3.673 219 236
51 H	3.758 871 514	4.972 628 729	−1.382 196 696
52 H	2.659 146 364	1.329 723 718	5.660 345 711
53 H	5.691 213 839	0.395 335 751	−0.778 695 403
54 H	6.585 379 716	0.470 896 913	−3.084 028 909
55 H	6.820 296 855	1.662 391 051	−5.244 198 713
56 H	1.753 960 262	3.637 220 279	5.390 575 918
57 H	1.976 165 218	4.825 625 934	3.226 264 233
58 H	2.856 367 107	4.893 049 855	0.913 821 302
59 H	4.789 565 463	0.316 875 319	1.518 340 071
60 H	3.897 754 05	0.240 759 136	3.814 594 817

Table A.2: the optimised coordinates of a tetracene dimer, as used in the calculations.

A.3 Pentacene Monomer

Atom	X	Y	Z
1 C	−4.434 544 461	2.790 578 95	0.222 565 069
2 C	−4.357 266 828	5.605 422 447	0.224 108 507
3 C	−5.585 702 234	4.957 971 94	0.180 019 232
4 C	−5.625 692 035	3.504 222 177	0.179 562 952
5 C	−0.734 623 252	3.369 089 305	0.354 872 134
6 C	−0.694 501 836	4.826 107 019	0.355 510 396
7 C	−1.899 028 545	5.539 163 943	0.312 400 7
8 C	−3.140 782 144	4.892 911 045	0.268 020 919
9 C	−3.180 920 715	3.435 903 335	0.267 393 904
10 C	−1.976 398 894	2.722 853 392	0.310 633 492
11 C	−6.822 842 971	5.673 488 258	0.134 987 554
12 C	−6.900 217 467	2.857 598 718	0.134 063 651
13 H	5.147 255 446	5.187 996 121	0.564 947 082
14 H	5.078 355 199	2.687 210 498	0.565 139 43
15 H	−1.869 367 799	6.632 125 599	0.312 789 526
16 C	−8.018 876 703	5.011 470 577	0.091 876 284
17 C	−8.058 023 09	3.584 303 967	0.091 793 041
18 H	−8.953 827 831	5.574 354 228	0.057 088 344
19 H	−9.022 606 935	3.073 484 666	0.057 351 845
20 H	−4.329 410 522	6.698 535 259	0.224 286 427
21 H	−6.794 897 754	6.766 076 627	0.134 703 234
22 H	−6.932 025 823	1.765 120 204	0.133 557 24
23 H	−2.006 066 749	1.629 886 962	0.310 134 922
24 C	3.024 899 709	5.404 132 737	0.488 703 54
25 C	1.750 339 752	4.757 464 088	0.443 158 636
26 C	1.710 207 168	3.303 717 435	0.442 638 649
27 C	2.947 338 648	2.588 177 973	0.487 678 83

28 C	4.143 419 838	3.250 141 25	0.530 623 206
29 C	4.182 608 988	4.677 266 17	0.530 747 193
30 C	0.559 245 578	5.471 267 559	0.400 208 991
31 C	0.481 740 528	2.656 252 515	0.398 553 583
32 H	2.919 389 98	1.495 582 528	0.487 831 093
33 H	−4.465 799 096	1.697 680 577	0.222 001 066
34 H	3.056 278 027	6.496 517 102	0.489 207 822
35 H	0.590 628 557	6.564 169 904	0.400 834 635
36 H	0.453 640 443	1.563 266 731	0.398 391 895

Table A.3: the optimised coordinates of a pentacene monomer, as used in the calculations.

A.4 Pentacene Dimer

Atom	X	Y	Z
1 C	−0.980 021 978	0.520 163 923	−5.209 266 6
2 C	−0.370 735 876	0.154 420 715	−6.386 905 655
3 C	0.878 044 883	−0.534 510 619	−6.378 074 445
4 C	1.510 544 699	−0.832 401 619	−5.194 863 858
5 C	0.918 552 307	−0.463 275 174	−3.942 076 462
6 H	−1.918 897 585	1.070 681 673	−5.214 246 9
7 H	−0.844 406 294	0.386 531 332	−7.339 601 246
8 H	1.333 230 368	−0.827 837 435	−7.321 829 337
9 H	2.450 297 151	−1.380 435 644	−5.188 820 813
10 C	1.573 791 826	−0.685 412 281	−0.261 866 212
11 C	0.979 420 287	−0.330 321 022	0.963 760 689
12 C	1.601 602 533	−0.620 910 412	2.203 657 305
13 C	1.005 801 349	−0.264 758 787	3.416 927 623

14 C	1.622 270 056	−0.565 736 185	4.677 626 82
15 C	−0.278 610 282	0.413 804 786	3.410 969 881
16 C	−0.903 538 801	0.702 108 836	2.194 874 86
17 C	−0.312 066 38	0.342 386 718	0.959 147 993
18 H	2.520 049 688	−1.224 190 21	−0.259 178 68
19 H	2.546 895 016	−1.161 570 666	2.208 196 516
20 H	2.562 340 902	−1.114 203 609	4.682 638 501
21 H	−1.848 342 539	1.243 371 063	2.192 652 907
22 H	−1.809 933 151	1.331 588 012	4.657 848 505
23 C	−0.935 964 421	0.632 622 492	−0.269 217 92
24 C	−0.341 216 094	0.278 447 326	−1.494 964 961
25 C	−0.962 249 197	0.570 754 295	−2.735 018 317
26 C	1.542 417 107	−0.753 571 676	−2.725 936 55
27 C	0.950 284 399	−0.394 639 355	−1.490 294 307
28 H	−1.882 392 7	1.171 114 444	−0.271 735 295
29 H	−1.907 149 176	1.112 197 202	−2.739 700 789
30 H	2.486 905 829	−1.295 358 277	−2.723 658 003
31 C	1.013 622 81	−0.199 031 981	5.855 291 597
32 C	−0.236 132 166	0.488 047 651	5.846 850 56
33 C	−0.869 960 855	0.784 046 67	4.663 727 77
34 H	1.489 157 288	−0.428 305 316	6.807 794 548
35 H	−0.690 438 827	0.782 249 9	6.790 796 125
36 C	−0.365 309 621	0.216 389 83	−3.948 281 237
37 H	5.460 415 428	4.898 306 514	−2.807 094 546
38 C	2.057 503 261	3.121 493 49	−0.211 972 611
39 C	2.639 610 402	3.408 116 855	−1.461 172 659
40 C	2.001 036 75	3.054 583 688	−2.674 678 553
41 C	2.581 488 594	3.345 914 382	−3.911 952 452
42 C	1.929 090 409	3.010 378 545	−5.143 907 612

43 C	2.513 635 719	3.324 982 725	−6.346 941 261
44 C	3.788 072 968	3.961 853 61	−6.395 379 05
45 C	4.449 911 482	4.304 645 158	−5.239 917 48
46 C	3.871 926 768	4.011 161 001	−3.960 305 171
47 C	4.513 121 813	4.362 343 859	−2.769 447 049
48 C	4.570 243 746	4.430 905 749	−0.306 172 455
49 C	3.988 557 752	4.143 934 548	0.942 770 963
50 C	4.627 241 718	4.497 892 244	2.155 918 234
51 C	4.048 563 504	4.205 701 948	3.393 287 887
52 C	4.702 117 58	4.542 685 748	4.624 287 801
53 C	4.119 183 305	4.227 976 131	5.828 086 575
54 C	2.846 128 131	3.588 549 21	5.878 035 615
55 C	2.183 766 146	3.243 164 189	4.723 457 292
56 C	2.759 083 694	3.538 420 168	3.442 770 823
57 C	2.116 991 198	3.187 922 256	2.251 893 661
58 C	2.695 743 306	3.475 896 336	0.991 101 152
59 C	3.932 869 75	4.075 569 197	−1.509 325 529
60 H	1.108 835 511	2.587 918 657	−0.175 990 879
61 H	1.051 999 689	2.521 919 232	−2.639 311 108
62 H	0.974 779 246	2.489 009 464	−5.108 324 364
63 H	2.000 185 554	3.090 241 78	−7.276 919 794
64 H	4.234 779 076	4.175 299 972	−7.363 728 853
65 H	5.402 892 188	4.829 238 74	−5.274 667 237
66 H	5.517 927 263	4.965 757 598	−0.341 833 403
67 H	5.575 852 69	5.031 088 802	2.120 153 463
68 H	5.655 396 324	5.066 121 026	4.586 875 021
69 H	4.632 992 634	4.464 568 117	6.757 265 983
70 H	2.401 835 923	3.374 466 274	6.847 245 893
71 H	1.233 325 382	2.714 090 159	4.759 786 507

72 H	1.169 670 642	2.651 889 622	2.289 469 276

Table A.4: the optimised coordinates of a pentacene dimer, as used in the calculations.

A.5 PbS+7C and Tetracene

Atom	X	Y	Z
1 Pb	26.043 257 16	19.389 059 69	14.525 296 47
2 Pb	17.719 860 62	26.452 819 52	22.918 885 26
3 Pb	26.363 538 17	17.207 583 94	29.642 480 58
4 Pb	27.891 067 37	23.383 635 77	20.520 894 04
5 Pb	26.019 961 25	10.229 037 62	20.989 195 02
6 Pb	22.926 020 89	19.121 808 38	29.491 731 87
7 Pb	29.104 387 86	20.608 964 17	17.497 877 86
8 Pb	30.400 949 41	24.725 634 11	23.231 980 6
9 Pb	26.940 951 71	26.696 967 41	22.818 295 71
10 Pb	26.919 607 68	16.550 038 71	17.514 481 77
11 Pb	23.250 154 6	18.291 402 19	17.133 310 83
12 Pb	27.886 989 5	23.764 687 8	26.523 979 86
13 Pb	24.635 288 7	13.221 399 78	29.313 734 78
14 Pb	14.591 609 18	15.770 763 01	20.064 479 65
15 Pb	24.142 509 77	15.749 771 2	20.687 729 81
16 Pb	27.901 283 7	13.945 223 42	20.787 260 85
17 Pb	15.549 209 38	12.898 032 44	23.276 963 16
18 Pb	20.572 471 07	27.441 433 1	26.077 391 66
19 Pb	14.717 571 15	15.945 750 45	25.753 556 95
20 Pb	26.037 418 3	19.355 029 48	20.232 711 03
21 Pb	24.543 013 88	15.415 932 02	14.537 100 71
22 Pb	23.389 146 27	16.274 215 28	32.452 221 57
23 Pb	24.048 210 95	16.084 302 02	26.433 600 37
24 Pb	28.177 396 55	14.063 464 55	27.311 066 94
25 Pb	24.176 273 06	25.632 536 1	26.258 407 9
26 Pb	13.650 851 16	18.882 613 57	23.162 277 41
27 Pb	25.120 017 24	22.491 406 24	17.270 063 29
28 Pb	21.474 716 55	24.195 102 3	17.124 970 31
29 Pb	20.649 155 84	27.370 033 93	19.654 379 51
30 Pb	29.672 877 57	17.718 837 6	21.002 034 4
31 Pb	31.180 487 22	14.696 516 17	23.348 785 16
32 Pb	32.243 819 03	18.795 213 36	23.471 392 44
33 Pb	31.226 867 89	21.520 914 39	20.545 026 39
34 Pb	28.742 255 14	20.773 230 28	23.665 347 93
35 Pb	26.825 579 98	16.598 541 27	23.722 875 78
36 Pb	25.764 674 3	19.816 082 41	26.501 763 05
37 Pb	25.702 247 14	20.182 650 57	32.882 889 93
38 Pb	24.936 746 08	22.905 891 84	29.174 118 54
39 Pb	25.165 206 22	22.505 220 56	23.366 933 15
40 Pb	20.851 468 77	24.615 641 03	29.388 137 28
41 Pb	21.527 097 07	21.896 533 99	32.279 745 86
42 Pb	21.185 191 05	24.722 545 61	23.080 227 87
43 Pb	23.119 112 73	18.778 987 48	23.294 441 21
44 Pb	30.042 812 56	17.836 101 48	27.303 393 41
45 Pb	31.619 324 59	21.737 735 06	26.403 682 02
46 Pb	21.865 313 51	11.978 170 85	20.267 105 28
47 Pb	22.904 617 95	9.300 760 499	23.674 063 07
48 Pb	19.124 590 4	11.035 170 15	23.420 629 39
49 Pb	21.753 835 94	12.411 052 56	26.479 226 83
50 Pb	22.972 074 92	28.061 924 1	22.961 838 6
51 Pb	22.016 717 31	21.983 633 46	26.042 158 87
52 Pb	24.451 465 29	25.404 936 47	19.939 853 05
53 Pb	20.465 657 2	17.616 736 92	14.197 970 95
54 Pb	20.950 484 59	14.291 189 08	17.145 701 4
55 Pb	17.383 295 64	16.655 728 33	17.017 958 07
56 Pb	18.438 395 53	13.892 363 98	20.182 157 76
57 Pb	20.169 034 98	17.766 718 9	20.271 017 21
58 Pb	20.790 164 83	14.900 511 15	23.354 756 49
59 Pb	17.269 888 01	17.188 935 14	22.915 059 99
60 Pb	18.182 544 12	13.832 597 56	26.200 197 15
61 Pb	20.019 550 42	18.176 935 82	26.248 211 47
62 Pb	20.630 494 97	15.117 126 17	29.509 308 71
63 Pb	16.746 161 93	16.924 668 84	29.394 544 93
64 Pb	19.915 752 07	18.148 614 77	32.044 968 28

65 Pb	28.778 338 21	21.024 727 75	29.662 904 61
66 Pb	22.649 041 58	21.161 491 16	14.245 012 59
67 Pb	28.401 854 6	11.103 815 15	23.975 694 84
68 Pb	24.832 500 34	12.998 069 54	23.434 197 55
69 Pb	22.025 853 16	21.660 778 84	20.130 848 72
70 Pb	25.488 326 7	10.212 868 9	27.040 092 33
71 Pb	19.467 575 52	20.352 794 82	17.044 442 35
72 Pb	25.709 238 38	12.398 646 35	17.302 838 84
73 Pb	16.550 260 32	19.673 578 43	19.854 437 71
74 Pb	18.125 548 39	23.525 664 91	19.722 841 13
75 Pb	19.273 493 48	20.744 888 98	23.173 132 82
76 Pb	15.064 279 31	22.804 628 37	23.350 558 7
77 Pb	16.153 430 05	19.688 909 23	25.966 548 97
78 Pb	17.944 122 92	23.809 344 01	26.025 703 29
79 Pb	18.993 363 05	21.156 816 45	29.291 893 57
80 S	22.057 115 56	21.891 488 09	29.480 686 13
81 S	21.112 194 18	24.628 663 21	26.179 612 29
82 S	29.549 963 56	18.026 244 78	23.873 818 36
83 S	24.030 378	15.627 002 28	17.088 862 65
84 S	26.272 574 07	19.336 994 93	17.482 199 89
85 S	24.968 916 62	12.954 790 32	20.597 274 22
86 S	22.241 214 02	21.526 820 42	16.841 152 65
87 S	27.716 204 76	23.835 013 6	23.518 511 14
88 S	23.305 547 74	18.556 074 48	14.321 288 73
89 S	27.080 172 4	16.718 544 7	20.736 609 06
90 S	24.738 169 99	12.894 504 5	26.668 052 62
91 S	23.212 495 91	18.905 776 97	20.504 157 78
92 S	31.475 387 39	21.906 551 57	23.501 348 62
93 S	14.407 437 86	16.003 783 3	23.078 156 01
94 S	23.827 702 05	15.908 120 93	23.397 954 5
95 S	25.815 355 24	19.497 270 26	23.718 546 14
96 S	21.663 065 97	24.638 960 91	20.222 981 47
97 S	26.794 657 14	16.797 560 44	26.679 039 01
98 S	25.281 750 09	22.585 566 86	19.990 341 79
99 S	29.114 146 86	20.914 272 18	26.536 993 77
100 S	22.623 319 36	18.989 815 52	32.526 213 45
101 S	20.309 610 12	27.409 280 36	22.733 309 67
102 S	23.158 527 69	18.972 753 76	26.617 693 66
103 S	21.944 779 9	11.957 168 26	23.449 711 77
104 S	23.605 904 96	16.026 676 64	29.700 346 08
105 S	25.803 989 8	20.081 966 74	29.770 946 45
106 S	28.530 403 18	20.469 514 86	20.483 765 78
107 S	22.052 267 56	21.946 717 63	23.005 764 53
108 S	24.185 564 79	25.456 371 57	22.650 482 44
109 S	24.985 170 52	22.591 497 86	26.092 695 37
110 S	25.877 901 57	10.407 495 24	23.652 626 79
111 S	20.239 426 79	17.790 785 25	16.929 536 35
112 S	21.338 225 28	14.845 880 33	20.384 366 02
113 S	17.420 958 3	16.664 649 04	19.849 775 02
114 S	18.173 568 17	14.014 32	23.385 865 9
115 S	20.182 155 03	17.786 446 46	23.268 968 95
116 S	20.891 254 4	15.032 476 99	26.269 341 11
117 S	17.352 233 46	17.187 320 07	25.958 364 86
118 S	19.727 504 84	17.985 486 25	29.173 073 29
119 S	19.482 152 91	20.575 472 55	20.259 068 78
120 S	16.417 957 06	19.935 997 7	23.039 219 45
121 S	18.366 463 55	23.786 330 51	23.238 182 38
122 S	19.174 959 1	20.808 653 1	26.023 628 4
123 S	27.889 112 49	13.743 775 28	23.715 184 23
124 H	18.263 665 07	23.428 599 33	16.949 218 77
125 O	18.975 351 38	23.184 913 87	17.614 442 29
126 O	17.834 379 35	26.437 419 96	25.494 973 23
127 H	19.103 898 07	11.121 325 55	20.347 003 86
128 C	28.286 032 8	21.462 991 39	13.965 142 12
129 O	28.061 071 59	20.685 708 99	15.009 994 27
130 O	27.474 450 03	21.906 546 04	13.167 713 18
131 H	29.294 347 95	21.851 596 94	13.854 419 55
132 H	21.605 194 45	12.372 651 39	29.651 422 82
133 O	22.189 210 69	12.858 264 19	29.075 233 86
134 O	22.199 822 43	14.651 451 66	14.382 312 15
135 C	21.271 220 24	13.852 180 67	14.051 099 16
136 C	22.733 673 54	29.349 681 12	19.644 797 55
137 O	22.640 630 97	28.392 533 68	20.492 856 99
138 O	21.827 964 98	29.635 569 26	18.831 775 65
139 H	23.753 380 9	29.830 702 27	19.746 528 44
140 C	18.131 017 67	13.659 748 73	29.976 026 31
141 O	18.023 756 93	14.538 956 63	29.042 481 12
142 O	19.238 042 63	13.411 576 9	30.554 215 62
143 H	17.198 955 37	13.149 857 88	30.242 557 53
144 C	20.141 566 77	28.679 507 15	28.870 751 29
145 O	20.127 516 84	29.500 247 36	27.909 188 93
146 O	20.655 946 74	27.516 163 35	28.770 544 76
147 H	19.572 393 93	28.907 862 6	29.790 921 62
148 H	22.869 218 61	28.850 320 35	25.916 912 36
149 O	22.851 860 92	28.017 570 68	25.469 934 25
150 H	15.933 111 03	27.675 393 11	17.887 108 4

151 O	16.854 011 46	25.414 229 55	18.659 850 06
152 C	26.051 816 08	29.336 557 29	21.562 212 21
153 O	27.217 962 6	28.929 715 2	21.279 032 38
154 O	25.295 963 09	28.905 156 63	22.520 246 13
155 H	25.651 151 78	30.221 480 19	21.030 844 26
156 H	25.815 659 11	21.958 824 03	13.962 747 86
157 O	25.039 627 29	21.533 65	14.713 432 84
158 C	30.009 178 43	17.342 279 35	17.422 879 17
159 O	29.294 609 09	18.266 447 75	17.996 079 19
160 H	27.257 179 97	26.488 242 03	26.765 105 5
161 O	26.647 908 35	25.899 005 05	26.260 548 52
162 O	15.727 127 85	22.729 440 71	25.535 410 57
163 H	15.170 995 91	23.364 479 55	26.017 036 02
164 C	22.698 501 53	8.935 936 821	20.177 552 36
165 O	23.427 793 76	9.508 606 36	21.051 019
166 O	21.955 218 31	9.480 336 346	19.274 682 15
167 H	22.516 058 23	7.825 027 226	20.139 532 85
168 H	18.818 139 02	21.381 338 29	32.201 897 97
169 O	19.515 586 48	20.968 384 78	31.662 179 97
170 C	18.998 850 49	20.030 961 9	13.584 097 4
171 O	20.116 357 3	20.098 456 14	14.258 842 01
172 H	18.342 326 62	11.137 923 71	26.443 708 98
173 O	18.929 827 06	11.671 449 11	25.939 173 16
174 O	20.569 514 46	13.221 688 08	14.873 493 04
175 H	21.050 855 64	13.636 040 54	12.963 038 18
176 C	32.389 526 35	12.013 298 95	22.760 857 33
177 O	31.154 932 06	11.707 546 85	22.781 124 39
178 O	32.931 669 32	13.172 866 9	22.698 959 12
179 H	33.058 332 38	11.111 088 21	22.628 209 14
180 C	28.556 691 14	21.291 629 61	33.256 168 37
181 O	28.073 624 3	21.006 448 18	32.086 556 8
182 O	27.953 965 92	21.215 083 71	34.322 853 99
183 H	29.613 255 01	21.692 403 52	33.197 006 78
184 H	15.534 609 53	22.368 977 02	19.450 797 09
185 O	16.240 704 57	22.018 619 36	20.071 550 62
186 H	16.259 838 5	27.617 922 79	26.061 577 69
187 O	19.554 557 16	11.554 757 91	21.023 300 65
188 C	20.229 433 83	7.463 935 299	24.169 553 13
189 O	20.411 381 24	8.737 109 183	24.326 480 46
190 O	21.065 759 04	6.707 432 96	23.658 184 28
191 H	19.331 670 14	7.096 973 336	24.504 347 18
192 H	30.676 229 57	14.914 953 18	28.048 305 15
193 O	29.912 291 14	15.491 033 22	27.981 843 56
194 H	31.031 538 82	17.639 686 36	17.235 312 46
195 O	29.600 093 09	16.207 311 64	17.228 762 69
196 H	18.105 206 91	13.493 021 95	17.314 555 88
197 O	18.615 561 43	14.315 794 82	17.670 504 37
198 O	13.168 247 91	24.362 332 09	23.845 274 99
199 H	11.930 377 33	26.728 847 48	23.077 654 21
200 H	29.618 074 75	27.291 336 42	22.150 434 58
201 O	29.258 048 87	26.380 588 25	22.085 604 85
202 O	27.772 062	10.955 299 29	16.423 897 45
203 H	28.414 285 89	9.212 957 029	17.386 337 38
204 C	32.143 144 85	20.485 710 64	16.791 405
205 O	31.651 774 37	20.921 625 63	17.913 395 05
206 O	31.472 198 41	20.262 284 7	15.795 067 6
207 H	33.297 818 75	20.482 499 5	16.730 811 93
208 H	15.884 809 61	10.365 435 5	23.137 561 64
209 O	16.571 252 98	10.897 076 32	23.639 269 67
210 O	32.450 456 29	17.640 080 79	28.096 953 73
211 H	34.220 954 54	18.497 025 17	27.679 287 94
212 C	30.350 038 08	25.263 188 37	27.111 616 22
213 O	30.547 203 62	24.361 665 08	26.195 514 98
214 O	29.269 166 62	25.519 284 12	27.712 016 03
215 H	31.257 135 29	25.989 865 76	27.270 714 83
216 H	33.635 295 88	16.405 474 64	23.025 709 28
217 O	32.648 565 94	16.598 424 93	23.082 854 15
218 O	26.773 078 62	25.572 707 05	20.797 530 52
219 H	27.224 049 33	26.301 096 32	20.330 297 49
220 C	14.365 503 02	14.577 620 76	28.784 185 75
221 O	14.478 800 12	15.873 633 78	28.798 976 12
222 O	14.374 978 99	13.895 745 82	27.797 348 51
223 H	14.200 377 09	14.178 535 28	29.774 896 96
224 H	20.731 937 91	24.697 472 9	32.244 142 42
225 O	20.541 293 57	23.947 989 49	31.684 318 78
226 O	26.952 051 3	10.073 500 79	18.363 890 66
227 C	27.737 567 38	10.071 439	17.331 184 63
228 C	29.273 003 46	11.038 115 85	27.421 687 65
229 O	28.316 674 2	11.027 546 4	26.569 804 59
230 O	29.602 790 63	11.999 029 62	28.164 783 04
231 H	29.694 397 1	10.014 931 95	27.666 778 56
232 H	16.019 776 24	19.793 269 91	17.149 456 81
233 O	16.873 623 67	19.388 608 55	17.372 150 01
234 C	13.704 706 92	25.481 411 19	23.543 488 67
235 O	14.989 534 83	25.540 531 75	23.262 723 07
236 H	18.186 143 86	23.906 841 65	29.753 298 31

237 O	18.773 736 58	23.500 995 35	29.085 360 69
238 H	26.621 437 5	10.276 660 33	31.131 093 59
239 O	26.446 206 27	9.025 093 007	29.579 212 76
240 H	21.166 938 26	11.300 305 31	17.632 456 19
241 O	21.041 493 42	12.198 512 1	18.071 798 25
242 H	28.061 805 12	23.616 084 21	29.557 136 03
243 O	27.544 398 27	23.025 408 5	28.918 898 96
244 H	28.160 393 1	13.498 546 9	17.832 812 1
245 O	27.286 625 54	13.607 252 38	18.259 751 71
246 O	23.990 223 81	25.113 309 62	28.434 199 7
247 H	24.410 989 74	25.803 253 03	28.967 866 7
248 H	24.013 114 37	24.978 329 48	16.368 598 37
249 O	23.877 858 32	24.446 738 8	17.172 244 71
250 C	16.711 481 81	26.651 775 97	26.123 984 87
251 O	16.200 774 54	25.772 408 04	26.855 107 19
252 H	29.504 987 61	17.762 578 44	30.030 328 86
253 O	28.826 662 82	18.144 472 33	29.371 519 33
254 O	26.080 513 04	11.238 932 94	29.363 391 97
255 C	26.389 569 2	10.166 158 65	30.042 055 21
256 H	12.636 174 53	21.769 823 25	24.204 364 21
257 O	13.360 583 05	21.224 993 95	23.799 915 34
258 O	32.732 372 48	19.380 513 81	26.586 442 24
259 C	33.115 905 35	18.516 138 58	27.394 069 62
260 C	31.181 391 79	22.946 914 53	29.706 853 84
261 O	31.404 665 75	21.965 217 71	28.862 515 14
262 O	30.083 497 19	23.149 866 97	30.228 049 16
263 H	32.015 990 2	23.620 310 75	29.958 018 57
264 H	13.323 079 52	19.012 797 9	25.993 726 17
265 O	14.011 013 83	18.570 385 17	25.393 673 65
266 O	18.774 547 82	19.189 505 28	12.691 822 76
267 H	18.025 929 03	21.561 961	14.776 765 98
268 C	25.193 354 12	23.456 344 71	32.355 478 84
269 O	25.629 814 83	24.017 834 07	31.320 435 28
270 O	24.485 459 5	22.430 427 74	32.463 475 98
271 H	25.520 907 77	24.018 643 72	33.250 411 74
272 C	27.966 985 56	23.853 246 52	16.844 621 11
273 O	28.186 494 3	23.221 766 64	17.941 173 31
274 O	26.873 256 85	23.939 041 37	16.240 635 06
275 H	28.790 480 63	24.470 562 02	16.402 362 71
276 C	13.635 405 59	18.938 770 59	19.040 503 72
277 O	14.352 730 22	19.882 406 16	18.648 890 72
278 O	14.004 145 69	18.157 074 85	20.032 598 41
279 H	12.445 527 68	17.433 721 7	18.135 334 85
280 H	15.193 552 54	13.468 195 44	26.202 272 51
281 O	15.713 791 21	13.893 154 37	25.516 391 48
282 O	17.571 970 07	16.133 464 15	31.953 622 1
283 H	16.021 952 38	16.646 195 51	33.211 312 71
284 H	30.992 467 27	14.709 707 43	20.610 428 62
285 O	30.410 781 85	15.194 376 72	21.229 517 04
286 H	26.306 553 74	12.858 448 63	14.597 689 68
287 O	25.837 026 36	13.510 073 73	15.170 587 79
288 C	29.555 928 33	11.110 953 24	20.795 258 47
289 O	28.497 922 22	10.868 317 91	21.536 892 25
290 O	29.684 123 01	12.033 239 8	20.006 694 57
291 H	30.446 769 39	10.448 574 39	21.006 065 3
292 H	20.646 833 85	15.094 146 79	32.495 687 91
293 O	21.088 063 54	15.864 050 07	32.118 069 35
294 O	15.913 237 66	17.568 103 37	31.434 252 96
295 C	16.559 292 52	16.854 767 34	32.315 358 44
296 H	32.513 183 26	18.786 195 34	20.592 932 81
297 O	31.928 895 69	19.246 955 77	21.160 773 55
298 H	27.702 518 73	17.156 370 29	33.433 161 22
299 O	26.356 559 77	15.578 06	33.387 871 09
300 H	27.622 545 4	16.368 675 81	14.875 054 81
301 O	26.741 327 58	16.618 327 87	15.132 425 23
302 O	25.884 078 59	17.610 094 42	32.545 210 34
303 C	26.697 494 31	16.766 952 73	33.113 595 74
304 C	13.783 922 72	15.013 466 98	17.196 795 38
305 O	14.841 719 7	15.806 833 25	17.315 372 34
306 O	13.061 125 12	14.839 968 45	18.256 593 6
307 H	13.179 982 53	14.793 642 88	15.261 515 01
308 C	20.847 480 95	27.011 208 86	15.973 793 81
309 O	20.673 802 26	25.957 935 14	15.292 307 96
310 O	21.281 719 28	26.971 387 81	17.210 779 96
311 H	19.525 013 55	28.529 824 47	15.259 186 37
312 C	16.000 865 64	12.119 030 29	19.246 764 32
313 O	15.665 282 4	12.902 813 2	20.296 814
314 O	17.166 922 35	11.985 626 86	18.860 940 88
315 H	15.181 247 65	11.548 346 8	18.827 203 07
316 C	22.462 918 31	9.310 366 175	27.179 542 2
317 O	23.184 276 46	9.498 523 187	28.206 057 82
318 O	22.818 777 51	9.487 532 629	25.967 627 56
319 H	21.397 143 8	9.120 369 991	27.434 140 99
320 C	16.000 481 95	20.517 256 74	30.062 276 81
321 O	16.770 377 04	21.499 519 28	30.413 966 99
322 O	16.232 929 91	19.617 895 15	29.181 213 87

323 H	15.063 177 75	20.453 105 35	30.678 097 49
324 C	17.543 779 57	15.816 261 23	13.968 520 99
325 O	18.620 100 92	16.012 008 53	14.601 676 52
326 O	16.458 490 08	15.614 533 04	14.630 588 91
327 H	18.494 487 12	15.709 438 71	12.008 243 59
328 H	27.612 779 48	14.461 646 95	30.093 661 7
329 O	27.030 091 42	14.546 613 5	29.336 432 78
330 H	31.032 695 48	24.581 063 6	20.581 638 5
331 O	30.530 164 21	23.877 297 28	21.065 450 32
332 C	16.905 328 73	26.479 121 24	19.351 248 02
333 O	17.788 794 56	26.621 007 06	20.301 169 47
334 C	20.277 752 01	18.910 835 92	9.578 877 211
335 C	19.060 371 48	19.093 748 78	8.591 928 813
336 C	17.724 272 2	18.592 871 25	9.352 043 107
337 C	17.579 240 4	17.068 785 88	9.608 104 02
338 C	16.297 358 78	16.745 721 41	10.462 126 64
339 C	16.493 667 88	16.688 592 01	12.008 908 22
340 C	17.488 588 96	15.652 036 96	12.460 766 57
341 H	21.195 140 73	18.967 818 42	9.000 567 897
342 H	20.077 869 35	17.964 003 48	10.091 317 87
343 H	20.328 882 89	19.594 493 34	10.382 059 95
344 H	19.123 373 29	18.374 978 3	7.677 146 011
345 H	18.932 509 29	20.110 873 24	8.274 708 467
346 H	16.916 356 21	18.879 657 11	8.727 196 929
347 H	17.629 965	19.156 142 44	10.286 967 14
348 H	18.373 761 32	16.648 263 24	10.222 731 07
349 H	17.525 452 27	16.595 987 73	8.618 309 981
350 H	15.996 628 91	15.747 272 66	10.192 719 53
351 H	15.364 070 99	17.278 094 36	10.165 401 36
352 H	15.445 377 42	16.412 745 41	12.350 325 27
353 H	16.780 632 11	17.718 236 65	12.292 082 39
354 H	17.044 097 45	14.674 848 73	12.349 203 31
355 C	22.538 828 32	29.942 495 02	9.441 106 964
356 C	22.006 796 92	29.132 582 67	10.651 868 71
357 C	22.701 501 19	27.789 073 68	10.819 379 94
358 C	22.356 403 68	27.017 253 79	12.199 248 54
359 C	22.472 114 78	27.873 954	13.506 528 56
360 C	21.119 080 88	28.559 721 61	13.902 948 73
361 C	20.585 191 43	28.395 706 29	15.311 050 51
362 H	23.658 429 21	30.022 731 59	9.611 001 526
363 H	22.134 647 34	30.925 892 67	9.395 859 002
364 H	22.352 821 95	29.473 613 31	8.508 255 679
365 H	20.889 707 48	29.004 838 17	10.423 128 37
366 H	22.069 106 42	29.669 305 86	11.610 006 19
367 H	23.699 353 28	27.853 141 81	10.722 570 8
368 H	22.347 377 98	27.188 641 18	9.985 008 227
369 H	22.983 650 57	26.147 177 16	12.260 819 5
370 H	21.276 276 22	26.723 402 18	12.210 833 64
371 H	23.254 739 18	28.699 194 09	13.423 248 93
372 H	22.742 279 05	27.242 372 32	14.320 222 36
373 H	20.340 842 77	28.150 025 76	13.245 725 79
374 H	21.124 235 55	29.655 976 69	13.653 234 01
375 H	21.095 841 73	29.152 115 85	15.825 030 67
376 C	11.751 904 98	7.365 089 338	13.141 087 4
377 C	11.005 869 72	8.534 622 396	13.820 571 92
378 C	11.926 989 54	9.687 801 22	14.029 833 08
379 C	11.631 306 41	10.838 165 92	15.161 948 71
380 C	12.750 510 09	11.912 328 96	15.050 498 46
381 C	12.778 966 52	12.927 983 56	16.266 987 95
382 C	13.671 845 13	14.153 930 73	15.935 012 04
383 H	12.229 523 4	7.679 331 014	12.178 756 37
384 H	11.111 760 72	6.463 998 068	13.082 048 42
385 H	12.639 081 22	7.152 961 826	13.799 007 32
386 H	10.632 109 82	8.212 983 082	14.829 080 37
387 H	10.123 783 48	8.792 005 293	13.271 183 26
388 H	12.153 237 3	10.140 569 61	13.050 438 44
389 H	12.901 967 82	9.274 113 682	14.251 085 97
390 H	11.620 529 24	10.381 180 16	16.131 056 52
391 H	10.630 841 59	11.266 143 48	15.068 677 46
392 H	12.710 909 68	12.441 267 34	14.121 206 24
393 H	13.692 884 6	11.336 426 8	15.048 937 63
394 H	13.264 615 62	12.435 244 41	17.102 217 76
395 H	11.741 755 95	13.073 087 75	16.691 779 53
396 H	14.650 254 43	13.893 989 85	15.591 703 63
397 C	8.452 695 572	17.821 844 56	11.892 642 62
398 C	9.542 184 332	18.772 528 09	12.443 946 44
399 C	9.878 547 167	18.275 092 69	13.873 994 76
400 C	10.766 286 47	19.098 204 28	14.705 748 76
401 C	11.109 907 2	18.608 751 73	16.109 570 58
402 C	12.207 207 11	19.337 142 47	16.917 744 75
403 C	12.419 363 51	18.580 401 97	18.223 267 25
404 H	7.803 009 213	17.553 607 56	12.743 512 62
405 H	8.891 884 789	16.885 276 88	11.550 305 6
406 H	7.779 045 456	18.274 079 32	11.206 061 35
407 H	9.262 865 135	19.883 556 24	12.434 776 36
408 H	10.400 083 2	18.683 053 61	11.748 721 1

409 H	10.291 310 68	17.228 592 86	13.785 245 19
410 H	8.957 369 092	18.145 336 85	14.410 638 95
411 H	10.268 645 03	20.096 996 55	14.769 540 66
412 H	11.668 148 77	19.477 271 91	14.200 703 46
413 H	11.449 227 44	17.533 787 05	16.091 884 28
414 H	10.170 147 09	18.548 688 19	16.699 382 83
415 H	11.907 791 56	20.434 813 66	17.110 540 67
416 H	13.126 952 8	19.387 953 19	16.311 801 4
417 H	11.509 261 92	18.707 346 28	18.767 959
418 C	13.448 468 26	23.754 682 49	9.643 919 564
419 C	14.026 641 67	24.039 947 85	11.030 388 73
420 C	13.462 279 85	23.028 574 75	12.017 134 7
421 C	14.387 839 66	21.822 866 2	12.302 246 26
422 C	15.791 672 5	22.111 500 16	12.975 006 74
423 C	16.592 747 19	20.805 879 68	13.295 483 75
424 C	17.992 795 37	21.139 352 07	13.753 832 9
425 H	13.583 024 63	22.684 198 01	9.338 712 87
426 H	13.776 527 94	24.585 851 87	9.009 151 42
427 H	12.330 566 62	23.927 840 62	9.735 662 494
428 H	13.821 074 15	25.088 683 61	11.272 406 15
429 H	15.103 679 6	24.121 782 47	11.166 273 88
430 H	12.491 448 93	22.632 303 49	11.571 415 7
431 H	13.260 298 76	23.544 117 01	13.022 098 59
432 H	14.591 636 76	21.403 740 03	11.322 983 22
433 H	13.754 218 16	21.245 757 91	12.974 639 58
434 H	15.781 585 68	22.568 859 61	13.945 083 89
435 H	16.366 648 95	22.689 332 64	12.253 681 34
436 H	16.583 749 05	20.212 168 15	12.337 350 46
437 H	15.985 669 02	20.204 195 66	14.011 764 68
438 H	18.352 849 97	22.006 604 75	13.139 105 27
439 C	14.630 827 97	34.360 898 89	24.110 475 87
440 C	14.960 020 72	32.993 298 78	23.386 772 92
441 C	14.018 452 02	31.873 402 56	23.639 874 02
442 C	14.374 435 73	30.508 729 38	23.165 185 36
443 C	13.440 119 38	29.386 367 18	23.694 918 34
444 C	13.769 282 14	28.032 080 52	23.014 847 18
445 C	12.920 346 24	26.835 472 53	23.553 610 76
446 H	13.510 677 28	34.680 115 31	24.225 793 21
447 H	14.889 203 59	35.118 469 34	23.357 934 07
448 H	15.147 045 06	34.700 015 8	25.045 654 08
449 H	15.945 742 93	32.692 446 66	23.777 050 17
450 H	15.066 701 25	33.169 940 2	22.300 847 7
451 H	13.049 522 45	32.112 868 92	23.309 071 45
452 H	13.841 330 56	31.855 775 65	24.692 947 38
453 H	15.354 370 32	30.387 063 68	23.717 173 33
454 H	14.564 218 36	30.517 674 37	22.077 163 17
455 H	12.298 570 16	29.498 215 14	23.626 214 88
456 H	13.594 460 6	29.289 245 99	24.804 785 65
457 H	14.873 760 95	27.802 907 66	22.972 311 39
458 H	13.667 168 9	28.216 380 49	21.912 522 23
459 H	12.753 682 01	27.089 883 97	24.670 554 85
460 C	19.477 295 12	34.417 342 64	18.137 341 41
461 C	18.658 379 03	33.523 503 34	19.077 655 63
462 C	18.372 159 08	32.092 310 12	18.556 626 42
463 C	17.765 451 69	31.062 594 48	19.562 305 23
464 C	17.412 696 2	29.718 294 87	18.913 777 22
465 C	16.244 269 03	28.913 903 97	19.637 094 1
466 C	15.953 466 5	27.561 162 08	18.972 045 08
467 H	20.563 703 53	34.136 264 42	18.158 232 2
468 H	19.374 245 75	35.536 001 93	18.445 795 86
469 H	19.096 100 37	34.344 066 67	17.079 622 61
470 H	17.685 223 65	34.054 121 31	19.274 824 2
471 H	19.165 352 14	33.566 680 07	20.106 294 23
472 H	19.276 526 78	31.617 314 41	18.180 006 59
473 H	17.650 455 83	32.294 287 14	17.739 744 3
474 H	16.850 060 3	31.509 495 51	19.984 382 54
475 H	18.355 342 11	30.873 528 8	20.473 450 15
476 H	18.276 820 65	28.980 875 03	18.964 628 15
477 H	17.066 438 19	29.844 344 7	17.872 110 95
478 H	15.457 107 04	29.666 562 8	19.592 425 86
479 H	16.450 565 91	28.784 860 65	20.688 797 55
480 H	14.985 766 11	27.093 787 33	19.158 950 19
481 C	8.748 859 228	29.297 076 88	10.446 208 07
482 C	8.580 935 436	29.950 474 83	11.610 716 38
483 C	9.012 582 823	29.441 471 39	12.876 446 25
484 C	8.874 197 313	30.068 432 81	14.079 261 3
485 C	10.060 929 06	28.322 238 72	15.286 993 75
486 C	10.260 696 99	27.662 154 42	14.061 051 24
487 C	9.697 729 228	28.159 414 5	12.885 824 86
488 C	9.913 135 339	27.525 914 14	11.580 573 89
489 C	9.416 330 731	28.049 213 54	10.411 237 91
490 C	10.109 997 62	29.948 985 61	20.234 605 76
491 C	9.620 799 091	30.506 167 82	19.037 491 7
492 C	9.690 810 065	29.752 737 56	17.801 277 38
493 C	9.225 395 052	30.226 635 5	16.579 711 06
494 C	9.314 637 254	29.540 276 41	15.331 771 94

495 C	10.552 529 7	27.824 879 5	16.527 909 5
496 C	10.355 875 17	28.488 433 79	17.776 685 08
497 C	10.822 940 87	27.911 687 25	19.011 693 04
498 C	10.669 447 7	28.620 792 17	20.193 065 05
499 H	8.408 511 027	29.735 514 56	9.482 158 715
500 H	8.191 038 898	30.982 839 45	11.535 356 81
501 H	8.388 208 841	31.029 532 55	14.144 194 52
502 H	11.008 792 02	28.185 698 63	21.110 199 86
503 H	10.900 074 69	26.804 319 01	13.994 530 52
504 H	10.499 322 59	26.652 228 12	11.537 664 41
505 H	9.649 772 372	27.495 047 04	9.536 647 578
506 H	10.072 392 5	30.550 742 74	21.144 898 32
507 H	9.174 233 809	31.510 408 9	18.984 408 94
508 H	8.774 205 225	31.168 633 49	16.531 107 72
509 H	11.139 170 92	26.943 955 48	16.495 174 29
510 H	11.290 432 43	26.897 233 75	19.044 126 02

Table A.5: the coordinates of the first time step in the MD simulation for the PbS QD with the 7C-ligand, used as the starting setup in the MD simulation.

A.6 PbS+9C and Tetracene

Atom	X	Y	Z
1 Pb	27.091 390 27	19.721 814 27	14.699 243 22
2 Pb	17.309 544 59	26.092 930 36	22.186 111 19
3 Pb	27.432 468 83	18.279 046 1	29.683 792 12
4 Pb	28.047 936 52	24.167 862 27	20.385 688 9
5 Pb	27.596 441 39	10.858 064 74	21.487 201 96
6 Pb	23.094 038 98	19.410 173 48	29.262 499 4
7 Pb	29.737 462 33	21.522 525 16	17.233 665 45
8 Pb	30.407 853 89	25.530 638 82	23.510 397 42
9 Pb	27.147 864 12	27.775 918 32	22.679 142 34
10 Pb	27.957 335 65	17.216 280 03	17.533 508 88
11 Pb	24.026 769 51	18.676 104 89	17.376 926 25
12 Pb	27.362 004 24	24.582 348 66	26.181 232 95
13 Pb	25.508 705 07	14.283 794 22	30.075 990 18
14 Pb	15.388 772 13	15.866 346 75	19.862 903 14
15 Pb	25.124 714 66	16.026 183 57	20.327 612 98
16 Pb	29.130 783 39	14.781 328 7	21.186 376 04
17 Pb	16.798 317 76	12.606 802 54	23.136 292 5
18 Pb	19.832 664 02	27.312 721	25.569 336 8
19 Pb	15.361 756 62	15.701 225 44	25.708 787 02
20 Pb	26.626 753 76	20.039 322 56	20.296 546 46
21 Pb	25.496 315 62	15.543 197 12	14.846 992 55
22 Pb	23.805 805 26	17.144 452 93	32.458 424 67
23 Pb	24.827 006 44	16.692 321 26	26.817 953 89
24 Pb	28.747 886 12	15.404 796 03	27.547 038 05
25 Pb	23.775 727 5	26.044 854 47	26.081 054 42
26 Pb	14.549 490 61	18.596 571 21	22.643 492 73
27 Pb	25.810 554 45	22.996 881 63	17.199 021 69
28 Pb	21.898 651 67	24.158 340 57	16.787 740 69
29 Pb	20.337 932 86	27.218 709 39	19.438 094 34
30 Pb	30.729 853 28	18.707 742 47	20.906 723 4
31 Pb	32.356 912 41	15.992 185 54	23.803 889 35
32 Pb	33.056 223 39	20.109 931 42	23.607 772 96
33 Pb	31.840 734 81	22.938 189 75	20.842 232 22
34 Pb	29.191 966 78	21.663 644 08	23.460 282
35 Pb	27.716 364 42	17.663 912 45	23.649 642 19
36 Pb	26.298 659 13	20.810 070 9	26.627 656 75
37 Pb	25.708 727 95	21.042 691 43	32.374 236 43
38 Pb	24.484 863 93	23.709 117 48	29.088 606 67
39 Pb	25.037 311 83	23.025 128 53	23.121 831 65
40 Pb	20.593 391 23	24.846 208 6	28.901 765 7
41 Pb	21.423 080 97	22.389 910 37	31.835 185 61
42 Pb	21.229 551 17	24.805 503 05	22.766 089 01
43 Pb	23.845 138 11	19.032 242 32	23.219 550 63
44 Pb	30.358 775 34	19.060 665 6	26.993 280 18
45 Pb	31.852 015 79	22.815 387 39	26.591 230 48
46 Pb	23.019 369 77	11.992 525 34	20.467 279 71
47 Pb	24.563 530 42	9.910 637 038	24.015 946 68
48 Pb	20.404 243 79	11.138 656 98	23.575 378 61
49 Pb	22.853 896 45	12.700 127 44	26.720 295 98
50 Pb	22.704 928	28.439 010 91	23.027 367 69
51 Pb	22.252 180 87	21.807 480 4	25.934 664 55
52 Pb	24.732 474 97	25.904 708 75	20.284 113 24
53 Pb	21.603 072 69	17.665 954 9	14.240 050 03
54 Pb	22.451 460 45	14.563 885 02	17.658 623 99
55 Pb	18.476 385 21	16.104 759 14	16.839 675 59

56 Pb	19.424 277 71	13.955 777 56	20.069 162 88
57 Pb	20.894 048 95	17.782 535 31	20.092 348 59
58 Pb	22.403 037 69	15.232 895 54	23.501 021 83
59 Pb	18.130 680 2	16.603 353 73	22.925 806 27
60 Pb	18.843 576 75	14.019 013 84	26.101 069 45
61 Pb	20.738 014 54	17.891 132 32	25.971 874 77
62 Pb	21.792 889	15.453 727 43	29.650 574 15
63 Pb	17.500 232 21	17.121 695 74	29.127 572 84
64 Pb	20.262 894 78	18.658 886 81	31.972 133 82
65 Pb	28.714 394 97	22.072 115 32	29.414 765 25
66 Pb	23.625 136 56	21.265 648 68	14.372 435 01
67 Pb	29.986 806 6	12.439 904 64	24.744 851 83
68 Pb	26.236 925 61	13.544 176 71	24.166 930 75
69 Pb	22.677 394 37	21.771 404 5	19.933 410 28
70 Pb	27.056 008 88	11.175 126 98	27.568 852
71 Pb	20.023 952 3	20.455 098 53	16.925 061 8
72 Pb	26.784 234 91	13.193 165 5	17.804 450 35
73 Pb	16.937 651 1	19.647 511 99	19.000 884 26
74 Pb	18.796 199 38	23.409 386 79	19.344 648 4
75 Pb	19.809 069 94	20.740 640 09	22.876 862 24
76 Pb	15.887 031 27	22.117 300 13	22.358 691 31
77 Pb	16.766 034 97	19.727 053 28	25.468 600 96
78 Pb	18.355 123 63	23.442 049 43	25.658 099 32
79 Pb	18.978 247 58	21.031 867 88	28.789 063 12
80 S	21.949 524 01	22.378 352 52	29.237 479 54
81 S	21.062 424 23	24.878 974 7	25.703 623 14
82 S	30.431 630 05	19.010 902 34	23.639 461 55
83 S	25.233 893 19	15.948 637 33	17.450 715 03
84 S	26.815 345 56	19.811 603 39	17.362 996 71
85 S	26.351 368 51	13.255 225 53	21.148 900 96
86 S	23.029 301 03	21.403 717 28	16.964 674 64
87 S	27.848 580 34	24.419 274 56	23.181 348 2
88 S	24.175 270 05	18.458 149 15	14.413 528 22
89 S	27.829 712 72	17.560 261 79	20.678 809 17
90 S	25.823 713 48	14.065 898 08	27.271 733 94
91 S	23.975 250 26	19.062 254 56	20.316 813 14
92 S	31.905 629 47	22.567 930 61	23.674 775 53
93 S	15.730 443 41	15.332 683 15	23.057 084 24
94 S	25.066 812 15	16.368 998 68	23.766 525 12
95 S	26.507 359 07	20.449 284 29	23.368 777 23
96 S	21.952 513 39	24.615 501 73	19.858 036 75
97 S	27.411 621 05	18.130 292 33	26.823 608 51
98 S	25.582 397 62	23.092 845 08	20.113 381 49
99 S	29.209 497 99	22.078 724 65	26.308 199 99
100 S	22.761 557 66	19.599 754 93	32.276 642 92
101 S	20.114 470 52	27.327 126 2	22.417 233 3
102 S	23.649 168 41	19.483 456 83	26.257 623 95
103 S	23.477 662 45	12.595 498 59	24.023 880 45
104 S	24.468 701 57	16.879 319 31	29.880 393 02
105 S	25.752 654 02	20.817 646 58	29.392 657 82
106 S	29.415 534 28	21.513 552 79	20.663 384 3
107 S	22.538 480 1	21.746 470 35	23.053 818 12
108 S	24.091 560 2	26.135 148 16	22.942 434 19
109 S	24.796 155 89	23.276 332 34	25.977 239 84
110 S	27.495 837 87	10.920 658 7	24.470 844 57
111 S	21.076 161 43	17.778 585 95	16.991 523 02
112 S	22.468 959 66	15.347 987 36	20.331 752 82
113 S	18.225 221 77	16.675 087 83	19.690 257 73
114 S	19.324 211 14	13.955 460 46	23.254 552 31
115 S	21.078 693 67	17.958 814 82	23.188 140 62
116 S	22.067 899 46	15.375 423 86	26.495 336 62
117 S	18.006 942 59	16.915 779 14	26.170 464 22
118 S	20.291 823 75	18.393 082 66	29.331 505 99
119 S	20.074 652 8	20.718 823 84	19.824 274 77
120 S	17.226 830 27	19.528 495 42	22.703 013 6
121 S	18.548 012 74	23.768 210 44	22.483 570 27
122 S	19.384 990 57	20.523 155 63	25.681 303 29
123 S	28.992 390 97	14.916 627 57	24.188 034 04
124 H	19.344 054 07	23.661 953 34	16.437 410 48
125 O	19.736 865 43	23.144 086 09	17.155 162 01
126 O	17.032 395 75	25.964 600 38	24.919 964 46
127 H	20.456 576 95	10.985 160 47	20.127 831 91
128 C	29.110 915 85	22.116 683 27	13.879 286 27
129 O	29.019 151 34	21.211 623 45	14.839 244 61
130 O	28.414 414 13	22.162 710 8	12.873 474 52
131 H	29.905 451 93	22.812 320 59	14.058 260 08
132 H	22.992 006 27	12.894 123 02	30.239 594 46
133 O	23.261 541 81	13.404 512 48	29.476 135 32
134 O	22.817 109 41	15.123 375 9	14.041 643 26
135 C	22.250 265 19	14.003 711 76	14.254 777 75
136 C	22.562 002 64	29.090 332 64	19.325 684 12
137 O	22.662 812 3	28.020 305 8	20.052 416 5
138 O	21.496 853 77	29.426 268 48	18.815 190 39
139 H	23.470 893 55	29.696 815 77	19.263 354
140 C	19.499 089 29	13.731 982 16	30.496 736 07
141 O	19.053 181 48	14.538 899 55	29.643 889 82

142 O	20.694 407 03	13.565 329 71	30.876 290 74
143 H	18.748 459 97	13.048 973 15	30.961 043 49
144 C	20.075 572 16	28.401 361 21	28.331 838 56
145 O	20.508 680 56	29.145 582 93	27.398 972 39
146 O	19.397 442 72	27.315 319 96	28.149 059 04
147 H	20.348 665 23	28.608 357 94	29.411 385 5
148 H	21.967 170 07	28.809 110 04	25.756 870 59
149 O	22.040 662 13	28.044 896 27	25.206 051 86
150 H	15.030 010 67	26.203 061 71	17.380 556 24
151 O	17.045 485 81	24.767 712 29	17.967 195 93
152 C	26.186 630 33	30.301 815 41	21.330 949 48
153 O	27.428 018 02	29.871 996 03	21.454 746 25
154 O	25.168 986 47	29.678 901 51	21.614 213 27
155 H	26.026 880 89	31.426 445 78	21.052 818 21
156 H	26.474 748 59	22.257 382 73	14.112 969 04
157 O	25.935 239 99	21.877 068 43	14.743 684 55
158 C	30.949 611 5	18.195 397 72	17.371 393 19
159 O	29.973 726 98	18.787 661 72	16.807 796 34
160 H	26.332 140 3	27.341 519 31	26.142 448 69
161 O	26.291 880 69	26.561 286 82	26.740 614 51
162 O	16.439 124 67	22.336 042 27	24.621 526 48
163 H	15.623 732 88	22.801 482 07	24.842 155 75
164 C	24.471 964 96	9.193 026 226	20.018 769 05
165 O	25.139 550 31	9.674 814 077	20.993 871 13
166 O	23.418 333 75	9.756 411 786	19.538 009 75
167 H	24.685 300 57	8.196 444 299	19.654 007 03
168 H	18.770 335 46	21.157 803 23	31.980 808 38
169 O	19.522 480 12	20.914 635 36	31.410 766 33
170 C	20.492 140 61	20.448 552 81	13.023 635 62
171 O	20.570 371 06	20.000 621 31	14.318 858 73
172 H	19.968 464 86	11.355 318 54	26.238 121 01
173 O	20.421 252 49	12.012 443 37	25.776 687 74
174 O	22.092 329 17	13.459 324 79	15.377 611 08
175 H	21.714 789 63	13.371 602 92	13.502 257 6
176 C	33.425 307 91	13.162 517 74	23.109 551 21
177 O	32.496 078 2	13.050 674 63	23.950 011 77
178 O	33.985 183 22	14.230 023 6	22.744 985 1
179 H	33.846 176 61	12.140 355 84	22.676 006 69
180 C	28.227 361 72	22.031 068 49	33.051 332 11
181 O	28.048 322 19	21.487 196 82	31.897 284 8
182 O	27.373 216 61	22.143 087 02	33.947 196 69
183 H	29.240 421 49	22.429 052 89	33.185 841 14
184 H	16.300 139 8	22.392 451 81	18.391 242 35
185 O	16.891 362 46	21.972 657 94	19.006 184 48
186 H	15.212 574 58	26.197 849 16	25.714 855 02
187 O	20.725 209 46	11.819 431 23	20.680 485 59
188 C	22.234 881 39	8.042 485 99	23.934 009 52
189 O	22.016 720 89	9.297 364 65	23.794 891 82
190 O	23.241 712 38	7.580 262 726	24.518 404 24
191 H	21.459 656 51	7.287 488 24	23.625 893
192 H	31.049 484 55	16.646 029 03	28.713 178 12
193 O	30.334 025 79	16.930 167 13	28.092 838 42
194 H	31.997 434 04	18.596 901 56	17.375 638 66
195 O	30.700 890 72	17.206 567 96	18.170 936 11
196 H	19.758 713 19	13.493 241 19	17.252 094 92
197 O	19.847 654 8	14.267 609 23	17.793 437 31
198 O	14.041 369 68	23.607 706 49	23.196 692 19
199 H	11.936 444 37	24.834 558 41	22.300 827 8
200 H	30.046 672 09	28.285 728 49	23.358 370 08
201 O	29.562 051 28	27.594 564 84	22.865 629 66
202 O	28.060 656 4	11.299 081 07	17.014 056 89
203 H	28.503 297 34	9.391 126 197	17.452 101 81
204 C	32.213 228 86	23.031 560 86	17.082 766 6
205 O	31.939 665 92	22.210 935 27	16.092 811 07
206 O	31.526 127 01	23.205 321 08	18.167 466 21
207 H	33.209 629 43	23.452 373 97	17.059 348 74
208 H	17.931 497 74	9.898 850 045	24.364 324 2
209 O	18.108 052 54	10.730 475 49	23.999 842 42
210 O	32.653 619 15	18.863 200 32	27.883 088 06
211 H	34.469 350 65	19.829 553 01	27.749 692 5
212 C	30.505 943 91	26.057 279 14	26.759 849 84
213 O	31.608 577 84	25.457 198 36	26.755 470 15
214 O	29.555 128 09	25.819 939 65	25.938 862 49
215 H	30.328 800 55	26.844 744 03	27.467 592 67
216 H	34.566 008 97	17.190 127 31	22.696 555 98
217 O	33.798 087 85	17.483 568 95	23.214 486 06
218 O	27.004 323 91	26.796 587 13	20.554 949 41
219 H	27.271 388 27	27.333 638 43	19.795 312 85
220 C	15.653 598 77	14.048 861 73	28.737 694 75
221 O	16.065 709 76	15.205 833 29	28.223 643 77
222 O	15.592 282 98	12.948 041 48	28.067 101 62
223 H	15.454 682 65	14.007 287 12	29.839 509 16
224 H	19.692 199 25	24.826 983 43	31.620 990 06
225 O	20.010 234 58	24.085 159 73	31.014 137 2
226 O	28.381 466 52	10.605 374 61	19.171 157 6
227 C	28.305 321 65	10.408 868 57	17.906 164 21

228 C	30.202 221 23	12.750 238 61	28.306 389 89
229 O	29.444 583 55	12.604 734 76	27.279 221 29
230 O	30.317 396 7	13.788 524 4	28.935 646 88
231 H	30.797 289 05	11.855 136 72	28.618 371 27
232 H	17.256 362 91	19.567 048 09	16.267 179 25
233 O	17.703 959 69	19.113 670 83	16.999 777 04
234 C	14.073 188 4	24.743 553 15	22.659 362 25
235 O	15.009 004 13	25.254 735 83	21.978 098 65
236 H	17.807 843 79	23.799 139 19	28.512 831 62
237 O	18.668 285 21	23.487 479 18	28.146 596 62
238 H	28.247 634 7	10.627 992 22	31.316 821 29
239 O	28.398 817 68	10.280 157 46	29.400 800 36
240 H	22.807 273 63	11.846 143 44	17.578 327 46
241 O	23.219 946 98	12.522 761 77	18.176 358 91
242 H	27.066 806 12	24.972 429 65	28.712 362 93
243 O	26.989 954 91	24.036 934 69	28.378 507 73
244 H	29.218 484 29	14.793 479 67	18.221 716 55
245 O	28.300 497 44	14.818 804 93	18.532 528 61
246 O	23.048 136 9	25.734 309 95	28.494 693 65
247 H	23.316 043 98	26.557 588 59	28.959 993 09
248 H	25.230 575 2	25.530 426 29	16.864 234 7
249 O	24.574 407 15	24.843 265 13	17.108 664 35
250 C	16.120 560 52	25.707 725 53	25.770 399 92
251 O	16.225 463 69	24.832 262 14	26.687 903 34
252 H	30.487 806 34	19.637 195 43	29.790 334 69
253 O	29.783 511 76	19.826 988 59	29.157 900 35
254 O	26.591 697	11.429 652 43	30.261 700 92
255 C	27.732 157 39	10.798 348 79	30.369 685 9
256 H	12.987 885 72	21.145 718 06	23.153 873 42
257 O	13.710 246 62	20.671 617 46	22.699 880 47
258 O	33.067 889 32	20.664 950 56	26.587 116 57
259 C	33.382 106 24	19.797 571 66	27.514 179 75
260 C	31.195 836 93	23.739 649 09	29.772 435 35
261 O	31.284 807 93	22.704 990 05	29.063 349 95
262 O	30.082 876 34	24.062 310 56	30.361 125 55
263 H	32.042 077 78	24.413 423 39	29.791 550 82
264 H	13.703 896 95	18.010 221 59	25.324 433 49
265 O	14.575 382 8	17.919 909 53	24.943 181 15
266 O	21.500 256 42	20.737 197 34	12.415 166 28
267 H	19.005 824 95	21.904 682 54	12.914 636 13
268 C	24.749 599 25	24.247 037 24	32.212 109 81
269 O	25.042 743 56	25.011 005 86	31.227 193 67
270 O	24.300 535 51	23.037 075 84	32.105 279 12
271 H	24.753 130 9	24.685 968 33	33.230 423 35
272 C	28.434 519 18	25.002 154 46	16.812 899 1
273 O	29.146 751 36	24.082 272 22	16.340 713 79
274 O	27.519 353 4	24.909 537 63	17.681 235 37
275 H	28.604 118 68	25.986 892 76	16.393 924 24
276 C	13.957 483	19.005 685 88	18.719 452 97
277 O	14.637 957 03	19.798 099 27	17.988 715 97
278 O	14.542 908 28	18.262 905 99	19.602 289 05
279 H	12.225 834 62	17.984 490 15	17.924 139 33
280 H	16.172 161 48	13.084 554 43	26.278 087 52
281 O	16.569 116 79	13.473 596 76	25.441 185 2
282 O	17.511 938 62	18.083 761 03	31.443 339 77
283 H	15.862 504 2	18.681 545 84	32.466 002 68
284 H	31.637 645 67	15.775 990 4	20.904 049 57
285 O	31.091 629 93	16.202 287 47	21.660 991 1
286 H	27.361 949 02	12.981 779 61	15.232 237 41
287 O	27.096 457 15	13.843 290 56	15.609 857 69
288 C	30.903 919 08	12.198 355 56	21.360 606 57
289 O	29.766 262 8	12.016 230 53	21.899 350 64
290 O	31.316 664 73	13.239 136 35	20.768 458 48
291 H	31.703 142 98	11.361 371 54	21.454 497 81
292 H	21.356 425 2	15.640 350 78	32.340 283 22
293 O	21.631 985 64	16.416 692 83	31.819 790 17
294 O	15.451 374	17.629 882 02	30.745 227 47
295 C	16.239 649 63	18.079 880 41	31.583 041 64
296 H	33.465 717 7	19.772 708 97	20.964 530 22
297 O	32.716 548 86	20.208 197 47	21.399 384 22
298 H	27.463 186 57	17.946 472 78	34.074 871 52
299 O	28.493 041 65	17.994 376 42	32.334 650 84
300 H	27.890 673 99	16.682 556 04	14.359 955 59
301 O	27.220 261 42	17.084 543 84	14.943 590 21
302 O	26.316 364 46	18.600 354 35	32.586 274 22
303 C	27.489 620 78	18.144 563 33	32.997 892 47
304 C	14.409 017 86	15.716 425 91	17.162 523 03
305 O	15.702 149 32	15.794 318 95	17.512 646 52
306 O	13.453 236 81	15.402 158 49	17.897 916 36
307 H	13.908 567 35	17.451 261 29	16.174 615 65
308 C	20.093 056 54	26.507 779 9	15.659 279 47
309 O	20.146 403 61	25.334 143 77	15.162 894 86
310 O	20.436 038 94	26.643 419 83	16.880 570 47
311 H	18.684 484 1	27.655 958 29	14.676 242 65
312 C	16.830 949 6	12.227 247 89	19.570 919 52
313 O	16.610 051 92	13.329 185 14	20.155 391 57

314 O	17.971 484 47	11.854 574 19	19.150 042 24
315 H	16.029 645 09	11.466 165 4	19.392 227 27
316 C	24.714 232 28	9.104 332 594	27.329 778 22
317 O	25.710 743 17	9.217 803 545	28.095 672 5
318 O	24.318 863 19	9.933 949 171	26.458 649 41
319 H	24.230 186 17	8.132 920 051	27.335 387 58
320 C	16.015 869 6	20.239 147 02	28.927 263 42
321 O	16.492 699 17	21.351 273 16	29.258 739 43
322 O	16.663 130 34	19.294 077 53	28.303 135 97
323 H	14.994 913 52	19.897 344 39	29.402 090 24
324 C	18.527 166 83	15.596 770 95	13.889 084 97
325 O	19.292 754 13	16.515 718 46	14.453 207 19
326 O	17.810 953 66	14.810 772 42	14.562 777 88
327 H	19.139 900 72	16.442 732 67	12.052 951 05
328 H	28.290 614 01	15.642 32	30.555 210 71
329 O	27.614 227 37	15.777 234 93	29.823 275 92
330 H	30.935 175 02	25.904 212 78	20.807 637 71
331 O	30.725 769 67	25.026 302 99	21.288 758 43
332 C	16.689 553 96	25.640 221 83	18.750 166 03
333 O	17.415 268 93	26.016 186 61	19.778 145 63
334 C	19.412 442 82	13.790 358 87	7.110 040 331
335 C	17.882 291 65	13.533 363 66	7.414 142 708
336 C	17.386 568 46	14.169 083 23	8.667 982 279
337 C	17.818 179 37	13.404 148 59	9.944 347 947
338 C	16.960 162 71	13.801 369 04	11.213 221 91
339 C	17.156 998 51	15.292 141 81	11.757 033 72
340 C	18.550 518 86	15.583 543 38	12.366 509 62
341 H	19.303 575 39	13.480 715 01	4.881 433 332
342 H	20.074 931 18	13.417 717 32	7.944 448 237
343 H	19.564 124 68	14.893 321 88	7.171 733 483
344 H	17.526 480 05	12.527 027 54	7.406 110 825
345 H	17.356 064 67	13.959 363 61	6.634 790 578
346 H	16.301 636 51	14.232 825 88	8.546 984 544
347 H	17.673 692 88	15.220 051 16	8.759 794 51
348 H	18.877 596 4	13.612 845 95	10.229 974 7
349 H	17.654 239 41	12.301 642 39	9.865 611 992
350 H	17.204 452 25	13.034 826 2	12.105 051 63
351 H	15.871 870 95	13.759 870 5	11.075 946 12
352 H	16.548 273 27	15.418 949 21	12.600 676 57
353 H	16.898 893 96	16.075 196 41	11.105 114 38
354 H	19.253 176 47	14.821 316 78	12.046 334 93
355 C	17.080 591 39	31.528 592 83	9.943 895 274
356 C	18.255 453 83	30.667 067 9	10.539 279 48
357 C	18.160 978 84	30.649 666 7	12.073 323 54
358 C	19.343 826 66	29.940 883 47	12.764 777 68
359 C	19.502 729 97	28.458 758 87	12.343 675 69
360 C	20.452 610 96	27.639 743 7	13.321 254 15
361 C	19.766 326 74	27.656 703 66	14.728 459 23
362 H	16.259 436 73	30.903 269 24	9.552 382 747
363 H	16.921 062 66	32.572 747 32	7.946 141 594
364 H	16.589 933 06	32.336 521 8	10.555 088 61
365 H	19.216 661 66	31.157 874 19	10.213 692 72
366 H	18.184 959 36	29.719 338 71	10.033 162 67
367 H	17.217 281 44	30.298 464 07	12.415 651 37
368 H	18.306 240 93	31.707 606 13	12.374 760 07
369 H	19.289 595 14	30.158 338 08	13.827 750 89
370 H	20.332 168 37	30.383 509 71	12.479 642 86
371 H	19.872 008 04	28.390 948 53	11.317 743 07
372 H	18.486 594 87	28.015 132 55	12.308 251 11
373 H	21.531 909 09	27.945 048 34	13.375 276 66
374 H	20.443 478 94	26.626 147 8	13.023 926 3
375 H	20.025 440 65	28.532 499 47	15.300 446 78
376 C	8.256 116 686	16.866 016 62	11.844 134 34
377 C	9.616 521 113	16.728 128 98	11.180 120 08
378 C	10.846 719 47	17.219 957 64	12.004 997 18
379 C	11.250 668 73	16.289 399 01	13.200 442 1
380 C	12.737 388 11	16.431 155	13.752 506 67
381 C	12.985 307 06	15.709 495 34	15.063 457 27
382 C	14.142 400 3	16.354 416 17	15.839 167 65
383 H	8.317 954 908	16.442 287 27	12.872 612 47
384 H	7.462 690 061	15.025 692 6	10.967 119 98
385 H	7.974 866	17.920 359 86	11.911 851 85
386 H	9.636 159 999	17.295 635 87	10.227 090 11
387 H	9.710 336 623	15.709 586 22	10.849 696 24
388 H	10.610 477 68	18.192 756 71	12.386 890 79
389 H	11.674 164 36	17.282 179 1	11.270 527 32
390 H	11.160 389 78	15.216 934 82	12.928 849 01
391 H	10.607 479 8	16.418 905 27	14.072 654 11
392 H	12.978 304 89	17.541 905 05	13.957 274 39
393 H	13.453 166 46	16.097 752 72	13.014 990 05
394 H	13.170 725 67	14.682 067 31	14.878 017 87
395 H	12.062 207 39	15.741 547 42	15.704 801 5
396 H	15.030 986 62	16.395 377 1	15.166 312 98
397 C	5.844 135 119	21.997 895 38	16.606 176 33
398 C	7.300 589 07	22.211 974 77	17.087 782 07
399 C	8.049 733 096	20.927 355 89	17.151 194 17

400 C	9.573 793 43	21.146 260 61	17.414 983 94
401 C	10.298 449 27	19.810 227 39	17.724 766 65
402 C	11.848 625 31	20.106 265 66	17.888 232 53
403 C	12.501 124 99	18.878 953 34	18.571 337 6
404 H	5.459 329 264	21.226 057 85	17.304 863 3
405 H	5.809 770 628	21.530 021 11	15.635 318 86
406 H	5.314 765 744	23.833 092 12	17.603 403 72
407 H	7.339 855 459	22.753 313 73	18.050 852 27
408 H	7.827 945 978	22.886 660 47	16.482 533 67
409 H	7.968 915 936	20.301 174 97	16.244 245 83
410 H	7.716 915 868	20.175 482 89	17.951 253 39
411 H	9.837 869 387	21.816 541 91	18.168 031 2
412 H	10.002 640 94	21.552 676 52	16.534 300 97
413 H	10.270 635 83	19.123 433 34	16.913 452 16
414 H	9.892 008 562	19.378 579 5	18.666 713 19
415 H	12.089 039 29	21.042 503 73	18.483 176 03
416 H	12.296 819 84	20.253 058 05	16.896 672 83
417 H	12.061 830 86	18.742 967 03	19.561 013 45
418 C	14.044 581 01	19.267 668 14	10.970 358 87
419 C	14.404 120 27	20.750 135 64	11.284 555 71
420 C	14.208 799 19	21.065 954 76	12.824 717 03
421 C	15.328 317 62	20.444 899 02	13.793 978 57
422 C	16.692 533 16	21.133 387 19	13.588 962 66
423 C	17.907 695 87	20.157 477 67	13.292 856 09
424 C	19.095 825 15	20.886 500 64	12.613 141 36
425 H	14.761 328 14	18.595 185 14	11.503 625 56
426 H	13.224 257 28	19.569 580 76	9.091 459 044
427 H	13.131 199 13	19.207 586 18	11.550 355 71
428 H	13.752 420 19	21.318 079 54	10.598 399 54
429 H	15.358 186 32	20.932 215 77	10.971 662 88
430 H	13.211 745 33	20.802 835 57	13.154 968 64
431 H	14.275 947 71	22.122 246 21	12.866 050 86
432 H	15.465 119 67	19.381 937 34	13.503 794 86
433 H	14.998 883 55	20.472 153 17	14.805 208 8
434 H	17.005 223 95	21.712 921 05	14.452 957 94
435 H	16.590 791 08	21.859 135 51	12.798 591 69
436 H	17.717 112 19	19.318 099 84	12.629 989 97
437 H	18.284 004 5	19.718 741 14	14.262 016 11
438 H	18.991 624 83	21.013 314 06	11.542 047 81
439 C	8.103 279 6	31.486 418 4	20.569 623 14
440 C	9.455 999 643	30.985 807 58	21.142 361 14
441 C	9.549 403 571	29.461 535 57	21.199 160 56
442 C	10.966 153 63	28.984 667 03	21.693 409 6
443 C	11.070 489 07	27.482 546	22.147 102 6
444 C	12.601 716 39	26.944 209 45	22.134 571 97
445 C	12.647 050 11	25.524 034 44	22.794 482 83
446 H	8.169 993 197	31.574 125 73	19.478 517 73
447 H	7.245 522 137	33.454 457 85	20.337 316 35
448 H	7.340 355 437	30.747 870 51	20.838 718 75
449 H	9.650 280 224	31.430 381 59	22.094 948 12
450 H	10.314 896 11	31.308 582 53	20.463 424 37
451 H	9.405 008 676	28.886 299 06	20.219 075 39
452 H	8.694 684 705	29.087 630 32	21.821 934 6
453 H	11.277 982 11	29.756 883 65	22.443 490 77
454 H	11.738 624 47	29.080 261 15	20.882 188 28
455 H	10.444 581 82	26.909 199 24	21.417 942 75
456 H	10.667 287 08	27.336 251 46	23.152 126 53
457 H	13.301 451 77	27.488 651 44	22.823 804 73
458 H	13.031 708 36	26.915 989 76	21.154 501 82
459 H	12.449 974 57	25.614 987 61	23.885 822 95
460 C	18.396 593 09	33.255 292 58	18.647 484 42
461 C	17.114 877 38	32.458 421 54	18.685 844 66
462 C	17.259 505 17	30.902 326 03	18.516 449 59
463 C	15.917 135 77	30.166 812 89	18.285 717 41
464 C	16.241 786 32	28.635 927 83	18.279 882 58
465 C	15.163 908 33	27.774 929 31	18.920 348 14
466 C	15.265 951 55	26.328 429 46	18.456 358 07
467 H	19.291 332 72	32.751 643 31	18.989 946 03
468 H	17.274 273 62	34.993 078 98	19.477 737 23
469 H	18.608 268 46	33.432 497 86	17.555 916 9
470 H	16.406 853 89	32.747 214 21	17.878 623 38
471 H	16.506 992 99	32.651 820 43	19.602 582 69
472 H	17.669 376 79	30.535 958 43	19.456 825 47
473 H	17.912 784 29	30.672 937 11	17.625 832 67
474 H	15.462 013 04	30.483 922 73	17.333 025 92
475 H	15.196 477 5	30.426 708 91	19.063 830 44
476 H	17.117 782 47	28.414 407 08	18.930 922 8
477 H	16.513 011 23	28.342 570 21	17.277 504 29
478 H	14.123 102 63	28.215 447 31	18.765 228 07
479 H	15.311 256 42	27.834 582 17	19.973 625 12
480 H	14.607 690 48	25.633 882 31	19.017 128 97
481 C	12.654 631 42	24.418 712 38	12.652 653 79
482 C	11.664 865 15	24.922 722 53	11.833 364 55
483 C	10.501 758 85	25.546 368 92	12.450 387 28
484 C	9.573 706 572	26.263 214 84	11.609 886 29
485 C	8.582 637 05	27.224 023 64	13.706 076 68

486 C	9.361 201 105	26.307 920 21	14.491 755 25
487 C	10.416 178 82	25.616 324 58	13.906 261 82
488 C	11.417 910 73	24.946 644 75	14.671 013 48
489 C	12.504 987 55	24.364 824 73	14.081 779 32
490 C	5.590 232 933	31.103 019 43	12.337 537 39
491 C	6.365 255 718	30.146 671 84	11.643 842 28
492 C	7.099 985 575	29.110 125 49	12.279 936 1
493 C	7.959 224 641	28.252 300 39	11.579 204 1
494 C	8.702 036 613	27.250 921 07	12.251 542 91
495 C	7.652 599 777	28.036 807 21	14.431 306 78
496 C	6.917 923 857	28.982 271 81	13.748 365 44
497 C	5.889 248 998	29.814 674 35	14.422 507 19
498 C	5.305 786 014	30.823 568 54	13.707 787 41
499 H	13.541 390 39	24.110 186 83	12.193 599 12
500 H	11.656 466 45	24.990 097 91	10.773 509 61
501 H	9.669 394 629	26.209 582 41	10.482 683 07
502 H	4.519 459 911	31.430 480 59	14.038 299 53
503 H	9.232 574 176	26.172 953 52	15.549 440 82
504 H	11.507 544 02	25.031 213 61	15.755 056 85
505 H	13.347 200 73	23.873 192 36	14.670 124 16
506 H	5.120 200 227	31.949 447 98	11.819 683 48
507 H	6.440 084 984	30.306 164 25	10.593 074 25
508 H	8.038 476 414	28.456 431 49	10.436 029 03
509 H	7.622 774 058	27.914 717 8	15.533 326 24
510 H	5.560 755 781	29.577 367 43	15.415 408 69
511 C	18.260 624 56	34.580 801 07	19.485 436 93
512 C	18.599 474 35	34.185 684 87	20.972 325 73
513 H	19.729 060 33	34.041 227 67	21.011 600 6
514 H	18.032 022 44	33.278 158 53	21.190 293 78
515 H	18.273 023 09	34.965 777 77	21.622 377 74
516 H	18.936 163 9	35.322 820 93	19.171 613 91
517 C	7.665 765 221	32.846 546 67	21.160 663 01
518 C	6.599 453 458	32.782 149 76	22.267 086 29
519 H	6.847 802 569	32.154 608 52	23.182 406 62
520 H	5.637 880 953	32.504 704 65	21.846 301 8
521 H	6.481 071 903	33.797 578 34	22.715 952 96
522 H	8.515 557 258	33.396 322 67	21.621 170 19
523 C	13.935 984 52	18.840 315 69	9.499 477 541
524 C	15.311 556 58	18.828 477 12	8.795 204 316
525 H	15.960 078 41	17.935 509 66	9.082 828 391
526 H	15.895 856 32	19.702 586 49	9.013 937 222
527 H	15.171 101 32	18.693 866 18	7.714 223 715
528 H	13.469 718 15	17.859 719 84	9.392 160 109
529 C	5.033 395 81	23.286 271 65	16.689 276 43
530 C	5.303 256 775	24.212 095 03	15.474 634 86
531 H	4.745 078 673	23.780 970 32	14.653 924 44
532 H	6.379 059 62	24.195 172 54	15.049 843 18
533 H	5.034 746 067	25.242 564 36	15.722 668 3
534 H	3.977 661 135	23.005 662 92	16.602 206 72
535 C	7.086 062 994	16.028 979 88	11.242 938 75
536 C	5.890 736 625	16.033 805 38	12.209 531 38
537 H	5.616 360 901	17.079 550 58	12.418 148 19
538 H	6.076 563 423	15.614 831	13.231 151 63
539 H	5.033 845 678	15.444 525 05	11.811 357 64
540 H	6.792 459 95	16.383 908 55	10.242 001 79
541 C	17.659 175 68	32.194 532 26	8.633 033 312
542 C	18.801 950 01	33.308 591 87	8.792 946 904
543 H	19.772 535 1	32.929 950 91	9.248 450 343
544 H	18.578 217 11	34.166 734 03	9.501 747 636
545 H	19.019 245 3	33.591 659 23	7.792 566 906
546 H	18.044 365 72	31.359 463 16	8.100 197 168
547 C	19.948 094 97	13.252 256 84	5.766 196 016
548 C	21.427 985 49	13.692 926 48	5.386 071 135
549 H	22.101 983 72	13.477 909 94	6.195 775 153
550 H	21.542 085 47	14.776 349 5	5.117 300 937
551 H	21.634 936 75	13.085 097 57	4.468 670 805
552 H	19.904 546 45	12.135 216 1	5.823 904 751

Table A.6: the coordinates of the first time step in the MD simulation for the PbS QD with the 9C-ligand, used as the starting setup in the MD simulation.

Appendix B

Excitation energy results

B.1 Tetracene

	PBE	PBE (hq)	B3LYP	B3LYP (hq)	CAMY-B3LYP	CAM-B3LYP	CAM-B3LYP (TDA)	M06-2X
S1 (mon)	2.17	2.15	2.45	2.42	2.69	2.75	3.03	2.92
S2 (mon)	3.03	3.02	3.49	3.46	3.64	3.65	3.71	3.67
S3 (mon)	3.25	3.22	3.61	3.60	4.13	4.21	4.41	4.32
S4 (mon)	3.64	3.61	3.97	3.91	4.30	4.51	4.57	4.49
S5 (mon)	4.43	4.38	4.70	4.64	4.88	4.93	5.29	5.24
T1 (mon)	1.39	1.39	1.23	1.22	N.A.	-0.14	1.42	1.21
T2 (mon)	2.69	2.69	3.60	3.57	N.A.	2.23	2.68	2.45
T3 (mon)	3.04	3.02	2.60	2.59	N.A.	3.30	3.38	3.26
T4 (mon)	3.05	3.04	3.20	3.17	N.A.	3.45	3.56	3.48
T5 (mon)	3.18	3.14	3.37	3.32	N.A.	3.90	4.18	3.91
S1 (dim)	1.30	1.28	1.90	1.85	2.56	-0.38	1.37	2.75
S2 (dim)	1.92	1.93	2.37	2.36	2.63	-0.36	1.37	2.86
S3 (dim)	2.13	2.11	2.41	2.38	2.70	2.16	2.62	2.92
S4 (dim)	2.14	2.13	2.53	2.55	3.24	2.17	2.63	3.41
S5 (dim)	2.59	2.57	2.55	2.53	3.64	2.68	2.87	3.65
T1 (dim)	1.27	1.25	1.18	1.18	N.A.	2.69	2.97	1.17
T2 (dim)	1.35	1.35	1.18	1.18	N.A.	2.90	2.91	1.17
T3 (dim)	1.39	1.38	1.90	1.85	N.A.	2.93	3.03	2.38
T4 (dim)	1.93	1.95	2.47	2.48	N.A.	3.51	3.53	2.40
T5 (dim)	2.56	2.55	3.37	3.32	N.A.	3.63	3.70	2.78

Table B.1: the excitation energies of the corresponding states as calculated for the corresponding functionals with the settings as described in the method section of tetracene, section 3.3.1. All values for the excitation energies are in eV and are relative to the ground state energy.

B.2 Pentacene

	PBE	B3LYP	CAMY-B3LYP	CAM-B3LYP	CAM-B3LYP (TDA)	M06-2X
S1 (mon)	1.62	1.89	2.14	2.20	2.50	2.11
S2 (mon)	2.37	2.92	3.38	3.39	3.46	3.33
S3 (mon)	2.93	3.22	3.42	3.49	3.71	3.40
S4 (mon)	2.97	3.24	3.62	3.83	3.88	3.73
S5 (mon)	3.99	3.96	4.50	4.55	4.86	4.48
T1 (mon)	0.93	0.71	N.A.	-0.90	0.95	-1.47
T2 (mon)	2.07	1.98	N.A.	1.55	2.08	0.66
T3 (mon)	2.38	2.92	N.A.	2.69	3.06	2.17
T4 (mon)	2.80	2.98	N.A.	3.10	3.19	2.95
T5 (mon)	2.93	3.00	N.A.	3.23	3.33	3.01
S1 (dim)	0.78	1.28	1.89	2.06	2.17	2.04
S2 (dim)	1.44	1.81	2.09	2.15	2.44	2.33
S3 (dim)	1.59	1.85	2.15	2.31	2.49	2.38
S4 (dim)	1.66	2.06	2.71	2.97	2.98	2.85
S5 (dim)	1.88	2.56	3.23	3.37	3.43	3.38
T1 (dim)	0.72	0.62	N.A.	-0.96	0.89	0.70
T2 (dim)	0.90	0.66	N.A.	-0.94	0.91	0.72
T3 (dim)	0.94	1.31	N.A.	1.46	2.01	1.80
T4 (dim)	1.51	1.90	N.A.	1.47	2.03	1.82
T5 (dim)	1.85	1.92	N.A.	2.22	2.23	2.10

Table B.2: the excitation energies of the corresponding states as calculated for the corresponding functionals with the settings as described in the method section of pentacene, section 3.3.1. All values for the excitation energies are in eV and are relative to the ground state energy.

Appendix C

Coupling of Setup 9C versus variables

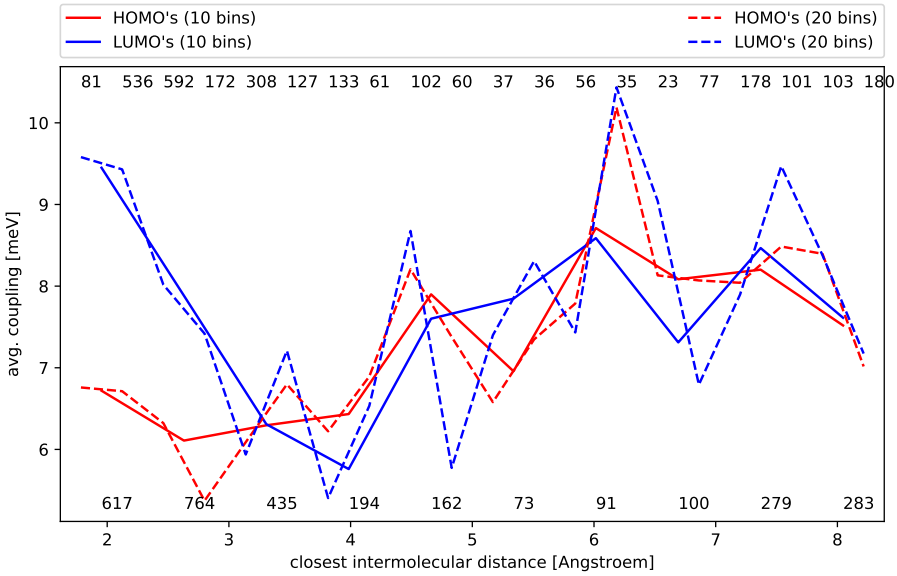

Figure C.1: the coupling of setup 9C averaged per closest intermolecular distance bin, one set of 10 bins (solid lines) and one set of 20 bins (dashed lines); the number of coupling values belonging to a bin is displayed at the top (for 20 bins) and bottom (for 10 bins) of the figure.

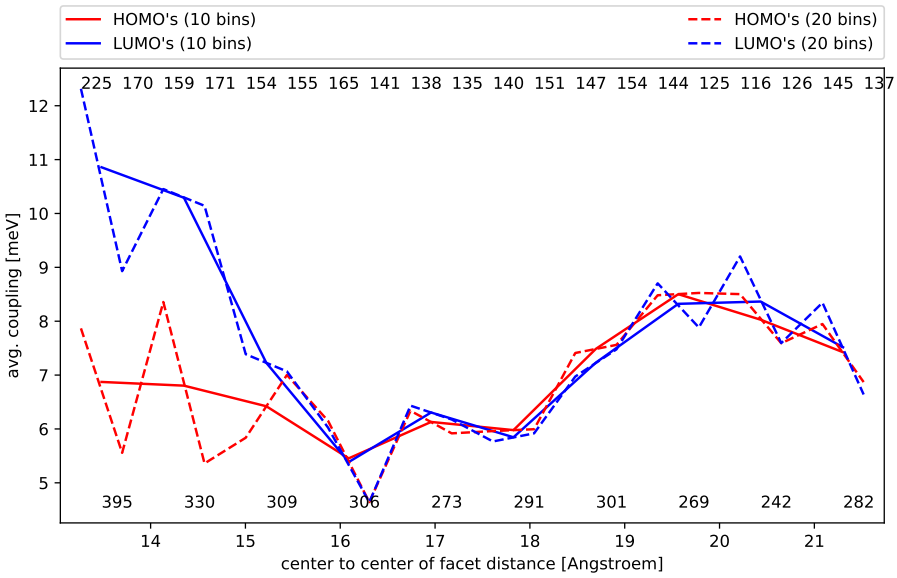

Figure C.2: the coupling of setup 9C averaged per distance bin, one set of 10 bins (solid lines) and one set of 20 bins (dashed lines); the number of coupling values belonging to a bin is displayed at the top (for 20 bins) and bottom (for 10 bins) of the figure.

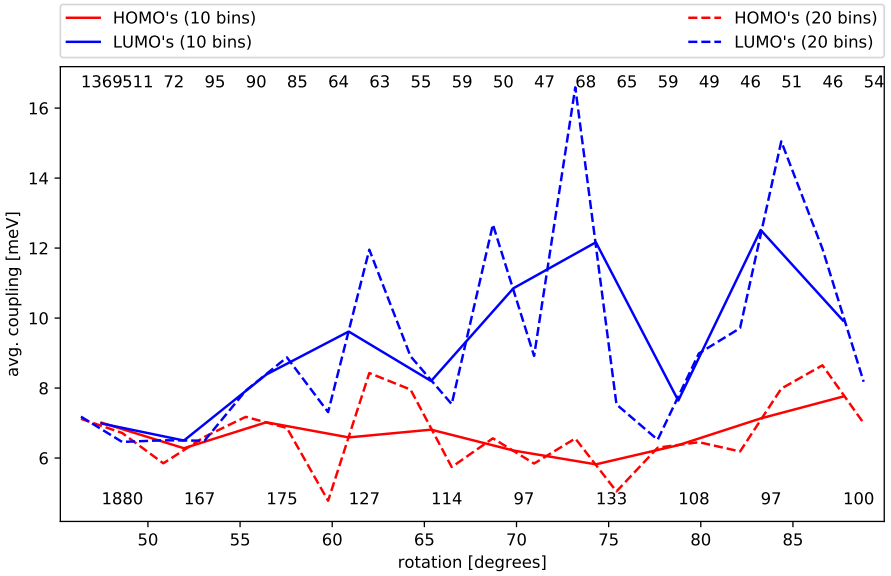

Figure C.3: the coupling of setup 9C averaged per rotational bin, one set of 10 bins (solid lines) and one set of 20 bins (dashed lines); the number of coupling values belonging to a bin is displayed at the top (for 20 bins) and bottom (for 10 bins) of the figure.

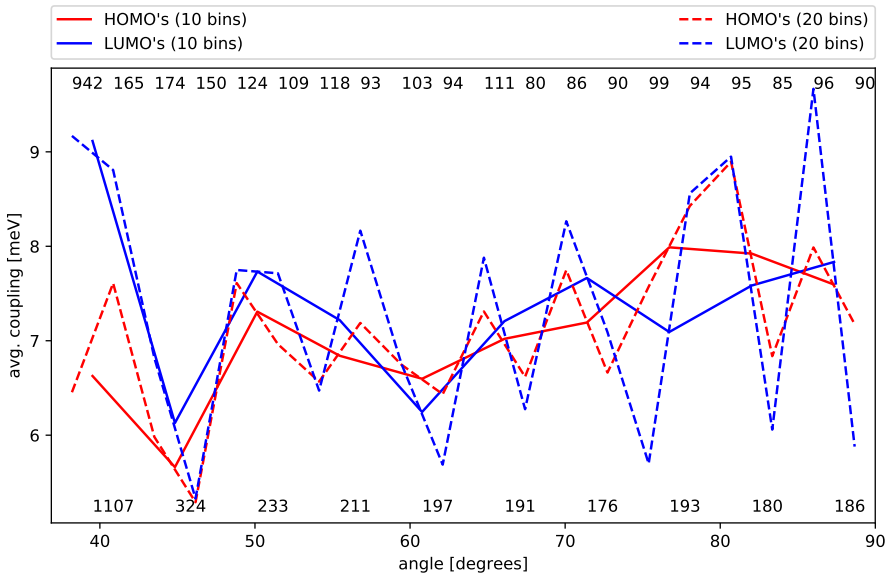

Figure C.4: the coupling of setup 9C averaged per angular bin, one set of 10 bins (solid lines) and one set of 20 bins (dashed lines); the number of coupling values belonging to a bin is displayed at the top (for 20 bins) and bottom (for 10 bins) of the figure.

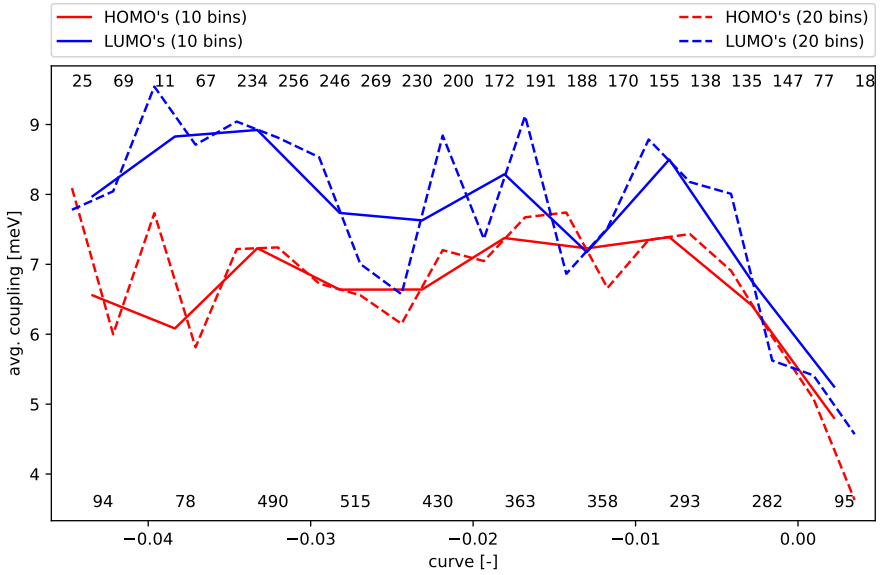

Figure C.5: the coupling of setup 9C averaged per parabolicity-bin, one set of 10 bins (solid lines) and one set of 20 bins (dashed lines); the number of coupling values belonging to a bin is displayed at the top (for 20 bins) and bottom (for 10 bins) of the figure.

Bibliography

[1] Alexey V. Akimov and Oleg V. Prezhdo. The pyxaid program for non-adiabatic molecular dynamics in condensed matter systems. *Journal of Chemical Theory and Computation*, 9(11):4959–4972, 2013. PMID: 26583414.

[2] Alexey V. Akimov and Oleg V. Prezhdo. Nonadiabatic dynamics of charge transfer and singlet fission at the pentacene/c60 interface. *Journal of the American Chemical Society*, 136(4):1599–1608, 2014. PMID: 24397723.

[3] Dylan H. Arias, Joseph L. Ryerson, Jasper D. Cook, Niels H. Damrauer, and Justin C. Johnson. Polymorphism influences singlet fission rates in tetracene thin films. *Chem. Sci.*, 7:1185–1191, 2016.

[4] Jon M. Azpiroz, Jesus M. Ugalde, Lioz Etgar, Ivan Infante, and Filippo De Angelis. The effect of tio2 surface on the electron injection efficiency in pbs quantum dot solar cells: a first-principles study. *Phys. Chem. Chem. Phys.*, 17:6076–6086, 2015.

[5] E.J. Baerends, T. Ziegler, J. Autschbach, D. Bashford, A. Berces, F.M. Bickelhaupt, C. Bo, P.M. Boerrigter, L. Cavallo, D.P. Chong, L. Deng, R.M. Dickson, D.E. Ellis, M. van Faassen, L. Fan, T.H. Fischer, C. Fonseca Guerra, M. Franchini, A. Ghysels, A. Giammona, S.J.A. van Gisbergen, A.W. Gotz, J.A. Groeneveld, O.V. Gritsenko, M. Gruning, S. Gusarov, F.E. Harris, P. van den Hoek, C.R. Jacob, H. Jacobsen, L. Jensen, J.W. Kaminski, G. van Kessel, F. Kootstra, A. Kovalenko, M.V. Krykunov, E. van Lenthe, D.A. McCormack, A. Michalak, M. Mitoraj, S.M. Morton, J. Neugebauer, V.P. Nicu, L. Noodleman, V.P. Osinga, S. Patchkovskii, M. Pavanello, P.H.T. Philipsen, D. Post, C.C. Pye,

W. Ravenek, J.I. Rodriguez, P. Ros, P.R.T. Schipper, H. van Schoot, G. Schreckenbach, J.S. Seldenthuis, M. Seth, J.G. Snijders, M. Sola, M. Swart, D. Swerhone, G. te Velde, P. Vernooijs, L. Versluis, L. Visscher, O. Visser, F. Wang, T.A. Wesolowski, E.M. van Wezenbeek, G. Wiesenekker, S.K. Wolff, T.K. Woo, and A.L. Yakovlev. *ADF2014*. SCM and Theoretical Chemistry and Vrije Universiteit and Amsterdam and The Netherlands, http://www.scm.com.

[6] Axel D. Becke. A new inhomogeneity parameter in density-functional theory. *The Journal of Chemical Physics*, 109(6):2092–2098, 1998.

[7] D. Beljonne, H. Yamagata, J. L. Brédas, F. C. Spano, and Y. Olivier. Charge-transfer excitations steer the davydov splitting and mediate singlet exciton fission in pentacene. *Phys. Rev. Lett.*, 110:226402, May 2013.

[8] Timothy C. Berkelbach, Mark S. Hybertsen, and David R. Reichman. Microscopic theory of singlet exciton fission. ii. application to pentacene dimers and the role of superexchange. *The Journal of Chemical Physics*, 138(11), 2013.

[9] Timothy C. Berkelbach, Mark S. Hybertsen, and David R. Reichman. Microscopic theory of singlet exciton fission. iii. crystalline pentacene. *The Journal of Chemical Physics*, 141(7), 2014.

[10] Patrick R. Brown, Donghun Kim, Richard R. Lunt, Ni Zhao, Moungi G. Bawendi, Jeffrey C. Grossman, and Vladimir Bulovi. Energy level modification in lead sulfide quantum dot thin films through ligand exchange. *ACS Nano*, 8(6):5863–5872, 2014. PMID: 24824726.

[11] J. Burgos, M. Pope, Ch. E. Swenberg, and R. R. Alfano. Heterofission in pentacene-doped tetracene single crystals. *physica status solidi (b)*, 83(1):249–256, 1977.

[12] D. M. Ceperley and B. J. Alder. Ground state of the electron gas by a stochastic method. *Phys. Rev. Lett.*, 45:566–569, Aug 1980.

[13] Wai-Lun Chan, Timothy C. Berkelbach, Makenzie R. Provorse, Nicholas R. Monahan, John R. Tritsch, Mark S. Hybertsen, David R. Reichman, Jiali Gao, and X.-Y. Zhu. The

quantum coherent mechanism for singlet fission: Experiment and theory. *Accounts of Chemical Research*, 46(6):1321–1329, 2013. PMID: 23581494.

[14] Wai-Lun Chan, Manuel Ligges, Askat Jailaubekov, Loren Kaake, Luis Miaja-Avila, and X.-Y. Zhu. Observing the multiexciton state in singlet fission and ensuing ultrafast multielectron transfer. *Science*, 334(6062):1541–1545, 2011.

[15] Christopher J. Cramer and Donald G. Truhlar. Density functional theory for transition metals and transition metal chemistry. *Phys. Chem. Chem. Phys.*, 11:10757–10816, 2009.

[16] P. A. M. Dirac. Note on exchange phenomena in the thomas atom. *Mathematical Proceedings of the Cambridge Philosophical Society*, 26(3):376385, 1930.

[17] Furio Ercolessi. A molecular dynamics primer. Technical report, International School for Advanced Studies, 1997.

[18] E. Fermi. Un Metodo Statistico per la determinazione di Alcune priorieta dell' atome. *Rend. Accad. Naz. Lincei*, 6:602, 1927.

[19] C. Fonseca Guerra, J. G. Snijders, G. te Velde, and E. J. Baerends. Towards an order-n dft method. *Theoretical Chemistry Accounts*, 99(6):391–403, 1998.

[20] Mirko Franchini, Pierre Herman Theodoor Philipsen, Erik van Lenthe, and Lucas Visscher. Accurate coulomb potentials for periodic and molecular systems through density fitting. *Journal of Chemical Theory and Computation*, 10(5):1994–2004, 2014. PMID: 26580526.

[21] Mirko Franchini, Pierre Herman Theodoor Philipsen, and Lucas Visscher. The becke fuzzy cells integration scheme in the amsterdam density functional program suite. *Journal of Computational Chemistry*, 34(21):1819–1827, 2013.

[22] Paolo Giannozi. Metodi numerici in struttura elettronica. Technical report, Università di Udine, 2010.

[23] Carlo Giansante, Ivan Infante, Eduardo Fabiano, Roberto Grisorio, Gian Paolo Suranna, and Giuseppe Gigli. darker-than-black pbs quantum dots: Enhancing optical absorption of

colloidal semiconductor nanocrystals via short conjugated ligands. *Journal of the American Chemical Society*, 137(5):1875–1886, 2015. PMID: 25574692.

[24] S.W. Glunz, F. Feldmann, A. Richter, M. Bivour, C. Reichel, H. Steinkemper, J. Benick, and M. Hermle. The irresistible charm of a simple current flow pattern 25% with a solar cell featuring a full-area back contact. *Proceedings of the 31st European Photovoltaic Solar Energy Conference and Exhibition*, pages 259–263, 2015.

[25] Martin A. Green, Keith Emery, Yoshihiro Hishikawa, Wilhelm Warta, and Ewan D. Dunlop. Solar cell efficiency tables (version 45). *Progress in Photovoltaics: Research and Applications*, 23(1):1–9, 2015. PIP-14-274.

[26] Eric C. Greyson, Josh Vura-Weis, Josef Michl, and Mark A. Ratner. Maximizing singlet fission in organic dimers: Theoretical investigation of triplet yield in the regime of localized excitation and fast coherent electron transfer. *The Journal of Physical Chemistry B*, 114(45):14168–14177, 2010. PMID: 20184354.

[27] D.J. Griffiths. *Introduction to Quantum Mechanics*. Pearson international edition. Pearson Prentice Hall, 2005.

[28] D. R. Hartree. The wave mechanics of an atom with a non-coulomb central field. part i. theory and methods. *Mathematical Proceedings of the Cambridge Philosophical Society*, 24:89–110, 1 1928.

[29] E. Heinecke, D. Hartmann, R. Muller, and A. Hese. Laser spectroscopy of free pentacene molecules (i): The rotational structure of the vibrationless s1s0 transition. *The Journal of Chemical Physics*, 109(3):906–911, 1998.

[30] P. Hohenberg and W. Kohn. Inhomogeneous electron gas. *Phys. Rev.*, 136:B864–B871, Nov 1964.

[31] Ivan Kondov, , Martin ek, Claudia Benesch, Haobin Wang, *, , and Michael Thoss*. Quantum dynamics of photoinduced electron-transfer reactions in dyesemiconductor systems: first-principles description and application to coumarin 343tio2. *The Journal of Physical Chemistry C*, 111(32):11970–11981, 2007.

[32] R. C. Johnson and R. E. Merrifield. Effects of magnetic fields on the mutual annihilation of triplet excitons in anthracene crystals. *Phys. Rev. B*, 1:896–902, Jan 1970.

[33] Jin Young Kim, Oleksandr Voznyy, David Zhitomirsky, and Edward H. Sargent. 25th anniversary article: Colloidal quantum dot materials and devices: A quarter-century of advances. *Advanced Materials*, 25(36):4986–5010, 2013.

[34] Thomas D. Khne. Second generation carparrinello molecular dynamics. *Wiley Interdisciplinary Reviews: Computational Molecular Science*, 4(4):391–406, 2014.

[35] Jingrui Li, Mattias Nilsing, Ivan Kondov, Haobin Wang, Petter Persson, Sten Lunell, and Michael Thoss. Dynamical simulation of photoinduced electron transfer reactions in dyesemiconductor systems with different anchor groups. *The Journal of Physical Chemistry C*, 112(32):12326–12333, 2008.

[36] Sanliang Ling. Optimisation of basis sets and pseudopotentials. Technical report, University College London, 2015.

[37] PerOlov Lowdin. On the nonorthogonality problem connected with the use of atomic wave functions in the theory of molecules and crystals. *The Journal of Chemical Physics*, 18(3):365–375, 1950.

[38] Fatemeh Mirjani, Nicolas Renaud, Natalie Gorczak, and Ferdinand C. Grozema. Theoretical investigation of singlet fission in molecular dimers: The role of charge transfer states and quantum interference. *The Journal of Physical Chemistry C*, 118(26):14192–14199, 2014.

[39] N. Monahan and X.-Y. Zhu. Charge transfer-mediated singlet fission. *Annual Review of Physical Chemistry*, 66(1):601–618, 2015. PMID: 25648486.

[40] Hazuki Morisaki, Takashi Koretsune, Chisa Hotta, Jun Takeya, Tsuyoshi Kimura, and Yusuke Wakabayashi. Large surface relaxation in the organic semiconductor tetracene. *Nat Commun*, 5, 11 2014.

[41] Dmitrii Nabok, Peter Puschnig, Claudia Ambrosch-Draxl, Oliver Werzer, Roland Resel, and Detlef-M. Smilgies. Crystal and electronic structures of pentacene thin films from grazing-incidence x-ray diffraction and first-principles calculations. *Phys. Rev. B*, 76:235322, Dec 2007.

[42] Noel M. O'boyle, Adam L. Tenderholt, and Karol M. Langner. cclib: A library for package-independent computational chemistry algorithms. *Journal of Computational Chemistry*, 29(5):839–845, 2008.

[43] Priya V. Parandekar and John C. Tully. Mixed quantum-classical equilibrium. *The Journal of Chemical Physics*, 122(9):094102, 2005.

[44] Priya V. Parandekar and John C. Tully. Detailed balance in ehrenfest mixed quantum-classical dynamics. *Journal of Chemical Theory and Computation*, 2(2):229–235, 2006. PMID: 26626509.

[45] John P. Perdew, Kieron Burke, and Matthias Ernzerhof. Generalized gradient approximation made simple. *Phys. Rev. Lett.*, 77:3865–3868, Oct 1996.

[46] John P. Perdew, Adrienn Ruzsinszky, Jianmin Tao, Viktor N. Staroverov, Gustavo E. Scuseria, and Gbor I. Csonka. Prescription for the design and selection of density functional approximations: More constraint satisfaction with fewer fits. *The Journal of Chemical Physics*, 123(6):062201, 2005.

[47] John P. Perdew and Yue Wang. Accurate and simple analytic representation of the electron-gas correlation energy. *Phys. Rev. B*, 45:13244–13249, Jun 1992.

[48] P.H.T. Philipsen, G. te Velde, E.J. Baerends, J.A. Berger, P.L. de Boeij, M. Franchini, J.A. Groeneveld, E.S. Kadantsev, R. Klooster, F. Kootstra, P. Romaniello, D.G. Skachkov, J.G. Snijders, C.J.O. Verzijl, G. Wiesenekker, and T. Ziegler. *BAND2014*. SCM, Theoretical Chemistry, Vrije Universiteit, Amsterdam, The Netherlands, http://www.scm.com.

[49] Felix Plasser, Giovanni Granucci, Jiri Pittner, Mario Barbatti, Maurizio Persico, and Hans Lischka. Surface hopping dynamics using a locally diabatic formalism: Charge transfer

in the ethylene dimer cation and excited state dynamics in the 2-pyridone dimer. *The Journal of Chemical Physics*, 137(22):22A514, 2012.

[50] Felix Plasser and Hans Lischka. Analysis of excitonic and charge transfer interactions from quantum chemical calculations. *Journal of Chemical Theory and Computation*, 8(8):2777–2789, 2012. PMID: 26592119.

[51] Felix Plasser, Michael Wormit, and Andreas Dreuw. New tools for the systematic analysis and visualization of electronic excitations. i. formalism. *The Journal of Chemical Physics*, 141(2), 2014.

[52] Albert Polman, Mark Knight, Erik C. Garnett, Bruno Ehrler, and Wim C. Sinke. Photovoltaic materials: Present efficiencies and future challenges. *Science*, 352(6283), 2016.

[53] Enrico Ronca, Gabriele Marotta, Mariachiara Pastore, and Filippo De Angelis. Effect of sensitizer structure and tio2 protonation on charge generation in dye-sensitized solar cells. *The Journal of Physical Chemistry C*, 118(30):16927–16940, 2014.

[54] E. Schrödinger. An Undulatory Theory of the Mechanics of Atoms and Molecules. *Physical Review*, 28:1049–1070, December 1926.

[55] J. C. Slater. A simplification of the hartree-fock method. *Phys. Rev.*, 81:385–390, Feb 1951.

[56] Millicent B. Smith and Josef Michl. Singlet fission. *Chemical Reviews*, 110(11):6891–6936, 2010. PMID: 21053979.

[57] P. J. Stephens, F. J. Devlin, C. F. Chabalowski, and M. J. Frisch. Ab initio calculation of vibrational absorption and circular dichroism spectra using density functional force fields. *The Journal of Physical Chemistry*, 98(45):11623–11627, 1994.

[58] A. Szabo and N.S. Ostlund. *Modern Quantum Chemistry: Introduction to Advanced Electronic Structure Theory*. Dover Books on Chemistry. Dover Publications, 1989.

[59] Maxim Tabachnyk, Bruno Ehrler, Simon Gélinas, Marcus L. Böhm, Brian J. Walker, Kevin P. Musselman, Neil C. Greenham, Richard H. Friend, and Akshay Rao. Resonant energy transfer of triplet excitons from pentacene to pbse nanocrystals. *Nat Mater*, 13(11):1033–1038, 11 2014.

[60] Yoshihiro Tawada, Takao Tsuneda, Susumu Yanagisawa, Takeshi Yanai, and Kimihiko Hirao. A long-range-corrected time-dependent density functional theory. *The Journal of Chemical Physics*, 120(18):8425–8433, 2004.

[61] G. te Velde and E. J. Baerends. Precise density-functional method for periodic structures. *Phys. Rev. B*, 44:7888–7903, Oct 1991.

[62] G. te Velde, F. M. Bickelhaupt, E. J. Baerends, C. Fonseca Guerra, S. J. A. van Gisbergen, J. G. Snijders, and T. Ziegler. Chemistry with adf. *Journal of Computational Chemistry*, 22(9):931–967, 2001.

[63] L. H. Thomas. The calculation of atomic fields. *Proceedings of the Cambridge Philosophical Society*, 23:542, 1927.

[64] Nicholas J. Thompson, Mark W. B. Wilson, Daniel N. Congreve, Patrick R. Brown, Jennifer M. Scherer, Thomas S. Bischof, Mengfei Wu, Nadav Geva, Matthew Welborn, Troy Van Voorhis, Vladimir Bulović, Moungi G. Bawendi, and Marc A. Baldo. Energy harvesting of non-emissive triplet excitons in tetracene by emissive pbs nanocrystals. *Nat Mater*, 13(11):1039–1043, 11 2014.

[65] V.K. Thorsmolle and R.D. Averitt. Photoexcited carrier relaxation dynamics in pentacene probed by ultrafast optical spectroscopy : Influence of morphology on relaxation processes. *Physica B*, 404(1):3127–3130, 2009.

[66] Y. Tomkiewicz, R. P. Groff, and P. Avakian. Spectroscopic approach to energetics of exciton fission and fusion in tetracene crystals. *The Journal of Chemical Physics*, 54(10):4504–4507, 1971.

[67] John C. Tully. Molecular dynamics with electronic transitions. *The Journal of Chemical Physics*, 93(2):1061–1071, 1990.

[68] R. Turton. *The Physics of Solids*. Oxford University Press, 2000.

[69] Paul J. Vallett, Jamie L. Snyder, and Niels H. Damrauer. Tunable electronic coupling and driving force in structurally well-defined tetracene dimers for molecular singlet fission: A computational exploration using density functional theory. *The Journal of Physical Chemistry A*, 117(42):10824–10838, 2013. PMID: 24053123.

[70] S. H. Vosko, L. Wilk, and M. Nusair. Accurate spin-dependent electron liquid correlation energies for local spin density calculations: a critical analysis. *Canadian Journal of Physics*, 58(8):1200–1211, 1980.

[71] Linjun Wang, Dhara Trivedi, and Oleg V. Prezhdo. Global flux surface hopping approach for mixed quantum-classical dynamics. *Journal of Chemical Theory and Computation*, 10(9):3598–3605, 2014. PMID: 26588504.

[72] G Wiesenekker and E J Baerends. Quadratic integration over the three-dimensional brillouin zone. *Journal of Physics: Condensed Matter*, 3(35):6721, 1991.

[73] Takeshi Yanai, David P Tew, and Nicholas C Handy. A new hybrid exchangecorrelation functional using the coulomb-attenuating method (cam-b3lyp). *Chemical Physics Letters*, 393(1):51 – 57, 2004.

[74] Jianhua Zhao, Aihua Wang, Martin A. Green, and Francesca Ferrazza. 19.8% efficient honeycomb textured multicrystalline and 24.4% monocrystalline silicon solar cells. *Applied Physics Letters*, 73(14):1991–1993, 1998.

[75] Yan Zhao and Donald G. Truhlar. The m06 suite of density functionals for main group thermochemistry, thermochemical kinetics, noncovalent interactions, excited states, and transition elements: two new functionals and systematic testing of four m06-class functionals and 12 other functionals. *Theoretical Chemistry Accounts*, 120(1):215–241, May 2008.

[76] Paul M. Zimmerman, Franziska Bell, David Casanova, and Martin Head-Gordon. Mechanism for singlet fission in pentacene and tetracene: From single exciton to two triplets. *Journal of the American Chemical Society*, 133(49):19944–19952, 2011. PMID: 22084927.

[77] Paul M. Zimmerman, Zhiyong Zhang, and Charles B. Musgrave. Singlet fission in pentacene through multi-exciton quantum states. *Nat Chem*, 2(8):648–652, 08 2010.